DISTRIBUTED COMMUNICATION AND CONTROL FRAMEWORKS FOR SMART DISTRIBUTION GRIDS USING THE INTERNET OF THINGS AND BLOCKCHAIN TECHNOLOGY

SHIVAM SAXENA

A DISSERTATION SUBMITTED TO THE FACULTY OF GRADUATE STUDIES
IN PARTIAL FULFILMENT OF THE REQUIREMENTS
FOR THE DEGREE OF

DOCTOR OF PHILOSOPHY

GRADUATE PROGRAM IN ELECTRICAL ENGINEERING AND COMPUTER SCIENCE
YORK UNIVERSITY
TORONTO, ONTARIO
JUNE 2021

Abstract

Smart distribution grids (SDGs) are power systems that seek to harness the advantages of distributed energy resources (DERs), such as renewable distributed generation and electric vehicles, to increase their operational efficiency and sustainability. However, the *uncontrolled* operation of DERs lead to severe operational challenges, resulting in the overloading of power transformers and voltage violations. Distribution system operators (DSOs) are responsible for preventing such issues, however, DERs are typically owned by agents such as homeowners and private enterprises, whose motivations revolve around financial incentives and maximizing operational convenience, which do not always align with the DSO's objectives. Thus, new communication and control frameworks are required to facilitate the coordination of control actions between agents and DSOs that are mutually beneficial. The architectures of these frameworks should be *distributed* to avoid unilateral authority, and *auditable* to alleviate any trust issues between participants.

To those ends, this thesis develops distributed communication and control frameworks for SDGs that are built upon modern communication technologies such as the Internet of Things (IoT), and blockchains, both of which provide architectures that are inherently distributed. The proposed control strategies of this thesis are inspired from principles related to transactive energy systems (TES), where distributed control techniques are combined with economically oriented decision making to improve overall energy efficiency.

Accordingly, this thesis is divided into three parts, where each part proposes a new framework that is validated by using simulated and real-world experiments at a microgrid in Vaughan, Ontario. Part I proposes a *fully* distributed communication framework

(DCF) that is built upon the IoT-based framework known as Data Distribution Service (DDS). Benchmarking of the DCF indicates that it can provide 1000 messages/second at 36 millisecond latency, which is well within the minimum latency requirements for smart grid applications. The DCF is also tested within the application of distributed voltage regulation, where agents use the DCF to execute the Asynchronous Weak Commitment (AWC) control strategy to resolve voltage violations despite intermittent agent connection failures. Part II proposes a blockchain-based TES to enable agents to bid and provide voltage regulation services in a competitive marketplace using the Extended Contract Net Protocol (ECNP) control strategy. Simulation results on a 69-bus test feeder show that the proposed system enables the simultaneous mitigation of multiple violations in less bidding cycles than conventional approaches. Part III develops a blockchain-based residential energy trading system (RETS), which enables residential communities and DSOs to participate in peer to peer energy trading and demand response. Experimental results indicate that the proposed system reduces the peak demand of the community by 48 kW (62%), which leads to an average savings of $1.02 M for the DSO by avoiding transformer upgrades. The proposed RETS is developed on the Hyperledger Fabric blockchain platform and deployed to the aforementioned microgrid to demonstrate its ability to minimize energy imports from the DSO. The proposed RETS is also benchmarked in terms of its transaction latency and provides transaction confirmation at an average of 17 seconds, which is sufficient for residential energy markets.

In summary, the findings of this thesis are intended to provide both quantitative and qualitative context for the new era of transactive energy in SDGs, where the underlying distributed communication and control frameworks require a thorough techno-economic evaluation. By demonstrating the efficacy of the proposed frameworks at a real-world microgrid, while also providing benchmarks that test their scalability, it can be concluded that the technologies of IoT and blockchains can indeed be utilized effectively to improve the operation of SDGs.

Dedication

To my parents:

Through all the long nights, early mornings, and extra weekends, your unconditional love and support is what drove me to the finish line.

This one is for you.

Acknowledgements

As I sit down to begin the final preparations of writing my thesis, I'd like to express my sincerest gratitude to all those who have helped me in this humbling journey.

My supervisor, Dr. Hany Farag, whose endless patience and guidance has taught me many things about smart grids, but more importantly, has taught me *many more* things about professionalism, kindness, and sincerity. Thank you for having me as your student, and helping me realize potential that I never knew I had.

My sincerest gratitude to my committee members, Dr. Aboelaze and Dr. Afshin, for their excellent insight and continued support throughout the PhD milestones.

My parents, for going to any extent to make my life easier so that I could fully focus on my work, no matter what level of inconvenience to them. My wife, Shweta, who has had to bear the brunt of my absent-mindedness for the better part of four years, but has graciously made every sacrifice to ensure that I continue my academic journey. My constant companion, Astro, for providing unconditional love. Thank you guys for always being there for me.

My colleagues in the Smart Grid Research Lab, Nader El-Taweel and Mohammad Zaki, thank you for helping me with your superb skills in mathematical optimization. To the extraordinary team at the Sustainable Technologies Evaluation Program, Leigh St. Hi-

laire, Amanda Yip, Gil Amdurski, Erik Janssen, Ricardo Brown, David Nixon, Svend De Bruyn, and Aidan Brookson, I'm grateful to you for your technical expertise in facilitating the real-world testing of the systems designed in this thesis. Aidan and Leigh, the knowledge you have shared with me in the field of transactive energy has been extremely valuable, and I learned greatly from our discussions together.

Dr. Henry Kim and Hjalmar Turesson from the York University blockchain.lab, thank you for giving me the opportunity to learn the concept of blockchains from you. This topic has enhanced the journey of my PhD significantly, and I am appreciative of the lessons learned as a result.

I'm grateful to all of you for your time, wisdom, and guidance. My hope is that this thesis reflects these sentiments.

Table of Contents

List of Tables

List of Figures

List of Attributions

Some of the graphics used in the generation of figures within this dissertation require attribution to the original creators of the graphics. Thus, the following table provides the necessary attributions.

Table 1.1: Attributions for graphics used in this dissertation.

Graphic Description	Figure #	Creator
Battery	1.1	Freepik
EV	2.1	OpenClipart
Heater	2.1	Arthur Schlain
End Loads (TV)	2.3	DinosoftLabs

Abbreviations

AC	Alternating Current: Current that reverses its direction at fixed frequency.
ACL	Agent Communication Language: Syntax used for agent communication.
ADMM	Alternating Direction Method of Multipliers: Algorithm for solving optimization problems.
AMQP	Advanced Message Queuing Protocol: A communication middleware based on the Internet of Things.
AMS	Agent Management System: An entity to manage agent lifecycle.
AWC	Asynchronous Weak Commitment: Algorithm to solve distributed constraint satisfaction problems.
BESS	Battery Energy Storage System: Technology used to store and recharge electric batteries.
BFT	Byzantine Fault Tolerance: Mathematical condition specifying that a network can function correctly as long as two-thirds of participants reach consensus.
CAPEX	Capital Expenditure: Monies required to acquire/upgrade an asset.
CFP	Call for Proposal: Initial request by an agent for task competion.
CNP	Contract Net Protocol: Algorithm for task assignment among multiple agents.

CNY	Chinese Yen: Currency used in the People's Republic of China.
DC	Direct Current: Unidirectional flow of electrical charge.
DCF	Distributed Communication Framework: An agent messaging framework proposed in this thesis.
DDS	Data Distribution Service: A distributed communication middleware based on the Internet of Things.
DER	Distributed Energy Resource: Small scale devices that can generate, store, or adjust energy consumption.
DF	Directory Facilitator: An entity that indexes agent services.
DG	Distributed Generation: Small scale energy generation devices. or adjust energy consumption.
DisCSP	Distributed Constraint Satisfaction Problem: Mathematical problem where agents cooperatively solve localized problems subject to local constraints.
DSO	Distribution System Operator: The supervisory controller of the power distribution system.
ECNP	Extended Contract Net Protocol: Algorithm for parallel negotiation/task assignment among multiple agents.
E-Load	Electric Load: Any load that can be electronically controlled.
EMS	Energy Management System: Control system that coordinates actions of devices to deliver optimal energy flow.
EV	Electric Vehicle: Any vehicle that stores electric charge on-board.
FIPA	Foundation of Intelligent Physical Agents: De-facto standards that govern multi-agent systems.
GDS	Global Data Space: A distributed layer of communication used in data distribution service.

GHG	Greenhouse Gas Emissions: Release of gases that contribute to creating the greenhouse effect in the earth's atmosphere.
HEMS	Home Energy Management System: Dystem that controls distributed energy resources to optimize energy flow within a home.
HIL	Hardware-in-the-loop: Testing infrastructure to validate performance of physical system by using emulated sensors or actuators.
HLF	Hyperledger Fabric: Permissioned blockchain framework.
IoT	Internet of Things: Network of connected devices that exchange information to complete tasks in a distributed manner.
JADE	Java Agent Development Environment: Platform for prototyping multi-agent systems and distributed control strategies.
KCM	Kortright Centre Microgrid: A research facility located in Vaughan, Ontario.
KM	Kilometer: Unit of measure for distance in the metric system.
kWh	Kilowatt-hour: Unit of measure of energy sustained for one hour.
MAS	Multi-Agent System: A system composed of distributed agents.
MCP	Market Clearing Price: Price of electricity during an energy market interval.
MSG	Message: A message type consisting of alpha-numeric characters.
MQTT	Message Queue Telemetry Transport: A communication middleware based on the Internet of Things.
MTS	Message Transport Service: An entity to manage agent messaging.
Q-caps	Quantity Demand Caps: Virtualized constraints enforced on energy markets to limit allowable quantity.
pBFT	Practical Byzantine Fault Tolerance: A consensus algorithm used by agents in permissioned blockchains.

P\Q	Active and Reactive Power
P-caps	Price Demand Caps: Virtualized constraints enforced on energy markets to limit allowable quantity by increasing price.
PCC	Point of Common Coupling: Interconnection point between distributed energy resources and the main grid.
POW	Proof of Work: A consensus algorithm used by agents in permissionless blockchains.
PV	Photovoltaic: Cells converting light into electricity using the photovoltaic effect.
PZC	Point of Zonal Coupling: Interconnection point between agent zones.
P2P	Peer to Peer: Agent communication without centralized intermediary.
QoS	Quality of Service: Configuration parameters that alter transport of messages.
RETS	Residential Energy Trading System: Electricity marketplace for homeowners.
SDG	Smart Distribution Grid: A power distribution system with bi-directional communication and control of devices.
SIL	Software-in-the-loop: Testing infrastructure to validate performance of a physical system represented by a mathematical model.
SLA	Service Level Agreement: A document representing terms/conditions of acceptable quality of performance between two agents.
ST	Smart Thermostat: Thermostat aware of energy preferences and controlling heating/cooling to optimize energy efficiency in accordance.
TES	Transactive Energy System: Control of energy systems in accordance with economic optimality for all users of the power system.
TOU	Time of Use: A fixed schedule to specify hourly electricity rates.

Chapter 1 - Introduction

1.1 Motivation

The conceptualization of the Smart Grid is motivated primarily by aggressive economic and sustainability initiatives, which seek to decentralize legacy power systems into modular subsystems that rely on distributed energy resources (DERs) to meet their local energy demand [1]. Particularly in power distribution networks, the rapid penetration of DERs such as renewable distributed generation (DGs), battery energy storage systems (BESSs), and plug-in electric vehicles (EVs) have resulted in a transition from passive to smart distribution grids (SDGs), which are capable of providing two-way communication between DER owners and distribution system operators (DSOs). Thus, DERs have tremendous potential to help satisfy key operational objectives of the DSO, which include, but are not limited to: lowering greenhouse gas (GHG) emissions, provision of ancillary services such as voltage regulation, as well as reducing feeder congestion via demand response [2].

However, the *uncoordinated* operation of DERs within SDGs leads to unintended technical challenges for DSOs that are primarily caused by the resultant and significant mismatches of local power supply and demand [3]. For example, coincident charging of EVs and BESSs at off-peak electricity rates leads to the overload of distribution transformers [4], while excess power production from renewable DGs, such as photovoltaics (PV), can cause overvoltage violations and

lead to the damage of critical DSO infrastructure [5]. DERs are often connected at the "grid-edge", which is defined as the intersection between the low-voltage (secondary) and medium-voltage (primary) side of the distribution system, where the ownership of the DERs may reside with the DSO, homeowners, or private entities [6]. Although the operation of the DERs must conform to grid interconnection standards, such as those specified in the IEEE 1547 standards [7], there is a noticeable shift in the desired operation of the DERs, since the role of the traditional end consumer of energy has evolved into that of a *prosumer*. Prosumers are motivated by their desire to operate their DERs to maximize their own convenience and financial benefit, without necessarily considering the impact of their actions on the DSO.

Consequently, DSOs are increasingly concerned with the negative impact of DERs at the grid-edge due to three main reasons. First, DSOs have limited visibility and control capability at the grid-edge because most DSO-owned control assets, such as load tap changers and line voltage regulators, are located on the primary side of the distribution system [8]. Second, DSOs cannot unilaterally control the DERs because the ownership of the DERs resides with the prosumer. Third, although recent work has proposed strategies whereby DSOs may offer incentives to prosumers in exchange for ancillary services [9], this may expose a trust issue between DSOs and prosumers, where DSOs do not have real-time mechanisms to ensure the correct operation of prosumer DERs, and prosumers cannot transparently determine the true value of the incentive they deserve [10].

To address the aforementioned concerns, work is being done in the field of distributed, multi-agent systems (MAS), where agents, analogous to prosumers, engage in coordination strategies without the need of a central intermediary [11]. Compared to conventional coordination strategies, which are centralized, a dis-

tributed approach is more scalable and reliable since it does not expose a single point of failure, or, rely on a unilateral authority to make decisions [12]. Recently, MAS research within SDGs has evolved into the concept of *transactive energy systems* (TES), which aligns distributed coordination techniques with the economic objectives of agents to realize a marketplace for the provision of energy and ancillary services [13]. The ethos of TES attempt to address trust issues between agents by requiring that all agent transactions be completely auditable, such that agent performance can be held accountable against certain standards of performance [14].

However, there are aspects within the work of MAS and TES that have not been well explored. To start with, the emphasis of research within MAS has traditionally revolved around the formulation of the control strategy, while the underlying communication architecture has been neglected [15]. In particular, there has been a lack of description as to how exactly messages between agents are generated, stored, and routed to the correct agent, with critical analysis missing as to how scalable the communication framework is in terms of its acceptable message latency and throughput. Furthermore, although the control strategies employed in MAS research are distributed, the architecture of the communication framework is typically centralized, which still exposes a single point of failure for the overall system [16–18]. Additionally, much of the work within TES assumes that the agents are cooperative and trustworthy, and does not consider the development of mechanisms that would enable agent auditability and enforcement of penalization policies for the incorrect provision of an ancillary service. [19–21].

As such, there is a need to develop distributed communication and control frameworks that seek to address the aforementioned gaps in facilitating coordination between agents within SDGs. Two promising new technologies in this regard are the Internet of Things (IoT) and blockchains. The IoT is a communication

framework that is based on distributed design principles that enable real-time, scalable messaging among agents [22]. Blockchain technology is comprised of a distributed ledger that is used to keep a record of all transactions between agents, where the authenticity of each transaction is cross-verified by the agents in consensus [23]. Blockchains utilize software applications known as smart contracts to automate the process of executing the transactions on the ledger, thereby serving as a single point of truth for all agents in the system, while also obviating the need for a central intermediary. Therefore, frameworks that utilize the IoT to enable real-time, local decision making between agents, while using blockchains to ensure the auditability and accountability of all agent transactions, have the potential to address concerns of communication vulnerability and trust for all agents within SDGs.

A block diagram of a potential framework that uses IoT and blockchain technologies is depicted in Figure 1.1, where agents utilize the IoT layer to engage in local, low-latency messages to coordinate DER control actions according to a particular control strategy. Agents then submit their proposed control actions to the blockchain layer using a smart contract, which the agents use to verify the authenticity and correctness of each control action. All valid control actions are then stored on the distributed ledger immutably, and are subsequently executed by each agent. Thus, distributed control can be achieved in a real-time, secure, and impartial manner.

As such, this thesis proposes the design and development of distributed communication and control frameworks for SDGs that are built on the foundation of IoT and blockchains. The thesis is divided into three parts, where each part will be prefaced with a fundamental research gap, a research objective that proposes a novel framework to address that gap, and a target SDG application to validate

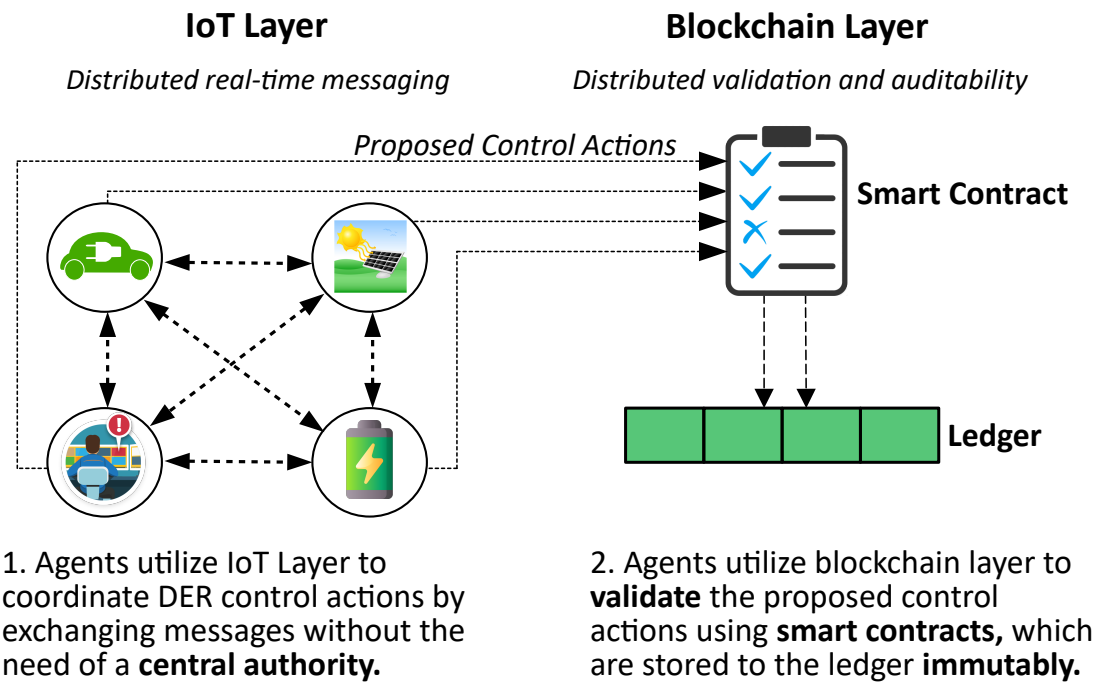

Figure 1.1: A control and communication framework using IoT and blockchains.

the efficacy of the proposed framework. The validation of the proposed solution will include experimental results from simulated SDGs, as well as from a real-world microgrid located in Vaughan, Ontario. A roadmap for the research objectives of the proposed thesis is shown in Figure 1.2.

As shown in the figure, the thesis is divided into three main parts. In Part I, a fully distributed communication framework (DCF) is developed to facilitate low-latency messaging between agents that is built on an IoT framework entitled Data Distribution Service (DDS). The performance of the DCF is validated by implementing it on real-time microcontrollers using a software-in-the-loop (SIL) approach, where its message latency is benchmarked and compared against acceptable limits of smart grid communication requirements [24]. The DCF is tested within the application of distributed voltage regulation, where agents use the DCF

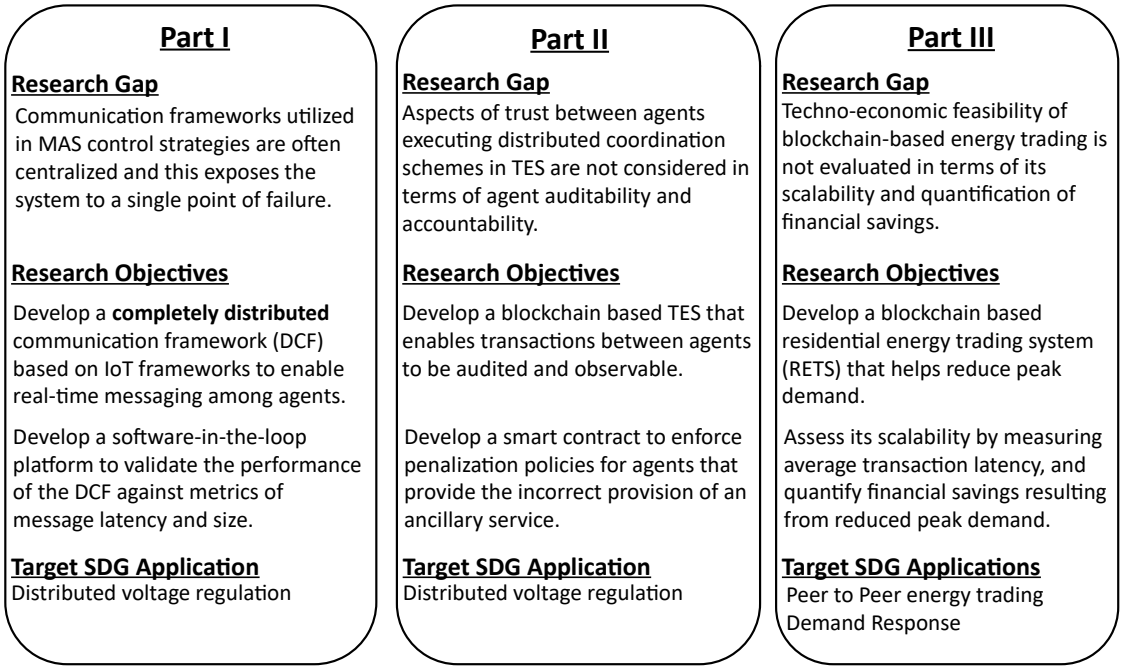

Figure 1.2: Roadmap of research objectives for the thesis .

to execute the Asynchronous Weak Commitment (AWC) control strategy to resolve voltage violations despite intermittent agent connection failures. In Part II, a blockchain-based TES is developed to establish a competitive marketplace for agents to sell voltage regulation services to each other by implementing the extended contract net protocol (ECNP) control strategy as a smart contract. A novel incentive mechanism is developed to penalize agents when they are unable to resolve a voltage violation they were assigned, which decreases their potential revenue. In Part III, a blockchain-based residential energy trading system (RETS) is developed to facilitate energy trades between homeowners with DERs in discrete market intervals, and also enables DSOs to engage in demand response to limit the maximum allowable demand within the market. A techno-economic assessment is carried out to evaluate the scalability of the proposed RETS by benchmarking

its average transaction latency, while also determining the total amount of capital expenditure (CAPEX) saved by the DSO as a result of the peak demand reduction realized by the marketplace. The proposed RETS is also deployed to the microgrid to demonstrate its ability to minimize the need to import energy from the DSO.

1.2 Research Objectives

A summary of the research objectives of the thesis is presented below:

1. Design of a completely distributed DCF for inter-agent messaging, which provides acceptable message latency as per smart grid communication requirements.

2. Development of an SIL platform to test the DCF, which demonstrates the ability of agents to execute the AWC control strategy to resolve voltage violations despite intermittent agent connection failures.

3. Development of a blockchain-based TES for distributed voltage regulation, which utilizes a smart-contract to enable agents to mitigate multiple voltage violations simultaneously using the ECNP control strategy, while also enforcing penalties for executing incorrect control actions.

4. Development of a blockchain-based RETS for homeowners with DERs that enables the peak demand of residential communities.

5. Techno-economic assessment of the proposed RETS by evaluating its scalability as a function of average transaction latency, as well as the total CAPEX saved by the DSO as a function of the reduction in peak demand.

6. Deployment and validation of the frameworks proposed in this thesis at a microgrid to demonstrate their efficacy in real-world settings.

1.3 Thesis Layout

The remainder of the thesis is organized as follows:

- **Chapter 2:** Provides background on SDGs and distributed control frameworks such as MAS and TEF. This is followed by an overview of IoT and blockchains, as well as a literature survey of control strategies that have utilized these technologies within SDG applications.

- **Chapter 3:** Introduces the design of the DCF based on DDS. The DCF is implemented on an SIL platform and aims to demonstrate its (i) scalability as a function of message latency and size; (ii) efficacy in enhancing the robustness of the AWC control strategy despite agent connection failures; and (iii) ability to resolve overvoltage violations at a real-world microgrid.

- **Chapter 4:** Presents a blockchain-based TES for voltage regulation services, where a novel incentive and penalization control strategy is proposed based on the ECNP. The objective of this chapter is to show how the proposed system can mitigate multiple voltage violations simultaneously, thereby being able to provide voltage stability in less bidding cycles when compared to conventional strategies.

- **Chapter 5:** Introduces a blockchain-based RETS for homeowner energy trading and demand response, where a techno-economic assessment is performed to (i) evaluate the proposed system's scalability as a function of average message latency; (ii) quantify the reduction of peak demand and corresponding CAPEX savings of the DSO in avoided transformer upgrades; and (iii) deploy the proposed system to the microgrid to demonstrate its ability to minimize energy imports from the DSO.

- **Chapter 6:** Summarizes the contribution of this thesis in relation to the target research gaps, and expands on the intention to pursue further work in these areas.

Chapter 2 - Overview of Distributed Communication and Control Within SDGs

Building upon the motivation and research objectives discussed in Chapter 1, this chapter provides an overview of the fundamental concepts of distributed communication and control within SDGs. The chapter begins with a formal introduction to SDGs and the grid-edge, with a special emphasis on summarizing the control issues that are caused by the uncoordinated operation of agent-owned DERs. Subsequently, distributed control concepts relating to MAS and TES will be discussed, which is followed by an overview of IoT and blockchains. Finally, a critical literature survey of IoT and blockchain-based control strategies within SDG applications will be provided to summarize the state-of-the-art, while also identifying research gaps that the thesis will address in later chapters.

2.1 Overview of Smart Distribution Grids

Power distribution grids are the interface that connect end consumers of electricity to the bulk power system, where the responsibility of the DSO is to deliver the power at an acceptable power quality and voltage level to all end consumers [25]. As discussed in Chapter 1, end consumers are rapidly investing in DERs, and thus, their role has transitioned to that of a rational agent that has the ability to operate their DERs according to their convenience and financial objectives. Accordingly,

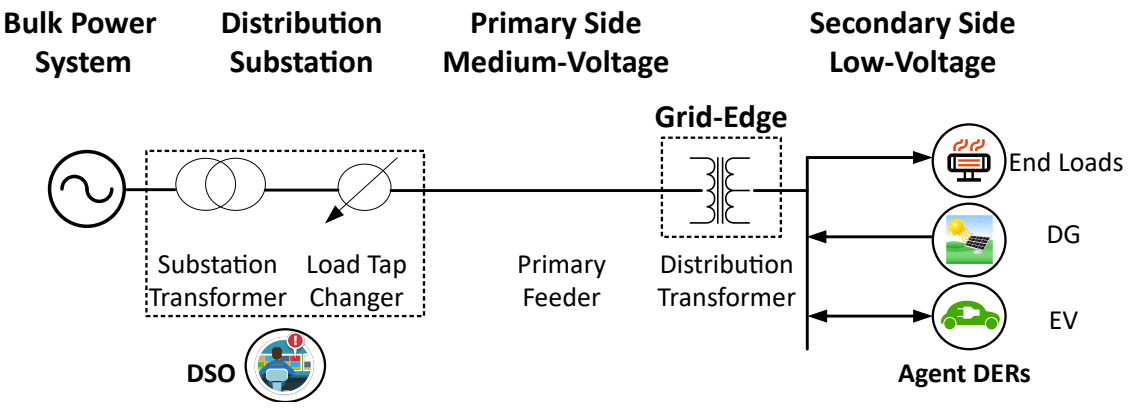

Figure 2.1: A schematic diagram of a typical smart distribution grid.

this transition has ushered in the era of the *smart* distribution grid, which must accommodate bi-directional communication and power flow as depicted in Figure 2.1. Conventional power flow dictates that the power from the bulk power system flows through the distribution substation, where the substation transformer steps down the voltage level of the power to between 4-35 kV. Load tap changers are also used to further regulate the voltage to within permissible limits when required [26]. The distribution substation is located on the primary, or medium-voltage side of the distribution grid, where power flows via primary feeders towards the grid-edge, which intersects with the secondary, or low-voltage side of the distribution grid. The distribution transformer at the grid-edge further steps down the voltage to an acceptable level for residential and commercial use, which is 120/240 V in North America [27]. On the other hand, the proliferation of agent-owned DERs at the grid-edge may cause power to flow in the *reverse* direction at times of excess power production and low demand. Careful coordination is required to mitigate significant power mismatches in SDGs, which leads to power losses, feeder congestion, and voltage violations that may result in damage and/or costly upgrades to DSO-owned infrastructure [28].

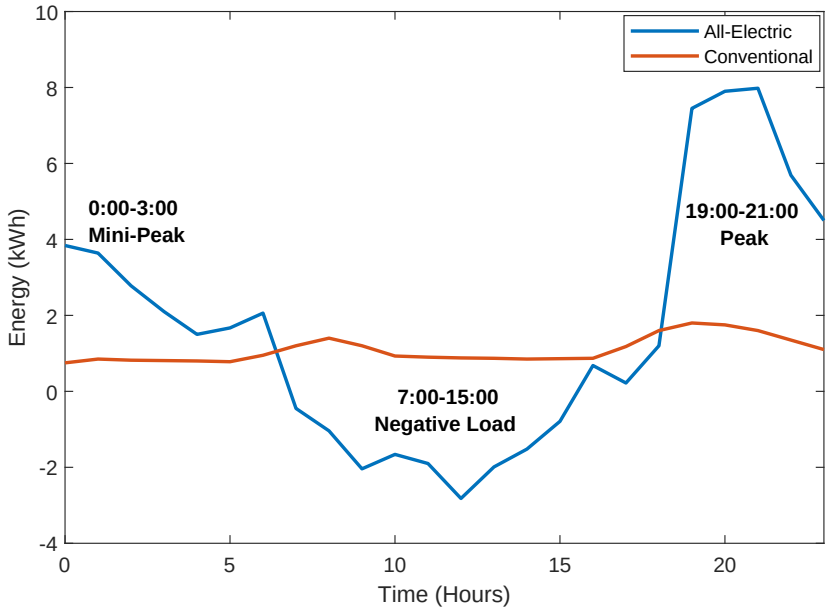

Figure 2.2: Load profile comparison between an all-electric and conventional home.

For example, the load profile of an all-electric home consisting of a 5 kW PV, 6 kW/25kWh BESS, a 6 kW/45kWh EV, as well as a smart thermostat (ST), is compared to a conventional home with no DERs in Figure 2.2. The load profile for the all-electric home is generated from real-world measurements taken from smart homes that exist at the Kortright Centre Microgrid (KCM), located in Vaughan, Ontario, while the conventional load profile is adapted from [29]. As seen in the figure, the load profiles are starkly different, where the load profile of the conventional home is relatively flat when compared to the all-electric home, which includes the creation of a new mini-peak between the hours of 0:00-3:00, negative loading between 7:00-15:00, as well as a 4.4x increase in peak demand during 19:00-21:00 (from 1.80 kWh to 7.98 kWh). The peaks are primarily caused by the charging of the BESS and EV during off-peak pricing hours, while the negative loading is caused by excess PV production during the afternoon. In executing simulations for

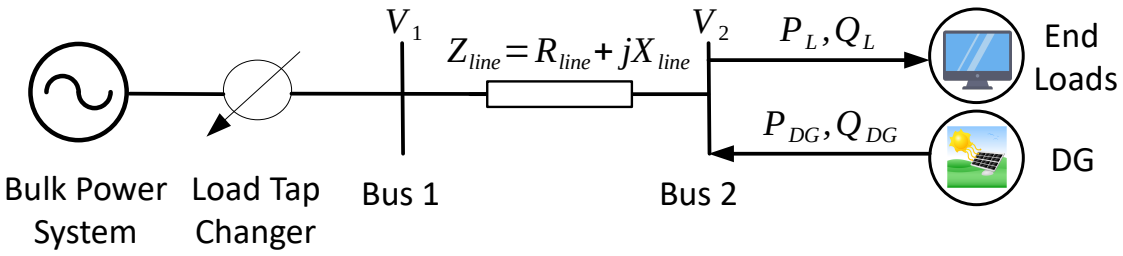

Figure 2.3: Simplified 2-bus SDG feeder.

an all-electric community of 8 homes, the peak load of the community is found to be 110 kW. This is well over the 50 kVA (45 kW with 0.9 power factor) capacity of the average distribution transformer that serves a typical 8-home community [30]. The simulation results for this scenario will be further expanded on in Chapter 5 of this thesis.

Another example to illustrate voltage regulation issues within SDGs is depicted in Figure 2.3, where an agent-owned DG is connected to the end of the SDG feeder. The voltage profile of any feeder is dependent on the feeder impedance (resistance and reactance), the active and reactive power, as well as the length of the feeder. Thus, the voltage drop between Bus 1 and Bus 2 of the feeder can be expressed as:

$$\Delta V = V_1 - V_2 = \frac{R_{Line}(P_L - P_{DG}) + X_{Line}(Q_L \pm Q_{DG})}{V_2} \tag{2.1}$$

where V_1 is the voltage at Bus 1, V_2 is the voltage at Bus 2, $\{R_{Line}, Q_{Line}\}$ are the resistance and reactance of the feeder, respectively, Z_{Line} is the overall impedance of the feeder, $\{P_L, Q_L\}$ are the active and reactive power consumption of the end loads, respectively, while $\{P_{DG}, Q_{DG}\}$ are the active and reactive power generation of the DG, respectively. It should be noted that the impedance of the feeder is a function of the feeder length, although this is not explicitly stated in equation (2.1). From equation (2.1), it can be seen that significant mismatches of P_{DG} and

P_L, as well as Q_{DG} and Q_L, may push the voltage outside acceptable limits. This is particularly true when the DG is fueled by intermittent renewable sources, such as PV or wind, which result in extreme fluctuations in power generation that cause both overvoltage and undervoltage violations [31].

A real-world example of this phenomenon can be seen at the KCM, which is a 240 V microgrid with a maximum allowable voltage of 254 V [32]. The KCM has a peak PV generation to load ratio of 40 kW to 15 kW, which results in a rapidly fluctuating voltage profile that is highly correlated with the experienced solar irradiance. The fluctuation of irradiance and resultant voltage profile of the KCM can be seen in Figure 2.4, while a data snapshot of the voltage of the KCM on a very sunny day can be seen in Figure 2.5, where the KCM is shown to regularly experience significant overvoltage violations. Since the DGs are owned by different stakeholders that have invested in the KCM, there is significant motivation to develop distributed control strategies that facilitate the pursuit of their individual objectives, while also staying within bounds of the voltage limits, as will be discussed in the next subsection.

2.2 Background of Distributed Control: MAS and TEF

Distributed control relies on the presence of multiple agents within an environment that work together to achieve a global objective, where decision making is shared among the agents [33]. In this thesis, agents are assumed to be independent entities that, in addition to the globally shared objective, also have local/individual objectives. This, in the context of SDGs, the environment is composed of the physical SDG infrastructure, as well as a set of virtual zones that are independently assigned to each agent. Each agent then utilizes the DERs within its zone to ensure the proper operation of its zone according to a specified control objective and a set of constraints. If an agent encounters a violation of constraints, it may request

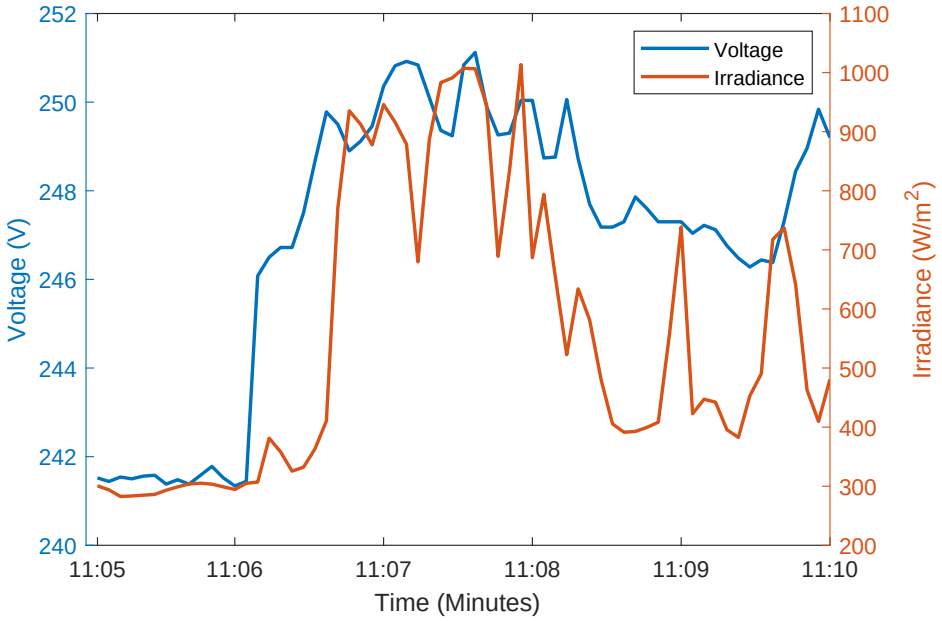

Figure 2.4: Significant fluctuation of voltage within KCM due to varying irradiance.

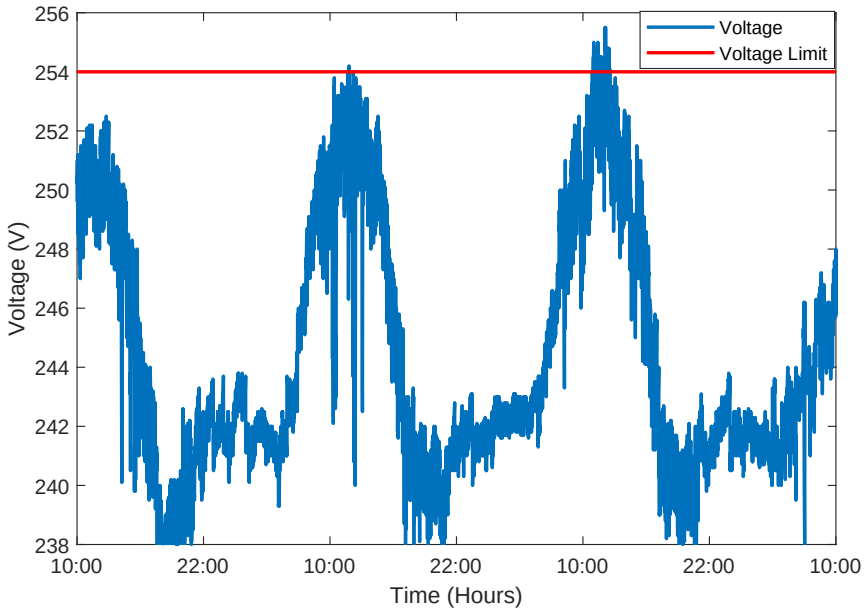

Figure 2.5: Evidence of overvoltage violations at the KCM.

help from neighboring agents, who will evaluate the request and determine whether it can be accommodated. Thus, the algorithm that defines the pattern of agent-requests, as well as the data to be exchanged at every iteration, is referred to as a distributed, MAS control strategy [34].

Standards for MAS have been developed by the Foundation of Intelligent Physical Agents (FIPA), which seek to standardize architectures that define how agents are deployed to, and interact with, any agent platform [34]. Figure 2.6 shows a block diagram of the FIPA Agent Management Reference Model, which defines the components that are used to manage the lifecycle and operation of existing agents. Each agent platform consists of agents, an agent management system (AMS), a directory facilitator (DF), as well as a message transport system (MTS). The AMS is used for registering the identities of all agents within a network, while the DF is used for registering a list of services that agents provide. The MTS is responsible for facilitating all messages between agents.

Inspired by the FIPA Agent Management Reference Model, many MAS development platforms have been proposed, where agents can be rapidly prototyped to test the efficacy of distributed control strategies [35]. The most popular MAS development platform is the Java Agent Development Environment (JADE), which is FIPA-compliant and can be hosted across multiple agent platforms [36]. It is interesting to note, however, that JADE utilizes a singular, centralized MTS to facilitate inter-agent communication, which is not robust since it exposes a single point of failure [37].

More recently, the application of MAS control strategies within SDGs has evolved into the concept of transactive energy, which is defined by the GridWise Architecture Council as a "combination of economic and control techniques to improve grid reliability and efficiency" [38]. It is important to highlight that the

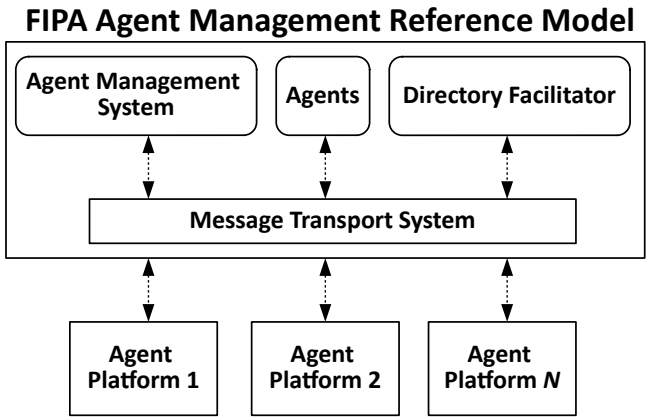

Figure 2.6: FIPA Agent Management Reference Model.

economic techniques include the incentivization of agents to control their DERs in a manner that aligns with the operational objectives of DSOs. TES' are inherently distributed, since all participants within the TES have the ability to engage in energy "transactions", where each transaction is usually attached to a financial incentive. In [38], the principles of TES' are discussed, which emphasize the need to enable the optimal integration of renewables and DERs, provide methods for non-discriminatory participation of agents, and allow for auditability of transactions such that all agents, including power system operators, such as DSOs, may be held accountable for standards of performance. It can be seen, therefore, that the principles of TES align well with the objectives of this thesis, which are to design auditable and distributed control and communication frameworks to address trust issues between agents, which would, in turn, increase the positive uptake of renewables and DERs. These objectives are better realized with the advent of modern communication frameworks in the form of IoT and blockchains, as will be discussed in the next subsection.

2.3 Background of Distributed Communication: IoT and Blockchains

2.3.1 Overview of the IoT

The IoT is a concept where every device, referred to as a "thing", has a presence on the internet, and can exchange information with other things to automate certain processes in a distributed manner [39]. The foundational element of IoT frameworks is middleware, which is comprised of communication interfaces and protocols that serve as a messaging layer between all agents, and is responsible for the transport, routing, buffering, and delivery of all messages [40]. IoT middlewares typically utilize a topic-based, publish-subscribe communication architecture for inter-agent messaging that defines a topic as a named channel of data that is comprised of a stream of messages. An example of this paradigm can be seen in Figure 2.7, where Agent 1 generates a request message and publishes it to Topic Y, and subsequently, the message is received by Agent 2 because it is also subscribed to Topic Y. In turn, Agent 2 publishes a response message to Topic Y, which is received by Agent 1 because it is also subscribed to Topic Y. The message buffering is handled by bi-directional message buffers, which store incoming published messages and release the messages to agents when they are online. It is worth noting that each topic can be configured with a quality of service (QoS) profile, which alters how the middleware transports the message [39]. Examples of QoS profiles include the ability to prioritize certain messages to improve their latency, defining a maximum acceptable duration latency, and specifying the exact order that an agent should receive messages in. Thus, it can be seen that the execution of distributed control strategies can benefit from utilizing the flexible range of QoS profiles to increase their operational efficacy.

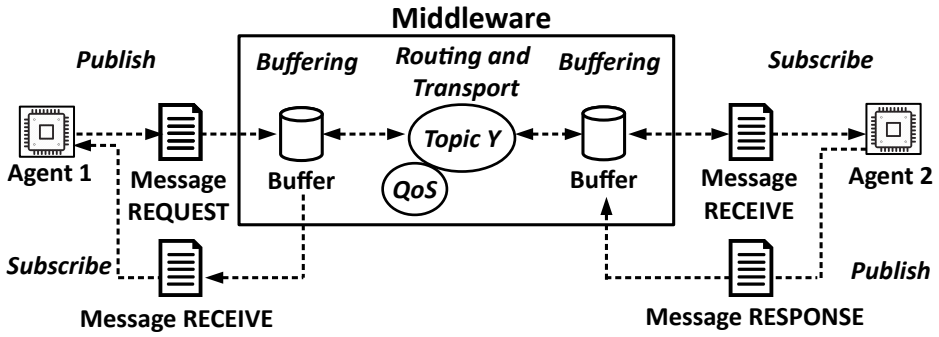

Figure 2.7: Message flow in topic-based, publish-subscribe middleware.

A popular type of IoT middleware is DDS, which is designed for low-latency, mission critical systems, and has the capability of sending millions of messages per second to millions of subscribers [41]. Unlike other popular IoT middlewares, such as Advanced Queue Messaging Protocol (AMQP), or Message Queue Telemetry Transport (MQTT), which utilize centralized message brokers to handle message transport and routing, DDS uses a completely distributed global data space (GDS) to enable inter-agent messaging [42]. The GDS is shown in Figure 2.8, and is comprised of topics and their associated QoS profiles. Agents merely need to declare their publishing/subscribing interest in a topic, and the GDS utilizes distributed multi-cast techniques to ensure that data flows directly from the publishing agent to the subscribing agent [43]. Additionally, DDS provides support for content filtering, where agents can specify conditional expressions that define a subset of messages they are interested in receiving from the GDS.

An example of content filtering is shown in Figure 2.8, where Agent 1 and Agent 2 publish messages to the Voltage topic in the form of voltage measurements, and Agent 3 and Agent 4 receive messages from the Voltage topic because they are subscribed to it. However, Agent 3 specifies a content filter that indexes all messages within the Voltage topic by the "Voltage" field, and accepts only the messages where

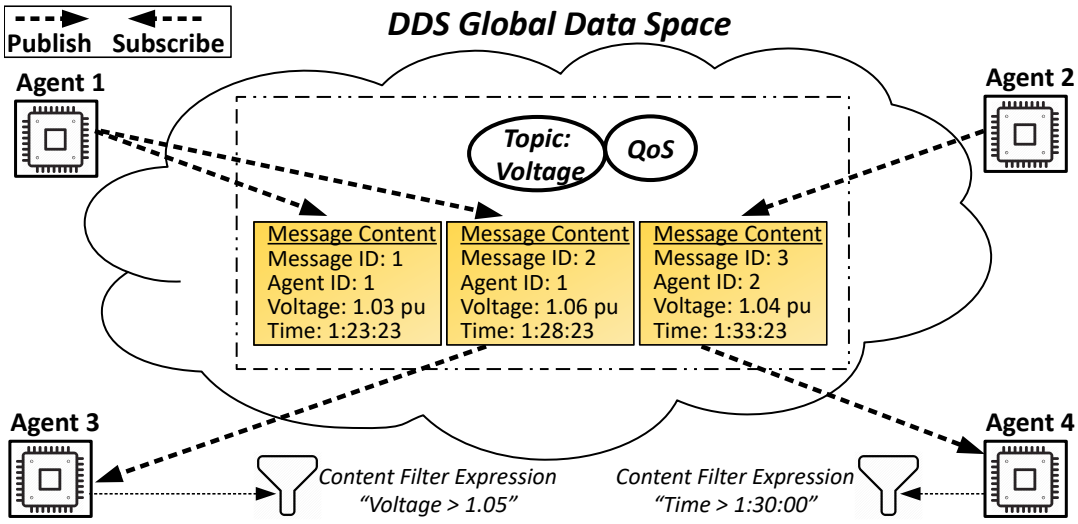

Figure 2.8: The DDS Global Data Space.

the voltage exceeds 1.05 p.u., while similarly, Agent 4 specifies a content filter that only accepts messages when the "Time" field exceeds 1:30:00. Since the GDS has the ability to understand and evaluate the data inside of a message, the GDS can execute content filters automatically, thus relieving Agents 3 and 4 of computational burden at the application level.

2.3.2 Overview of Blockchains

At its core, a blockchain is a decentralized, transaction-based state machine that immutably tracks P2P transactions from different agents and utilizes distributed consensus techniques to ensure that all agents are in agreement with the current system state [44]. All transactions are stored on a ledger that is shared and maintained collectively by all agents within the blockchain network, where transactions are any pieces of data or commands that might alter the current state of the system. Examples of transactions may be a money transfer between agents, or a measurement of a unit of renewable energy from the DG of an agent. All transactions are

collected together into discrete blocks of data that are chained together in chronological order, such that the evolution of system state is transparent to all agents on the network over time.

Figure 2.9 shows a symbolic representation of a general blockchain network, which depicts the process of how transactions are committed to the ledger. Each agent, P, utilizes a computing resource, referred to as a node, N, to interface with the blockchain network. Multiple agents can be assigned to a single node [45], and thus, an agent can be denoted as P_a^p, where a is the index of the agent assigned to the node ID, p. Upon joining the blockchain network, the agent receives a digital wallet that stores its account balance, B_a^p, as well as its public/private keys, $\{SK_a^p, PK_a^p\}$, that are used to sign each transaction to establish the identity of the transaction owner. Transactions are made by the agent by invoking a smart contract, which are software applications that automatically execute agent transactions based on ledger data and an associated set of terms and conditions [46]. Smart contracts are deployed to the blockchain in much the same manner as regular transactions and must be validated by agents on the network. As the smart contracts have access to the shared ledger, they have the ability to enforce the terms and conditions of the contract. An example of a smart contract could be the transfer of ownership of an asset contingent upon the transfer of a sum of money, or the checking of power measurements on the ledger to determine if an agent operated a DG correctly to resolve a voltage violation.

Although the smart contract is used to initiate transactions, before the transaction can be fully committed to the ledger, the transaction must be validated by the agents using a consensus mechanism, where popular consensus mechanisms include proof-of-work (PoW) and practical byzantine fault tolerance (pBFT) [47]. The objective of a consensus mechanism is to ensure that a distributed set of agents are in

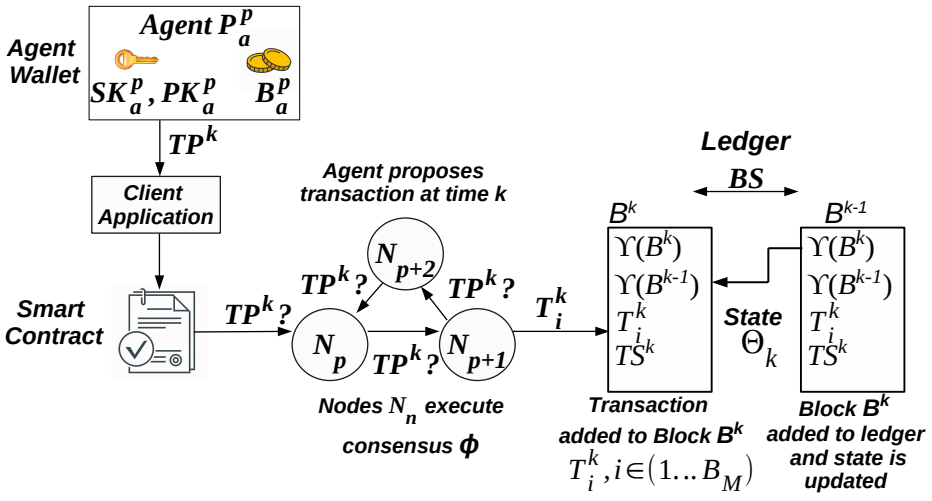

Figure 2.9: A generalized representation of a blockchain network.

agreement with the authenticity and validity of each transaction on the ledger [48]. Consensus mechanisms will be discussed in more detail in the next subsection. As depicted in Figure 2.9, an agent initiates the consensus mechanism, ϕ, at time k by generating a transaction proposal, TP^k. Subsequently, TP^k is forwarded to other nodes that individually verify the validity of the transaction according to rules that are determined within the smart contract. If a minimum of two-thirds of the nodes report that TP^k is indeed valid, it is added to a block of transactions, B^k, which stores the transaction into the block as an ordered set, $T_i^k, i \in (1...B_M)$, where i is the index of the transaction and B_M is the maximum block size. The block also contains a timestamp, TS^k, as well as a block hash, $\Upsilon(B^k)$, that is uniquely composed of all the transactions within the block, and is updated with every new transaction. A new block is created when the block has reached its maximum block size, or, when a certain amount of time has elapsed since the last block was created, referred to as the block speed, BS. The new block is appended to the end of the ledger and pointed at the block hash of the previous block, $\Upsilon(B^{k-1})$, resulting in

ledger data that is transparent and tamper-proof. Thus, the current state of the blockchain, denoted as Θ_k, is a reflection of the transactions of the latest block on the ledger after having been verified by ϕ, as well as the blocks that came before it, and can be formulated as:

$$\Theta_k = \phi(B^k, B^{k-1}, B^{k-2} \ldots B^0) \tag{2.2}$$

2.3.3 Consensus Mechanisms

As mentioned earlier, consensus mechanisms play a vital role in blockchains to verify the authenticity and validity of all transactions between agents. Due to the fact that the ledger is shared amongst all network participants and must reflect a single point of truth, there must be general consensus amongst all agents with respect to the current system state. In general, consensus mechanisms aim to be Byzantine Fault Tolerant (BFT), which refers to the ability for a network of agents to reach consensus even if a number of agents experience communication loss, or intentionally send incorrect responses to other agents during the validation process [49]. To establish BFT, it has been mathematically proven that a minimum of two-thirds of the number of agents must return the *same result* when verifying a block of transactions (or the anticipated result of the execution of a smart contract) [49].

The most popular consensus algorithm in use today is PoW, used in platforms such as Bitcoin and Ethereum [50]. In PoW, all agents are incentivized to participate in the consensus process, where agents leverage computational resources within their node to validate transactions for a monetary reward (often referred to as mining). The validation of an upcoming block of transactions involves solving a cryptographic puzzle that is composed of a unique combination of $\Upsilon(B^k)$ and $\Upsilon(B^{k-1})$, and the first miner to solve the puzzle receives a reward. Once a miner solves the puzzle, it broadcasts the solution to all other miners that verify

its correctness, and the new block is added to the end of the chain. However, PoW relies on brute force methods to solve the puzzle, resulting in significant scalability concerns due to the computational complexity and energy expenditure required by the consensus process [51]. The energy consumed from the PoW consensus process on the Bitcoin network in the year 2017 was equivalent to the annual energy consumption of Ireland, which is in excess of 30 TWh [52].

In contrast, an example of a consensus algorithm that does not use mining techniques is pBFT, which is used by platforms such as Hyperledger Fabric (HLF) [53]. Within pBFT, one agent is designated as a leader, and the other agents are designated as followers. During the validation process, the leader agent broadcasts the block of transactions (or proposed smart contract to be executed) to all other followers, who in turn, validate the transactions. The transactions are successfully confirmed only when more than two-thirds of the agents return an identical confirmation result. Compared to PoW, pBFT is minimally computationally intensive, however, its communication complexity is $O(n^2)$ because every agent must communicate with every other agent during the validation process [54]. As a result, pBFT is ideally suited when there are a limited set of agents within the network.

2.3.4 Permissioned and Permissionless Architecture

Generally, blockchains can be divided into two categories: permissionless (public), or permissioned (private or hybrid) [53]. Permissionless blockchains, such as Bitcoin and Ethereum, are open to the public, and any agent can begin to make transactions after registering on the network. In contrast, permissioned blockchains, such as HLF, require an invitation to join the network. As a result, the identities of the agents within the network can be known. Permissioned blockchains have found success in use cases where there are shared business networks in which agents i)

might have conflicting incentives or ii) do not necessarily trust each other, yet must still conduct transactions for a shared business objective [55]. Since an invitation is required to participate in a permissioned blockchain, the consensus algorithm does not require all agents to participate in the consensus process, thereby alleviating the concerns about excessive energy use associated with permissionless blockchains [56].

2.4 Literature Survey and Identification of Research Gaps

2.4.1 Prior Use of DDS in SDG Applications

The utilization of DDS within SDG applications is a fresh research stream, with the earliest publications starting in 2013 and continuing to present day. In [57], DDS is proposed as the middleware framework to handle message passing for the application of substation automation in a manner compliant with the IEC 61850 interoperability standard. Case studies highlight the speed and reliability of DDS, with a throughput of 2 million messages per second at 100% reliability for message sizes less than 256 bytes. The authors in [58] utilize DDS to test the feasibility of information exchanges between DSOs and metering devices, with several case studies exploring the effect of different QoS profiles on latency and jitter. It is found that the effect of the reliability QoS on message latency increases the overall latency from 15 milliseconds (ms) to 20 ms within a network comprising of 6 publishers and 6 subscribers, which is an increase of 33%. Nevertheless, even at 20 ms, DDS still provides acceptable message latency for SDG applications, which require an overall latency between 15-200 milliseconds [24].

DDS has also been utilized as the communication middleware of choice within SDG control strategies, which include the real-time control of microgrids. In [57], the authors develop a control strategy to facilitate the synchronized islanding/re-

connection of multiple microgrids, where DDS is used by multiple distributed applications to share data for forecasting, visualization, pricing signals, and DER status. The work in [59] proposes a fuzzy logic-based energy management framework to optimize the energy consumption of small microgrids, where DDS is used to disseminate information to simulated loads, meters, and forecasting systems. The same authors develop a DDS-based hardware-in-the-loop (HIL) testbed for a variety of SDG applications, such as generator synchronization, load balancing, and network topology reconfiguration [60]. In [61], a hierarchical microgrid control strategy is developed with agents defined at the utility, microgrid, and DER level. Benchmarking of DDS within this work reveals that DDS is capable of providing point to point message latencies of 0.3 ms at 1000 messages/second with a message size of 32 bytes. The authors in [62] propose a DDS-based protection scheme to island microgrids when they experience a cyber-attack. Furthermore, the work in [63] utilizes DDS to manage data flow in a demand response market for microgrids.

Although the aforementioned works have made strong contributions in exploring the usage of DDS within smart grid applications, improvements can be made in the following aspects. First, the scalability of inter-agent DDS messaging has not been appropriately evaluated. The work in [57–59, 61, 64] benchmarks the transmission latency of DDS messages on a single computer, and without a physical router, which does not adequately reflect the entire agent communication process that occurs between multiple agents on multiple platforms. Second, the aforementioned work does not discuss how the QoS profiles of DDS can be tailored to mitigate the issue of agents acting on outdated messages that are improperly ordered when agents experience frequent connection failures [65]. The issue of improper and outdated messaging is common in distributed systems, where message brokers are not aware that a message is outdated, and pass the burden of checking for outdated messages

to the agents themselves. This leads to unnecessary computational burden for the agent, and also introduces the risk of misaligned execution for a distributed control strategy. Third, the previous works do not enforce the compliance of DDS with FIPA standards, which would prevent their positive uptake in real-world applications [66]. Interoperability and plug and play operation is a vital pillar of SDGs, and it is important to conform to accepted standards that would ease future integration efforts [67] These shortcomings will be addressed in Chapter 3, which will introduces the development of a distributed communication framework based on DDS that is FIPA-compliant, and automatically discards outdated messages while executing control strategies. The proposed framework is also benchmarked on multiple microcontrollers to determine its scalability as a function of its message latency and size.

2.4.2 Prior Use of Blockchains in SDG Applications

Blockchains have recently been applied to SDG applications within the context of TES, including EV charging management, microgrid energy management, and peer to peer (P2P) energy trading. In [68], an optimal EV charging schedule is developed to minimize power mismatches of an SDG, where the charging schedule of all EV owners is recorded on the ledger, and a smart contract is used to establish pricing initiatives to incentivize EV owners to change their schedule to flatten the overall load demand. The work in [69] develops a smart contract to enable bi-directional EVs to provide ancillary services to the DSO, where the smart contract autonomously levies penalties on EVs that disconnect while providing the service. The smart contract also stores the user preferences of EV owners on the ledger. Furthermore, in [70, 71], the authors propose a blockchain-based TES that utilizes contract theory to model the preference of EV owners to prioritize energy trading

with solar energy aggregators, where smart contracts are used to audit all energy transactions.

Within the field of microgrid energy management, the work in [72] aggregates DGs and a variety of flexible loads to build an optimal, day-ahead dispatch schedule for a microgrid. The smart contract is used to resolve the distributed marginal locational price for each agent using the Alternating Direction Method of Multipliers (ADMM) method, while also rendering all payments to agents in a secure fashion. Furthermore, the authors in [73] implement a multi-microgrid trading platform, where the smart contract is used to execute a double auction to set the price of electricity using the Vickrey second price auction method. The authors in [74] develop a multi-objective demand response system that calculates dynamic pricing for consumers based on their preferences for allowable emissions, where the blockchain ledger is used as a single point of truth for energy auditing. It is found that the proposed system increases the profitability of the agents by 1.68%, while reducing GHG emissions by 0.97%.

There has also been a great deal of work on evaluating the financial feasibility of blockchain-based energy trading systems [75–78]. In [75], a system is proposed to facilitate trades between homeowners and a community BESS, which leads to monthly savings of $75.92, or 44.2%. The work in [76] develops a game-theory based system to enable homeowners to form coalitions and negotiate electricity rates that lead to monthly savings of $378.2 across 300 homeowners. The authors in [76] implement a smart contract, based on non-cooperative game theory, to generate daily savings of 24 Chinese Yen (CNY) across 6 households equipped with PV and interruptible loads. The work in [77] develops an energy trading algorithm that minimizes the number of transactions on the ledger to reduce communication overhead.

Again, while the aforementioned work has greatly enhanced the state-of-the-art, there are several factors that can be improved. To begin with, although the works in [69–71] model bidding preferences for EV owners, they do not explicitly model any strategies for BESSs or flexible loads, such as STs. Thus, the results derived from these works do not accurately represent the complete range of DERs that would be able to participate in an energy trading system [79]. Second, the aforementioned works in [75–78] do not discuss the financial impact of their proposed systems on the presiding DSO, which leaves the financial analysis incomplete. Third, with the exception of [69], there is a lack of discussion that relates to enforcing contract-based penalties on those agents that do not fulfill the terms and conditions of their contract. Fourth, none of the aforementioned works conduct any practical benchmarking of their proposed blockchain-based systems, even though concerns of scalability are a major barrier to adoption for blockchains [44]. Last, but certainly not least, the aforementioned work does not deploy their proposed systems within real-world settings, where lessons learned on practical implementation can be derived.

The aforementioned shortcomings will be addressed by this thesis in Chapters 4 and 5, where blockchain-based systems are proposed within the applications of voltage regulation and P2P energy trading. Chapter 4 will introduce a blockchain-based TES that will enable enforcement penalties for voltage regulation services provided by agents, while Chapter 5 will introduce a RETS, which will include the design of novel bidding strategies for BESSs, EVs, and STs, as well as a techno-economic evaluation of the proposed system in terms of its scalability, financial savings to the DSO, and real-world deployment at the KCM.

Chapter 3 - A Distributed Communication Framework For Multi-Agent SDGs Based on Data Distribution Service

With the background of IoT and message-oriented middleware established in Chapter 2, this chapter introduces the design of the proposed DCF that is built upon DDS middleware. The chapter begins with a brief recap of the problem description that the proposed DCF is designed to address, which is to provide a fully distributed MTS that is capable of preventing agents from acting on outdated messages. Subsequently, details of the architectural design of the DCF are discussed, including the SIL platform that is implemented to validate the proposed DCF. Following this, a subsection is dedicated to illustrate how the DCF can be applied to the SDG application of distributed voltage regulation within SDGs, where the necessary background of the AWC control strategy is also provided. Next, results from simulated and real-world experiments are provided to validate the efficacy of the proposed DCF, after which, the chapter is concluded with a discussion that summarizes the major outcomes of this work.

3.1 Problem Description and Hypothesis

As mentioned previously, the emphasis of previous works within MAS SDG applications have focused on the formulation of the control strategy, while the underlying communication framework has often been neglected [15]. Specifically, the issue of outdated and improperly ordered messages being sent to agents when they reconnect to a network is not discussed. This issue is significant because it results in the misaligned execution of agents participating in a control strategy [80]. Furthermore, much of the previous work employs the popular JADE platform as the communication framework [16, 17, 81–83]. However, JADE utilizes a singular, centralized MTS to facilitate inter-agent communication, which is not robust since it exposes a single point of failure [37]. Hence, the hypothesis that governs this chapter is that DDS middleware can be utilized to provide a robust, distributed messaging system that can be customized further to enhance the efficacy of distributed control strategies.

As such, this chapter proposes a novel DCF for MAS in SDG applications that is built on top of DDS middleware. The DCF is implemented as a *fully distributed* entity that provides robust message transmission since it is not vulnerable to a single point of failure. Further, the DCF is designed with QoS profiles that automatically discard outdated messages, thereby preventing agents from taking incorrect decisions that could result in the misaligned execution of their control strategy. The DCF is also designed to be compliant with FIPA standards, thereby reducing the integration effort required from developers of distributed control strategies that also follow FIPA standards [66].

3.2 Design of the Proposed DCF

3.2.1 DCF Architecture

The proposed architecture of the DCF is designed to leverage the strengths of DDS while also including all of the essential components of MAS communication architecture as specified by FIPA. As discussed in Chapter 2, these components include an AMS, a DF, as well an MTS. The AMS is used for registering the identities of all agents within a network, while the DF is used for registering a list of services that agents provide. The MTS is responsible for facilitating all messages between agents. To mitigate the vulnerability of using a centralized MTS implementation, as observed in JADE, the architecture of the proposed DCF is designed using a distributed approach. The AMS, DF, and MTS are all moved into the distributed GDS that is shared by all DCF agents, and mapped to separate topics that the agents subscribe to. Accordingly, the three main topics defined in the GDS are *Services*, *AgentID*, and *MsgBus*, which are mapped to the DF, AMS, and MTS, respectively, and are shown in Figure 3.1.

The *Services* topic allows an abstract definition of services to be defined for each agent, where in the context of SDG applications, services may comprise of ancillary services such as voltage regulation and demand response. The *AgentID* topic provides a lookup table of agent identities, which are indexed by the specific subsystem, or spatial zone of operation that they govern. The *MsgBus* topic is used by all agents to exchange messages in real-time. Figure 3.1 shows the underlying data structure of the *MsgBus* topic, which conforms to the agent communication language (ACL) specifications as per FIPA, where the sending (*Sender_Agent_ID*) and receiving (*Receiver_Agent_ID*) IDs of the agents, as well as the performative and content of the message are explicitly defined.

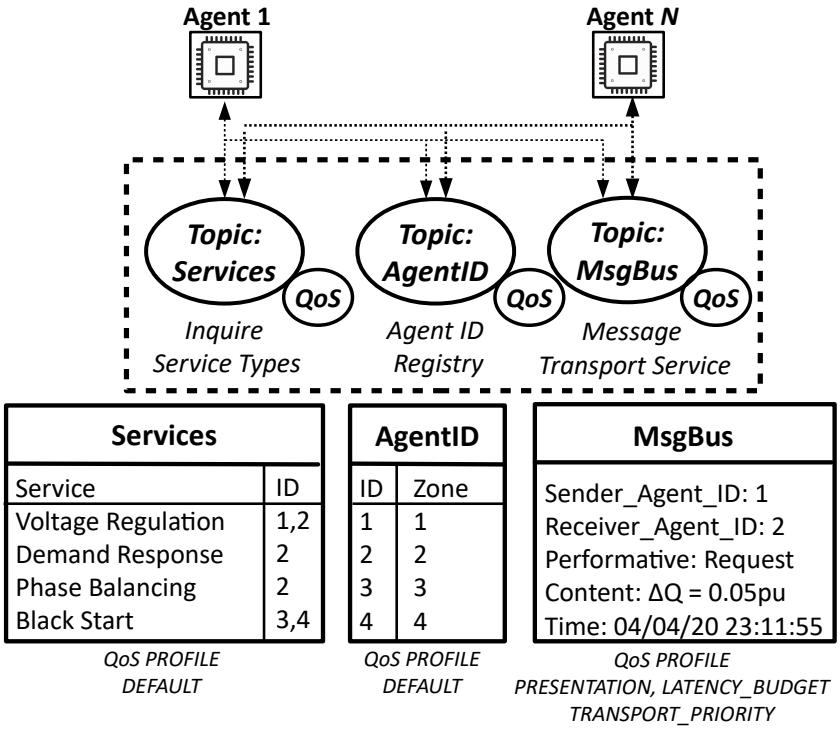

Figure 3.1: Depiction of the topics and underlying data structures of the DCF architecture.

The *MsgBus* topic is also configured with three unique QoS profiles. The TRANSPORT_PRIORITY profile prioritizes the delivery of messages within the *MsgBus* topic over all other topics, while the LATENCY_BUDGET defines the maximum allowable latency for each message associated with the *MsgBus* topic. The PRESENTATION profile ensures that messages are received by an agent in the exact order they were sent, thus preventing agents from acting on misrepresented data.

The mapping of FIPA-specified components to topics in the DCF has four major advantages. First, since the GDS is inherently distributed, the *MsgBus* topic does not expose a single point of failure for agent communication, unlike JADE. Second, by abstracting the *Services* and *AgentID* topics away from the *MsgBus* topic, agents

can receive the latest updates to agent IDs and services by subscribing to these topics, thus leaving the *MsgBus* topic to facilitate high-priority messages when executing distributed control strategies. Third, to route messages correctly and efficiently, the DCF specifies content filters on the *Receiver_Agent_ID* field and the *Time* field within the *MsgBus*. These content filters enable the *MsgBus* to automatically filter out messages that are not intended for the correct agent, as well as messages that exceed a configurable period of time and are outdated. Fourth, the unique QoS configuration of the *MsgBus* topic with the PRESENTATION profile enables agents to receive messages in order, which prevents the misaligned execution of distributed control strategies.

A potential security concern with the *MsgBus* topic may be realized if a malicious agent sends fraudulent messages by incorrectly specifying the *Sender_Agent_ID* field within a message, or eavesdrops on unauthorized messages by specifying an incorrect *Receiver_Agent_ID* field. To mitigate this, the DCF sets access control privileges for each field inside the *MsgBus* topic by specifying read/write access levels for all agents. The DCF architecture imposes read-only access to the *Receiver_Agent_ID* field when establishing a subscription to the *MsgBus* topic, and similarly imposes read-only access for the *Sender_Agent_ID* field when publishing to the *MsgBus* topic. The DCF presets the correct ID for the agent as soon as the agent joins the network, and as such, agents using the *MsgBus* topic can only access messages they are authorized to access.

3.2.2 Messaging Workflow of DCF Agents

An example of the messaging workflow of agents using the DCF is given in Figure 3.2. When launched, all agents must initialize their settings by establishing publish/subscribe access to the mandatory DCF topics, which are *Services*, *AgentID*,

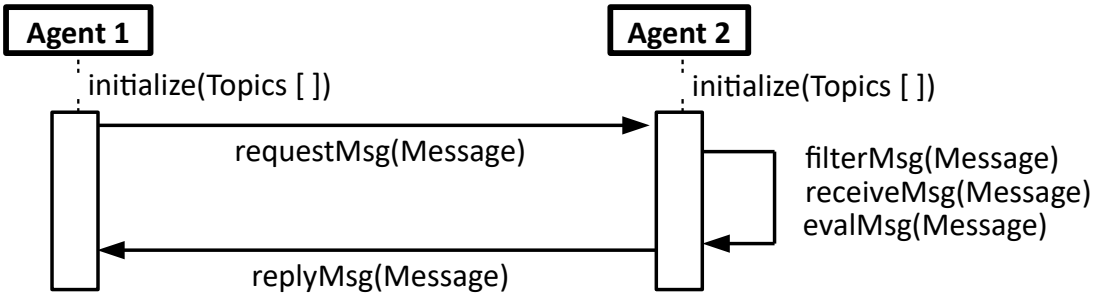

Figure 3.2: Typical agent workflow for message exchange.

and *MsgBus*. Agents may then engage in request/response messaging as shown in Figure 3.2, where the format of the message would be identical to the data structure of the MsgBus depicted in Figure 3.1. Namely, Agent 1 would send a request message to Agent 2 by specifying the *Sender_Agent_ID* field as *1*, the *Receiver_Agent_ID* field as *2*. the *Performative* field as *Request*, the *Content* field with the appropriate content, and the *Time* field with the current timestamp. The DCF would filter the message for Agent 2 by the *Receiver_Agent_ID* field, and send the message to Agent 2, which would send back an appropriate message response depending on the control strategy that is being executed.

3.2.3 Proposed SIL Platform for DCF Implementation

To validate the ability of the DCF to execute distributed control strategies for SDG applications, a SIL platform is developed. The SIL platform is composed of networked real-time microcontrollers that host multiple agents, all of which use the *MsgBus* topic to exchange messages. The mathematical system model of any power system can be inserted directly into the simulation loop as a special agent, referred to as the model agent, as seen in the block diagram in Figure 3.3.

The model agent begins the simulation process by generating a state vector that represents the power system state at a discrete time step k, denoted as $X(k)$. The

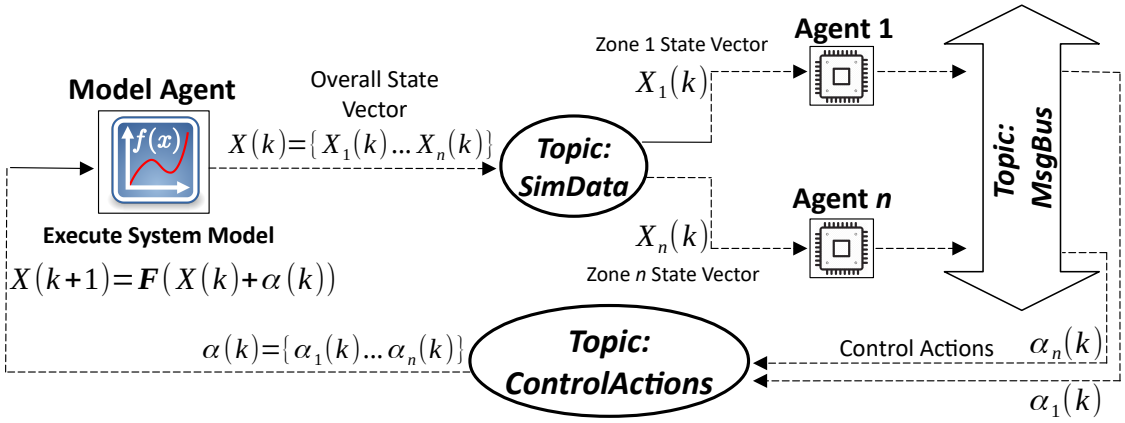

Figure 3.3: Block diagram of the proposed SIL platform.

state vector is published to the *SimData* topic, which each agent is subscribed to, and each agent content-filters a subset of the overall state vector that pertains to their zone of operation, which is denoted as $X(k) = \{X_1(k)...X_n(k)\}$. The agents then use the *MsgBus* to exchange messages and coordinate their control actions according to a specified control strategy, where the control actions are represented by $\alpha(k) = \{\alpha_1(k)...\alpha_n(k)\}$. The finalized control actions are then published to the *ControlActions* topic, which is subscribed to by the model agent. The model agent gathers all control actions, updates the overall state vector, and executes the system model to generate a new state vector at time $k+1$. The process repeats at the next time step, and is represented as follows

$$X(k+1) = \boldsymbol{F}(X(k) + \alpha(k)) \tag{3.1}$$

where $\boldsymbol{F}$ is a symbolic function for the system model. In this chapter, the system model will be representative of a physical SDG, and agents will utilize the *MsgBus* to exchange messages in accordance with the distributed AWC control strategy for the application of distributed voltage regulation.

3.2.4 Application of DCF in Improving Distributed Control Strategies

Many conventional distributed control strategies, such as the AWC strategy utilized in this work, define two assumptions that limit their efficacy [84]. First, it is assumed that the agents have prior and continuous knowledge of the physical network address of each agent, such that messages can be directed to the intended agent correctly. Second, it is assumed that the agents receive messages exactly in the order that they were sent. These assumptions are unrealistic because they imply that the agents remain connected to the network at all times. Yet, agents frequently disconnect and rejoin the network when communicating over unreliable physical interfaces, and upon rejoining the network, they are assigned to new network addresses, and begin receiving an influx of messages that are out of order and may be outdated [80].

The design of the DCF removes the need for these assumptions. First, agents do not need to know the physical address of other agents because they exchange messages by explicitly defining the *Receiver_Agent_ID* within the message via the *MsgBus* topic, and content filters are utilized to ensure that the message is routed to the correct agent. All agents are also subscribed to the *Services* and *AgentID* topics within the DCF, and are instantaneously updated if there are changes to an agent ID, which obviates the need for agents to poll for the latest physical network addresses. Second, the QoS profile of PRESENTATION for the *MsgBus* topic ensures that messages are received by the agent in the exact order in which they were sent. Third, a content filter is placed on the *Time* field of the *MsgBus* topic, and thus, the DCF is able to filter out any outdated messages based on a reference point of time, thus ensuring that agents do not act on outdated messages.

As such, the DCF enables the execution of distributed control strategies to support scenarios where some agents may frequently disconnect and rejoin a network,

but will still be able to execute the control strategy in alignment with the rest of the agents, which increases its robustness. An example of this scenario will be presented in the experimental results in Chapter 3.4.3.

3.3 The Application of DCF Within Distributed Voltage Regulation

This section seeks to illustrate how the DCF can be utilized within the SDG application of distributed voltage regulation. Within this application, agents formulate the application as a Distributed Constraint Satisfaction Problem (DisCSP), and utilize the DCF to execute the distributed AWC control strategy to resolve all voltage violations in a cooperative manner. An illustration of this can be seen in a multi-layered, cyber-physical representation of an SDG in Figure 3.4, where Layer 1 depicts the physical infrastructure of the SDG clustered into virtual zones of operation, Layer 2 depicts how agents formulate the DisCSP, and Layer 3 shows how agents execute the AWC control strategy to regulate the voltage of each zone, where the message exchange is handled by the *MsgBus* of the DCF.

3.3.1 Layer 1: Modeling and Virtual Zoning of ADNs

In Figure 3.4, two types of DERs are connected to the SDG feeder, which are renewable DGs, and BESSs. BESSs are assumed to be capable of operating in the four quadrants, i.e., being able to modulate their active and reactive power output, while renewable DGs are assumed to operate at the maximum power point tracking setting [85]. In general, at timestep t, the active and reactive power flow in branch i, and the voltage at bus i, can be represented with respect to bus j as follows [85]:

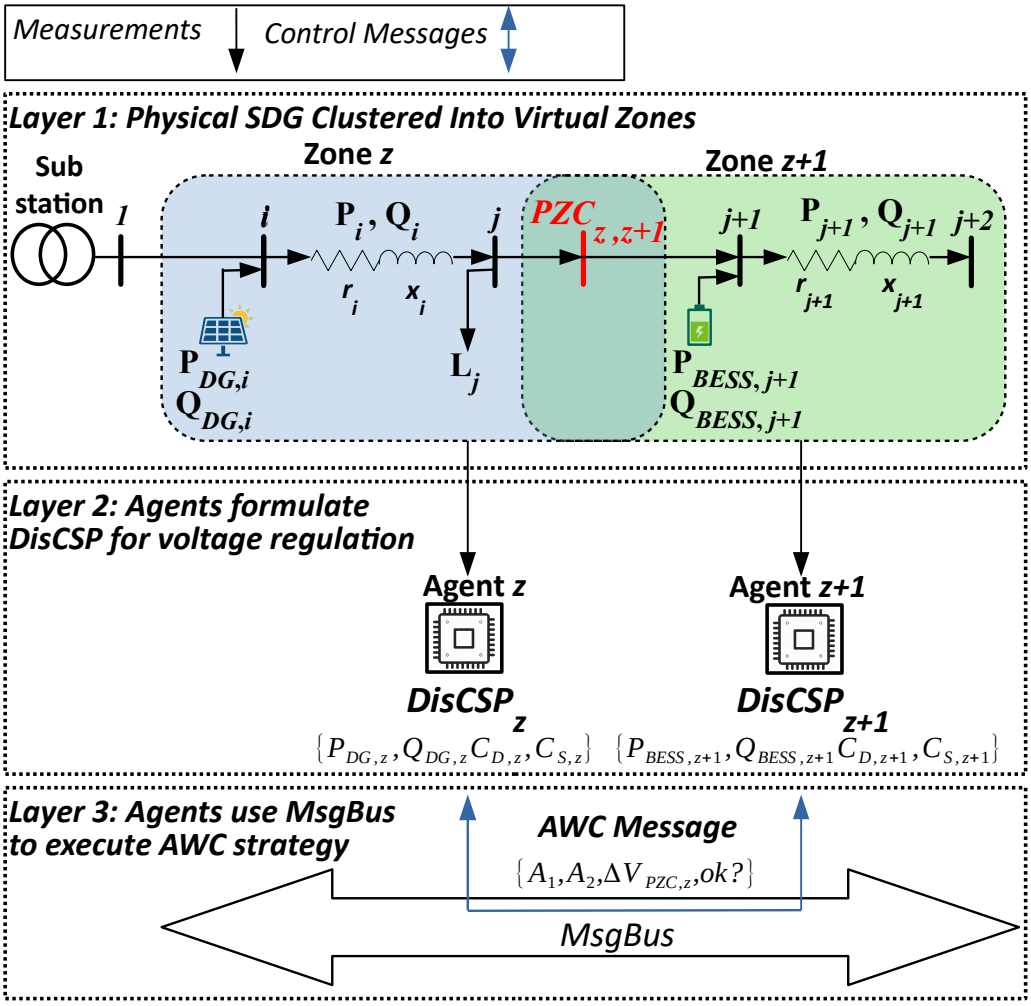

Figure 3.4: Cyber-physical example depicting DCF agents resolving voltage violations using the AWC.

$$P_i(t) = P_j(t) + \sum_{n=i}^{n=j-1} \left(P_{L,n}(t) - P_{BESS,n}(t) - P_{DG,n}(t) \right) \tag{3.2}$$

$$Q_i(t) = Q_j(t) + \sum_{n=i}^{n=j-1} \left(Q_{L,n}(t) - Q_{BESS,n}(t) - Q_{DG,n}(t) \right) \tag{3.3}$$

$$V_i^2(t) = V_j^2(t) - 2\sum_{n=i}^{n=j-1}\left(r_n P_n(t) + x_n Q_n(t)\right) \tag{3.4}$$

where n is the branch iterator, $\{Pn, Qn\}$ are the output active/reactive powers, $\{P_{L,n}, Q_{L,n}\}$ are the active/reactive loads,$\{P_{BESS,n}, Q_{BESS,n}\}$ are the injected active/reactive powers from the BESS, $\{P_{DG,n}, Q_{DG,n}\}$ are the injected active/reactive powers from the DG, V_i is the voltage at each bus, and $\{r_n, x_n\}$ is the resistance/reactance of each feeder. It can be observed from (3.2)-(3.4) that the voltage profile across the feeder depends on the change of the branches' active and reactive power flow along the feeder, which may cause voltage violations due to the intermittent changes of DGs. Simplifying (3.4) by linearization and neglecting the change in load demand during these events, the change in voltage can be expressed as:

$$\Delta V_i(t) = \frac{1}{V_i(t-1)}\left[V_1(t-1)\Delta V_1(t) + \Delta P_{DG,i}(t)\sum_{n=i}^{i-1} r_n + \Delta Q_{DG,i}(t)\sum_{n=i}^{i-1} x_n\right] \tag{3.5}$$

Since the voltage at the substation,V_1, is typically held steady [86], ΔV_1 can be set to zero, resulting in:

$$\Delta V_i(t) = \Delta P_{DG,i}(t)\frac{\sum_{n=i}^{i-1} r_n}{V_i(t-1)} + \Delta Q_{DG,i}(t)\frac{\sum_{n=i}^{i-1} x_n}{V_i(t-1)} \tag{3.6}$$

Hence, the sensitivity at each bus due to active/reactive power injections can be calculated as follows:

$$SP_i = \frac{\partial V_i}{\partial P_i} = \frac{\sum_{n=i}^{i-1} r_n}{V_i(t-1)}, SQ_i = \frac{\partial V_i}{\partial Q_i} = \frac{\sum_{n=i}^{i-1} x_n}{V_i(t-1)} \tag{3.7}$$

A BESS deployed to a bus within the feeder can be used dynamically to regulate the voltage via active/reactive power modulation. Thus, any change in the power output of a BESS located at bus j will impose a change upon node i voltage as

follows:

$$\Delta V_i(t) = \frac{1}{V_i(t-1)}\left[V_j(t-1)\Delta V_j(t) + \Delta P_{BESS,i}(t)\sum_{n=i}^{i-1} r_n + \Delta Q_{BESS,i}(t)\sum_{n=i}^{i-1} x_n\right] \tag{3.8}$$

The physical SDG can then be clustered into z zones of operation and assigned to an agent that uses the control actions of the BESS and/or DG of its zone to regulate the zonal voltage. Each zone shares a bus with its adjacent zone, which is referred to as the point of zone coupling (PZC). Thus, the agents are jointly responsible for regulating the voltage at the PZC (V_{PZC}), and must communicate with each other when executing control actions that may affect V_{PZC}. However, the control actions are subject to certain constraints, which will be exemplified in the next subsection that discusses the DisCSP.

3.3.2 Formulation of Distributed Voltage Regulation as a DisCSP

The formulation of a DisCSP involves a set of agents that execute control actions to arrive at a state where all system constraints are satisfied [84]. In this work, the agents seek to adjust the control agents of their BESS/DG units to regulate the voltage of their zone, subject to constraints of device ratings and feeder capacity. If the constraints do not permit the local mitigation of a voltage violation, the agent may exchange messages with neighboring agents, who, in turn, adjust the control actions of their BESS/DG units to help mitigate the violation. The application of distributed voltage regulation as a DisCSP can be formulated as follows:

$$DisCSP_z = \boldsymbol{F}(\Delta P_{BESS,z}, \Delta Q_{BESS,z}, \Delta P_{DG,z}, C_{D,z}, C_{S,z}) \tag{3.9}$$

where $\{\Delta P_{BESS,z}, \Delta Q_{BESS,z}, \Delta P_{DG,z}\}$ represent the control actions available to each agent in zone z when resolving a voltage violation, which are constrained

by both device constraints, $C_{D,z}$, as well as system constraints, $C_{S,z}$. The limits of these constraints form a domain from which the control actions can be determined. The device constraints include the manufacturer's limits for the range of operation for the BESS capacity, state of charge (SoC), the maximum apparent inverter capacity, as well as the minimum power factor, as shown below.

$$C_{D,z} = \begin{cases} P^{Pre}_{BESS,z}(t+1)\Delta t \leq B^{cap}_{BESS,z} \\ SoC^{min}_{BESS,z} \leq SoC_{BESS,z}(t) \leq SoC^{min}_{BESS,z} \\ \sqrt{P^2_{BESS,z}(t+1) + Q^2_{BESS,z}(t+1)} \leq S^{cap}_{BESS,z} \\ PF_{BESS,z}(t) \leq PF_{min} \end{cases} \tag{3.10}$$

where $P^{Pre}_{BESS,z}$ is the predicted active power at the next timestep, $B^{cap}_{BESS,z}$ is the BESS capacity in kWh, $SoC^{min}_{BESS,z}$, $SoC^{max}_{BESS,z}$, $SoC_{BESS,z}$ are the minimum, maximum, and current SoC of the BESS, $S^{cap}_{BESS,z}$ is the BESS inverter capacity in MVA, and PF_{min} is the minimum power factor. On the other hand, the system constraints describe the limits of the voltage at every bus within the zone as well as the current flowing through the zonal feeder.

$$C_{S,z} = \begin{cases} I_i \leq I^{cap}_{f,z} & \forall\ i \in F^z \\ V_{lb} \leq V_{i,z} \leq V_{ub} & \forall\ i \in N^z \end{cases} \tag{3.11}$$

where $I^{cap}_{f,z}$ is the carrying capacity of a zonal feeder, F^z is the set of all feeders within zone z, $\{V_{lb}, V_{ub}\}$ are the lower and upper voltage limits for $V_{i,z}$, and N^z is the set of all nodes within zone z. Note that $V_{i,z}$ includes the PZC, which is a common constraint to adjacent zones and requires message exchanges between agents to ensure that any control action does not violate PZC constraints.

3.3.3 Solution of DisCSP: Asynchronous Weak Commitment

The AWC is a distributed control strategy to solve DisCSPs [84]. As shown in Figure 3.5, every agent executing the AWC maintains a local agent-view that stores requests from other agents, where the agents must evaluate the requests against local constraints before determining a control action. Thus, there are five main message types within the AWC paradigm, which include: i) an *ok?* message that represents an agent's request to another agent, ii) a *good* message that a responding agent sends when the *ok?* request satisfies all constraints, iii) a *no-good* message that is the opposite of a *good* message, iv) an *execute* message that a requesting agent sends to confirm execution of a control action, and v) an *executed* message that a responding agent sends when the control action is executed. Since all agents operate concurrently, it is possible that they may encounter two separate agent requests at the same timestep. To avoid deadlock, the agent prioritizes the agent request that violates the least number of constraints, which is referred to as the *min-conflict heuristic* [84]. Thus, mapping the AWC technique to the proposed application, an agent that detects a voltage violation initiates a DisCSP by specifying the change in voltage needed at its PZC, $V_{PZC,z}$, and encoding it within an *ok?* message to its neighbors. The neighboring agents evaluate the message and determine if it violates any device or system constraints, and send back an appropriate *good* or *no-good* message. If an agent has more than one request in its agent-view, as shown in Figure 3.5, it uses the min-conflict heuristic to prioritize the violation with the highest $V_{PZC,z}$. If a *good* message is sent back, a subsequent *execute* message will actuate the agent's BESS/DG units to resolve the voltage violation.

It is worth noting that all message exchanges for the AWC are facilitated by

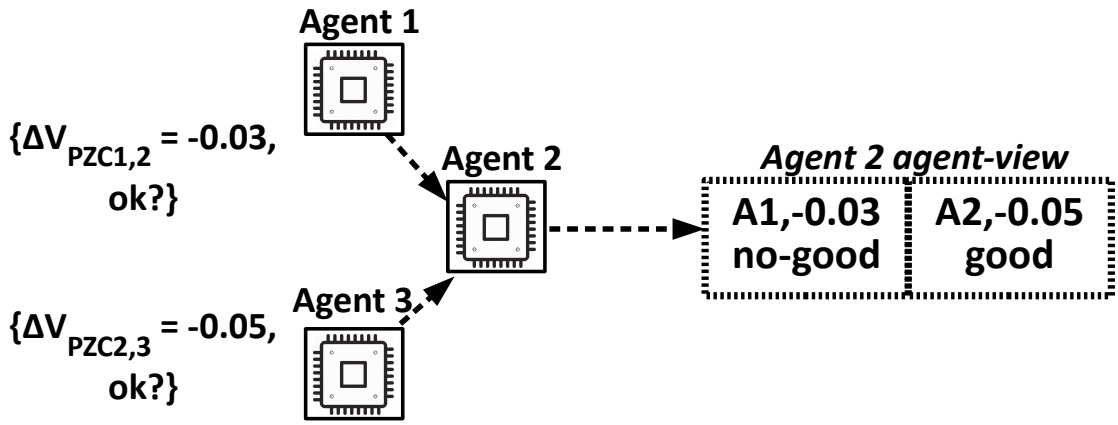

Figure 3.5: Message exchange during AWC and an agent's agent-view.

the *MsgBus*. A generic message format can be formulated as follows

$$\{A_{ID}^{FROM}, A_{ID}^{TO}, \Delta V_{PZC,z}, timeRef, msg\} \tag{3.12}$$

where A_{ID}^{FROM}, A_{ID}^{TO} represent the sending and receiving IDs for the agents, respectively, $timeRef$ is a time reference, and msg is the message type (*ok?,good,etc.*). The $timeRef$ parameter is analogous to the $Time$ field as discussed in Section 3.2.1, and is crucial in ensuring that the *MsgBus* can filter out any outdated messages based on the reference point of time to prevent misaligned execution of the AWC. With this in mind, the remainder of the subsection will formally discuss the AWC implementation:

First: Each agent performs state estimation for its zone to determine the zonal voltage profile. Further discussion of the state estimation techniques are outside the scope of the thesis, but can be found in [87]. The determination of the change in voltage needed to mitigate a voltage violation at bus i in zone z can be expressed as

$$\Delta V_{z,i} = \begin{cases} max(V_{z,i}(t) - V_{ub}), & \forall\, i \in N^z \,\&\, V_i > V_{ub} \\ min(V_{z,i}(t) - V_{lb}), & \forall\, i \in N^z \,\&\, V_i < V_{lb} \\ 0, & \forall\, i \in N^z \,\&\, V_{ub} \geq V_i \geq V_{lb} \end{cases} \tag{3.13}$$

Second: The agent predicts the magnitude of the voltage at the violated bus ($V_{z,i}^{pre}$) at the next timestep, determines a target for the required voltage adjustment needed ($\Delta V_{z,i}(t+1)$), and defines a tolerance for the target voltage deviation (ϵ) to account for any estimation error as follows:

$$V_{z,i}^{pre} = V_{z,i}(t) + \Big(V_{z,i}(t) - V_{z,i}(t-1)\Big) \tag{3.14}$$

$$\Delta V_{z,i}(t+1) = \begin{cases} max(V_{z,i}^{pre}(t+1) - V_{ub}) - \epsilon, & \forall\, i \in N^z \,\&\, V_i > V_{ub} \\ min(V_{z,i}^{pre}(t+1) - V_{lb}) + \epsilon, & \forall\, i \in N^z \,\&\, V_i < V_{lb} \end{cases} \tag{3.15}$$

Third: The agent calculates the assignment for its local control actions of $\Delta P_{BESS,z}$ and $\Delta Q_{BESS,z}$, considering the constraints given in (3.10)-(3.11) and the predicted active and reactive powers ($P_{BESS,z}^{Pre}$) and ($Q_{BESS,z}^{Pre}$) in the next step, respectively, as follows [86]:

$$\Delta Q_{BESS,z}(t+1) = \Big((P_{BESS,z}^{pre}(t+1) + \Delta P_{BESS,z,j}(t+1)) \times tan(cos^{-1}(PF_{min}))\Big) - Q_{BESS,z}^{pre}(t+1) \tag{3.16}$$

Fourth, If the local control action assignment violates any constraints, it can request assistance from neighboring agents. The violated agent calculates the required change in voltage at its PZC ($V_{PZC,z}$) with the neighboring agents that will resolve

the voltage violation [88]:

$$V_{PZC,z}^{limit}(t{+}1) = V_{PZC,z}^{pre}(t{+}1) + \Delta V_{PZC,z}(t) \tag{3.17}$$

$$\Delta V_{PZC,z}(t) = \begin{cases} \frac{\partial V_{PZC,z}}{\partial V_{z,i}}\Big(V_{ub} - V_{z,i}^{pre}(t{+}1)\Big) - \epsilon, \forall\, V_{z,i} > V_{ub} \\ \frac{\partial V_{PZC,z}}{\partial V_{z,i}}\Big(V_{z,i}^{pre}(t{+}1) - V_{lb}\Big) + \epsilon, \forall\, V_{z,i} < V_{lb} \end{cases} \tag{3.18}$$

Subsequently, the violated agent sends its neighboring agent an *ok?* message that specifies the $\Delta V_{PZC,z}$ required to maintain the PZC voltage as a common constraint. Any agent request that cannot be satisfied by the neighboring agent will be passed on to *its* neighboring agent, based on the current voltage at their PZC.

Fifth, if the violated agent receives a *no-good* message from the neighboring agents, its last resort is to curtail the power from the DGs in its own zone, as follows:

$$\Delta P_{DG,z}(t+1) = \begin{cases} \frac{\partial P_{i,z}}{\partial V_{z,i}}\Big(V_{ub} - V_{z,i}^{pre}(t{+}1)\Big) \forall\, i \in N^z \& V_{z,i} > V_{ub} \\ \frac{\partial P_{i,z}}{\partial V_{z,i}}\Big(V_{z,i}^{pre}(t{+}1) - (V_{lb})\Big) \forall\, i \in N^z \& V_{z,i} < V_{lb} \end{cases} \tag{3.19}$$

Thus, the execution of the AWC control strategy is completed when all agents have processed all requests in their agent-view in accordance to all constraints, meaning that all voltage violations have been resolved.

3.4 Experimental Results

This section presents the results of three experiments that evaluate the efficacy of the proposed DCF and its implementation as a SIL platform, including i) benchmarking the SIL platform in terms of average message latency against the recommended latency requirements of SDG [24], ii) prototyping the modified AWC strategy on a 39 bus test feeder and validating its performance on the SIL platform, and iii) deployment of the DCF at a Canadian microgrid to mitigate overvoltage

violations. The results are prefaced by a description of the experimental equipment used to conduct the experiments.

3.4.1 Experimental Equipment

The simulated experiments are conducted using the SIL platform described in Chapter 3.2.3. The agents are implemented in the LabVIEW programming environment, which are subsequently deployed on four National Instruments myRIO-1900 Linux-based real-time microcontrollers with a processing speed of 667 MHz and 256 MB RAM. The model agent utilizes a desktop computer that hosts the Windows 10 operating system, with an i7-2.60 GHz processor and 8 GB RAM, and executes the mathematical model of the SDG in the MATLAB environment. The SIL platform retains connectivity with the agents by way of a 2.4 GHz wireless-N router (WiFi). The first experiment involves the benchmarking of the DCF and a comparison with other IoT middlewares, such as AMQP and MQTT, where the *MsgBus* topic is implemented on AMQP and MQTT as well. However, since the myRIO microcontrollers do not support the native client libraries of AMQP and MQTT, the benchmarking of these middlewares is conducted on the desktop machine instead. The DCF is benchmarked on both the myRIO microcontrollers, as well as the desktop machines. Table 3.2 provides the software versions and libraries used to conduct the experiments, where "DCF-PC" indicates the use of the DCF on the desktop machine, while the "DCF-RIO" indicates the use of the DCF on the myRIO.

The real-world experiments are conducted at the KCM, where the agents are deployed to a National Instruments PXI-8840 real-time controller running Windows 7, with 8 GB RAM and 2.4 GHz processing speed. The agents control two DERs in the experiment, which are the SolarEdge 6000SE inverters (4 x 5 kW), and the

Table 3.2: Software versions used in the benchmarking procedure.

	Client Library	Broker	Host Platform/OS
AMQP	Python AMQP 2.5.2	RabbitMQ	Windows 10 PC
MQTT	Python Paho 1.5.0	Mosquitto	Windows 10 PC
DCF-PC	RTI DDS LabVIEW	-	Windows 10 PC
DCF-RIO	RTI DDS LabVIEW	-	Linux myRIO-1900

Schneider Xantrax 6848 XW+ BESS (6.8 kW/75 kWh). The SolarEdge inverters are connected to approximately 20 kW of PV arrays that are manufactured from Morgan Solar.

3.4.2 Experiment 1: Validation of DCF Using SIL Platform

The experimental methodology for benchmarking the SIL platform consists of three experiments that measure the average latency of messages exchanged using the *MsgBus* topic as a function of message rate (messages/second), message size (bytes/message), and the number of agents. At the start of each experiment, all agents are launched simultaneously, and publish messages of a configurable size to the *MsgBus* topic by specifying a random agent ID in the *Receiver_Agent_ID* field. Subsequently, the agents begin to receive messages from the *MsgBus* topic, which are timestamped and logged to disk. Since the messages are timestamped at both the sending/receiving ends, the message latency is calculating by subtracting the two measurements from each other. Monte Carlo experiments of 1000 trials are repeated for each experiment, with the average message latency being taken as the final result.

Experimental results are depicted in Figs. 3.6-3.8. Figure 3.6 shows the result for message latency as a function of message rate, where the number of agents

is fixed at 4 and the message size is fixed arbitrarily at 8192 bytes. The average message latency increases with the increase of the message rate for all three middlewares, except for the DCF-PC implementation, where the recorded latency is consistently below 2 ms. Within the DCF-RIO implementation, the average message latency exceeds 10 ms only after reaching messaging rates of 1000 messages/second, which may also be attributable to the fact that the myRIO processor gives unstable performance at process rates above 1 kHz [89]. Nonetheless, the DCF-RIO implementation significantly outperforms the PC implementation of MQTT (faster by a factor of 5.2), and is at par with AMQP-PC (slower by a factor of 1.26) despite using a platform that has significantly less computational power. The DCF-PC implementation is faster than the AMQP-PC and MQTT-PC by a factor of 47.8 and 112.3, respectively. It is worthwhile to note that the benchmarks for all three frameworks satisfy the minimum latency requirements for smart grid applications, where the lowest specified latency recommendation is in the range of 15-200 ms [24]. However, the trend shown in Figure 3.6 shows that the implementation of the DCF is consistently more scalable than AMQP or MQTT.

Figure 3.7 shows the result of the second experiment, where the message rate is fixed at 10 messages/second and the number of agents is fixed at 4. The DCF-PC implementation shows superior performance to AMQP-PC and MQTT-PC by a factor of 1.18 and 5.67, respectively, and all three implementations show consistent performance in holding the average message latency to below 10 ms. The DCF-RIO delivers message latency below 10 ms until the message size reaches 16,384 bytes, with the maximum latency observed at 27.9 ms for a message size of 32,768 bytes. Given that distributed control strategies tend to limit the message size to reduce communication costs [85], a maximum message size of 8,192 should suffice to ensure compliance with latency requirements in [24].

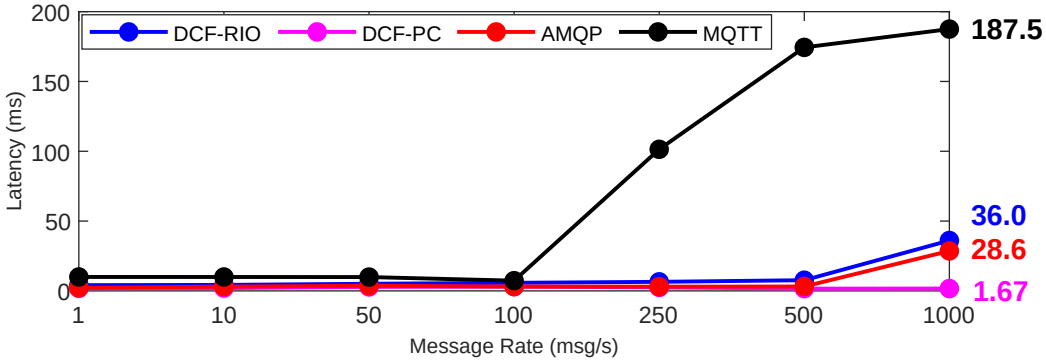

Figure 3.6: Benchmark of message latency vs message rate.

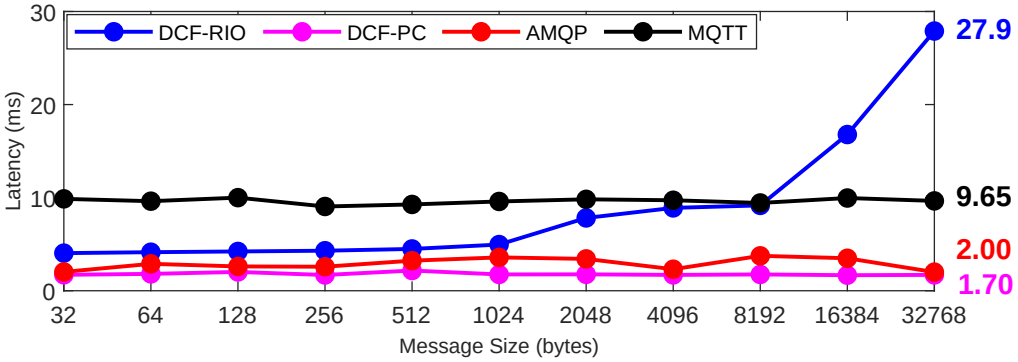

Figure 3.7: Benchmark of message latency vs message size.

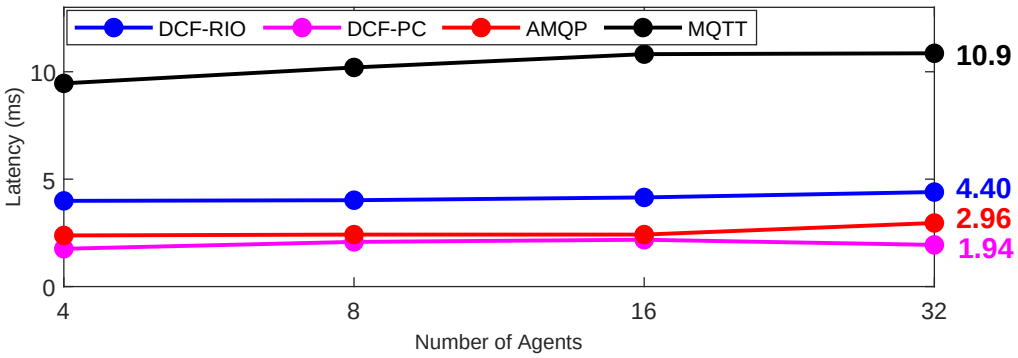

Figure 3.8: Benchmark of message latency vs number of agents.

Figure 3.8 shows the result of the third experiment, where the number of agents is increased while fixing the message size and rate at 256 bytes and 10 messages/sec-

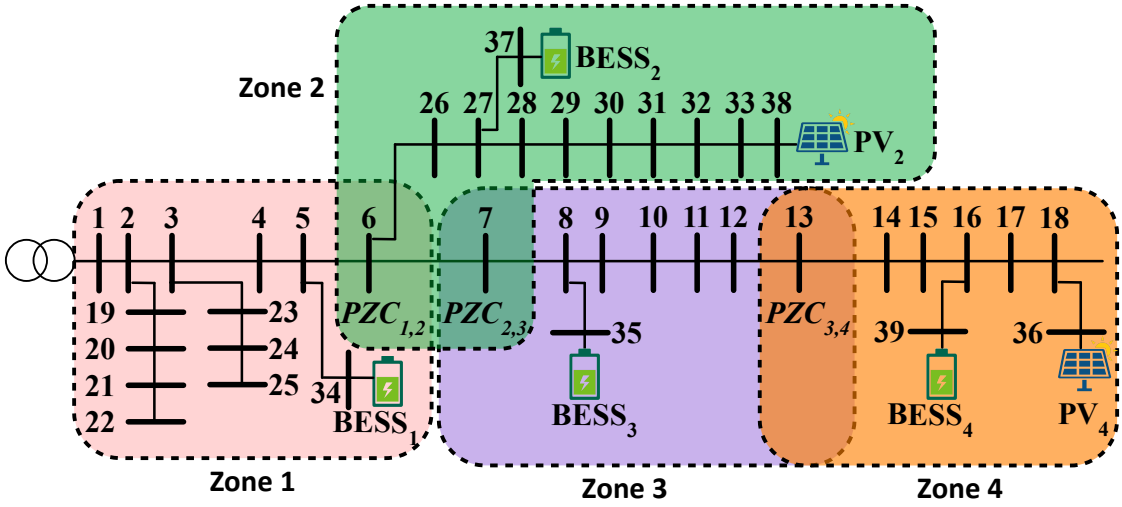

Figure 3.9: The 39-bus test feeder divided into 4 zones.

ond, respectively. Figure 3.8 shows consistent performance of all middlewares on all platforms, with DDS-PC, DDS-RIO, and AMQP-PC recording average message latencies below 5 ms when 32 agents are deployed. In summary, the results of this experiment show that the DCF-PC implementation is superior to both MQTT-PC and AMQP-PC implementations, and that the DCF-RIO implementation is still within the tolerable requirements for smart grid communication standards.

3.4.3 Experiment 2: SIL Simulation of Voltage Regulation Scheme

In this experiment, the SIL platform is used to validate the implementation of the modified AWC strategy in regulating the voltage of an SDG. A modified 39-bus SDG feeder is used as the test system [90], which is divided into 4 zones as seen in Figure 3.9, where PV DG units of 1.0 MW capacity (PV_2 and PV_4) are deployed at buses 38 and 36, respectively, and $BESS_1$-$BESS_4$ are deployed at buses 34, 37, 35, and 39, respectively. $BESS_1$, $BESS_2$, and $BESS_4$ have identical sizing, with a maximum capacity of 300 kWh, a minimum power factor of 0.89, and maximum

apparent power of 0.3 MVA, while $BESS_3$ has a slightly larger apparent power rating of 0.4 MVA. The upper bound for the voltage limit is set at 1.05 p.u. The simulation is carried out on the SIL platform as per Figure 3.3, with the plant agent being implemented in MATLAB to execute the SDG system model, while the agents are deployed on the myRIOs and implemented in LabVIEW.

For this particular experiment, the PV generation results in overvoltage violations most prominently in Zone 4, and as such, Figure 3.10 shows a plot of the voltage magnitude at the bus of PV_4 under different scenarios, including the conventional (old) AWC, the modified AWC as implemented by the DCF (mod), as well as with no AWC. To support this figure, Figures 3.11-3.13 show the resultant control actions from the agents in terms of their modulation of BESS active/reactive power and PV curtailment in order to resolve the overvoltage violations. Additionally, the issue of the DCF handling outdated messages when executing the AWC is highlighted in Figure 3.14, which prevents misaligned execution and unnecessary energy loss.

As shown in Figure 3.10, an overvoltage violation of 1.0534 p.u. is detected at the bus of PV_4 by Agent 4 at timestep 2. Agent 4 reacts by setting a voltage target of 1.042 p.u. at the next timestep and uses (3.16) to find a solution that does not violate any of the agent constraints, which is ΔP_{BESS_4}=0.171 MW and ΔQ_{BESS_4}=0.0876 MVAR. A similar event occurs at timestep 4 in Zone 2, where Agent 2 detects the maximum voltage to be 1.506 p.u., and resolves the violation by adjusting ΔP_{BESS_2}=0.13 MW and ΔQ_{BESS_2}=0.066 MVAR. At timestep 6, both Agents 2 and 4 detect voltage violations of 1.0526 p.u. and 1.0586 p.u., respectively, but their BESS inverter capacities have been reached, thus requiring agents to utilize the AWC technique.

As shown in Figure 3.14, Agents 2 and 4 calculate the ΔV_{PZC} required to

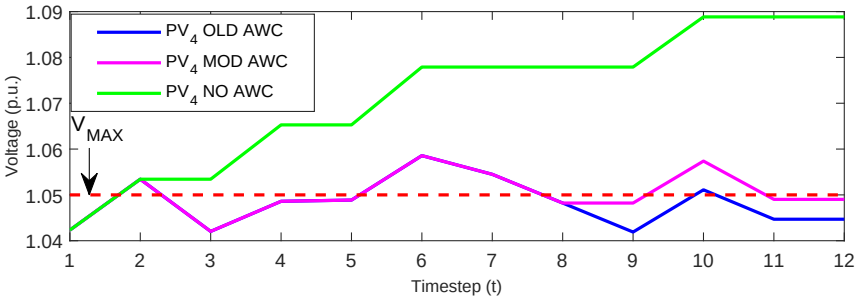

Figure 3.10: PV_4 voltage under different AWC implementations.

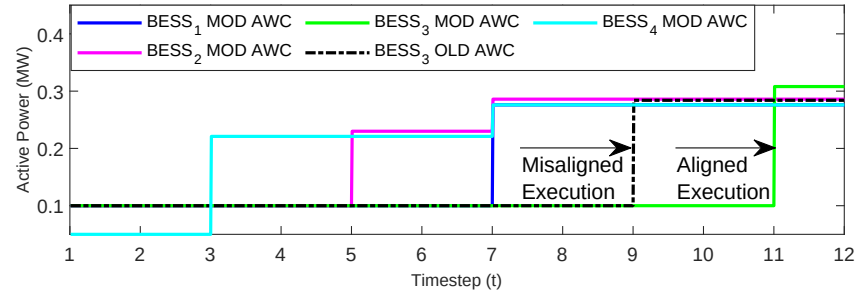

Figure 3.11: BESS active power charging at each timestep.

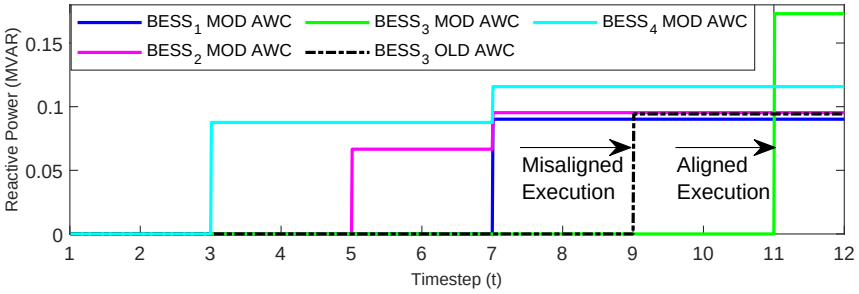

Figure 3.12: BESS reactive power absorption at each timestep.

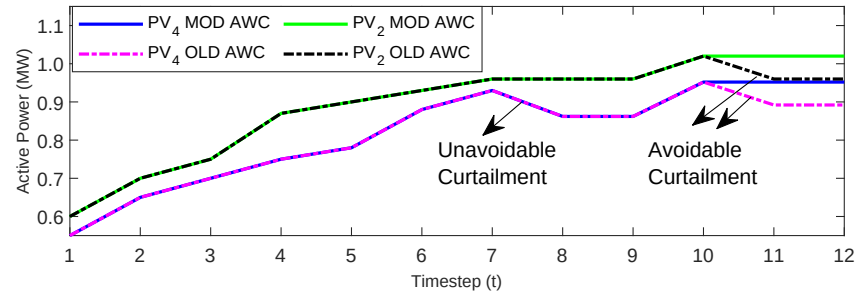

Figure 3.13: PV power generation at each timestep.

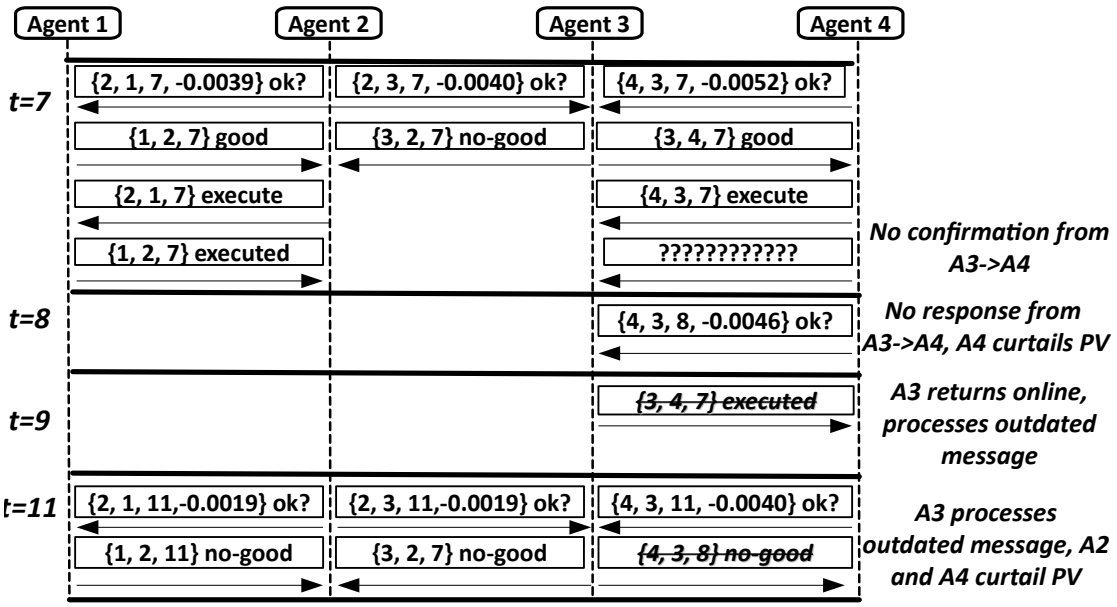

Figure 3.14: Erroneous message exchange using conventional/old AWC.

mitigate the voltage violations using (3.18) at timestep 7, and send *ok?* messages to Agents 1 and 3, respectively, using the syntax defined in (3.12). Both agents store the requests in their agent-view, where Agent 1 determines a solution set of ΔP_{BESS_1}=0.176 MW and ΔQ_{BESS_1}=0.0902 MVAR that does not violate any constraints, and sends back a *good* message to Agent 2. Agent 3 evaluates both requests from Agent 2 and Agent 4, and according to the min-conflict heuristic, gives priority to Agent 4's request by sending back a *good* message after determining a solution set of ΔP_{BESS_3}=0.184 MW and ΔQ_{BESS_3}=0.0943 MVAR. In response, Agents 2 and 4 send back *execute* messages, to which Agent 1 responds, but Agent 3 does not respond since it suffers a disconnection from the network. Thus, at timestep 8, the violation still exists in Zone 4 as seen in Figure 3.10, and Agent 4 sends another message to Agent 3 with a new target V_{PZC}, which again remains unanswered. With no answer from Agent 3, Agent 4 curtails its PV at timestep 8 by -0.068 MW to resolve the violation.

It is at this point where the difference between the conventional AWC and the modified AWC can be seen. As shown in Figure 3.14, Agent 3 rejoins the network at timestep 9 and erroneously executes the outdated *execute* message sent by Agent 4 at timestep 7, even though there is no voltage violation. This results in unnecessary, misaligned execution of BESS3 as seen in Figures 3.11-3.12. At timestep 10, both Agents 2 and 4 again detect overvoltage violations, and *ok?* messages are sent in the same fashion as timestep 7. Agent 3 again erroneously processes the *ok?* message from timestep 7, resulting in an inconsistent agent-view. Due to the unnecessary, misaligned execution of the control action of $BESS_3$ at timestep 9, $BESS_3$ has reached its maximum capacity and sends back a *no-good* message to Agent 4. At this point, all other BESSs have also reached their maximum inverter capacity, resulting in the curtailment of both PV_2 and PV_4 to resolve the violation, which leads to unnecessary energy loss.

Within the modified AWC strategy implemented by the DCF, which has the capacity to automatically filter the outdated messages, Agent 3 *does not* process the *execute* message from Agent 4 at timestep 9, and therefore, does not unnecessarily execute any control actions. At timestep 11, Agent 3 receives the correct *ok?* message from Agent 4, and has sufficient capacity to resolve the voltage violations for both Agent 2 and Agent 4, thereby obviating the need to curtail PV power, as shown in Figure 3.13 by the annotation of "Avoidable Curtailment".

3.4.4 Experiment 3: Real World Implementation

The DCF agents are implemented at the KCM, where the configuration of DERs used for the real-world experiments is represented as simplified single line diagram in Figure 3.15. At Bus 3, Agent 1 controls 4 x 5 kW SolarEdge 6000SE inverters, while Agent 2 controls the Schneider Xantrax 6848 XW+ BESS at bus 4. An Accuenergy

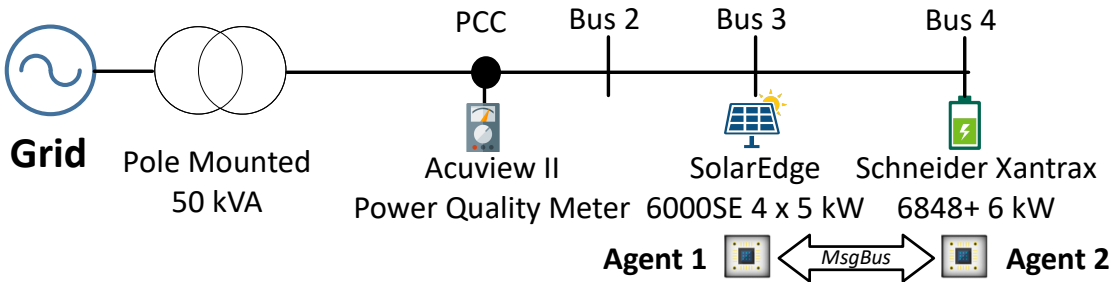

Figure 3.15: Single line diagram of the Kortright Centre Microgrid.

power quality meter of Acuview-II vintage is used to observe measurements of voltage and power flow at the point of common coupling (PCC) between the KCM and the main grid. All DERs and meters devices are controlled by the agents via the MODBUS protocol. As discussed in Chapter 2, the KCM experiences severe overvoltage violations due to a combination of very light loading and high renewable power production on its main feeder, and as such, the proposed DCF is deployed to mitigate these voltage issues.

3.4.4.1 Outdoor Voltage Sensitivity Trials

First, outdoor trials are conducted to determine the sensitivity of the KCM feeder voltage to active and reactive power injections from the SolarEdge inverters. These trials are conducted by manipulating the setpoints for active and reactive power on the inverters in fixed increments, while observing the resultant impact on the voltage profile of the feeder. The measurements are taken at a sampling frequency of 1 Hz. The trials are conducted on a bright and sunny day, where there is no cloud cover to disrupt the generation of the PV array that is connected to the inverters. Additionally, the maximum power output of the inverters is curtailed to an aggregate of 12 kW instead of their nameplate capacity of 20 kW. This step is taken to avoid inconsistencies in power output when the inverters reaches their

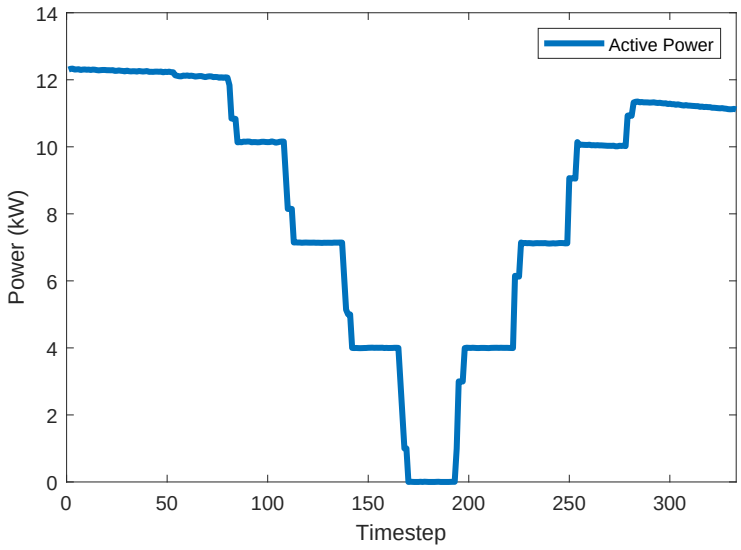

Figure 3.16: Active power modulation of SolarEdge inverters.

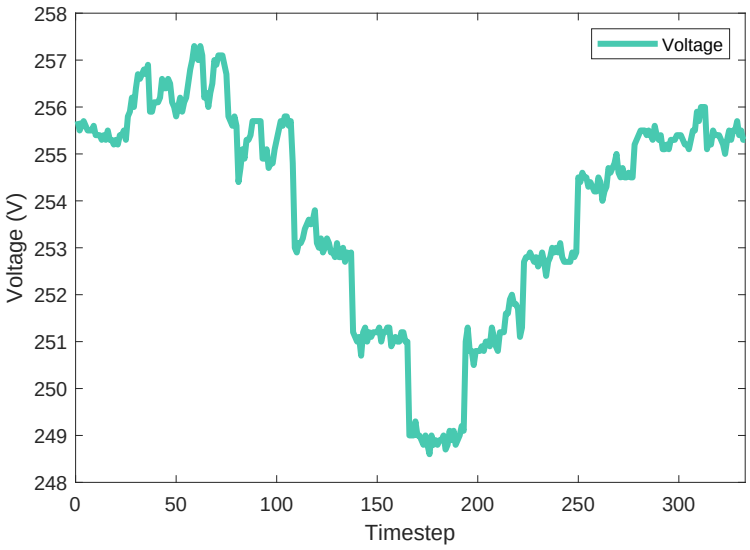

Figure 3.17: Voltage profile of KCM feeder in response to active power modulation.

maximum capacity of 20 kW.

The results for the active power sensitivity trial of the KCM can be seen in Figure 3.16, where the active power is curtailed in increments of 20% of the nameplate

Table 3.3: Voltage sensitivity calculations at the KCM as a function of active power

Setpoint (%)	Average Power (kW)	Average Voltage (V)	Interim Sensitivity (kW/V)
60	10.14	255.23	-
40	7.14	253.11	1.41
20	3.99	251.11	1.57
0	1.66	248.94	1.85
20	3.99	251.17	1.79
40	6.00	252.81	1.22
60	8.99	254.59	1.72
		Average Sensitivity	**1.59**

capacity of 20 kW. The resultant impact on the KCM feeder voltage profile can be seen in Figure 3.17, where it is evident that there is a strong degree of correlation between active power and the voltage profile. The waveforms shown in the figures have very similar profiles throughout the modulation process and their amplitude is steady in between the perturbations to the system. Table 3.3 summarizes the calculations used to determine the sensitivity of the voltage of the KCM feeder to active power injections. For each setpoint, the measurements for active power generation and voltage are averaged. Subsequently, the interim sensitivity is calculated between setpoints by taking the difference between the calculated average power generation and dividing it by the difference in the calculated average voltage measurements. Finally, the average of averages are taken to be the final sensitivity, which is 1.59 kW/V. This means that for every 1 volt differential of the KCM feeder voltage, it will require a differential of +/- 1.59 kW of active power.

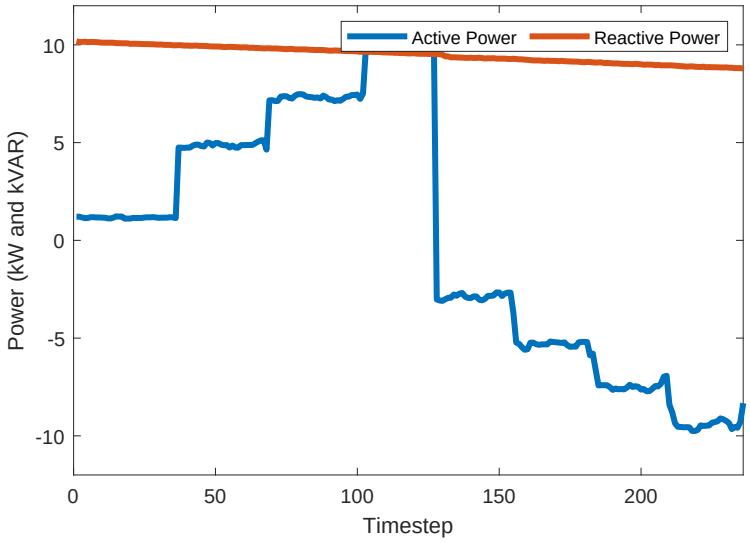

Figure 3.18: Reactive power modulation of SolarEdge inverters.

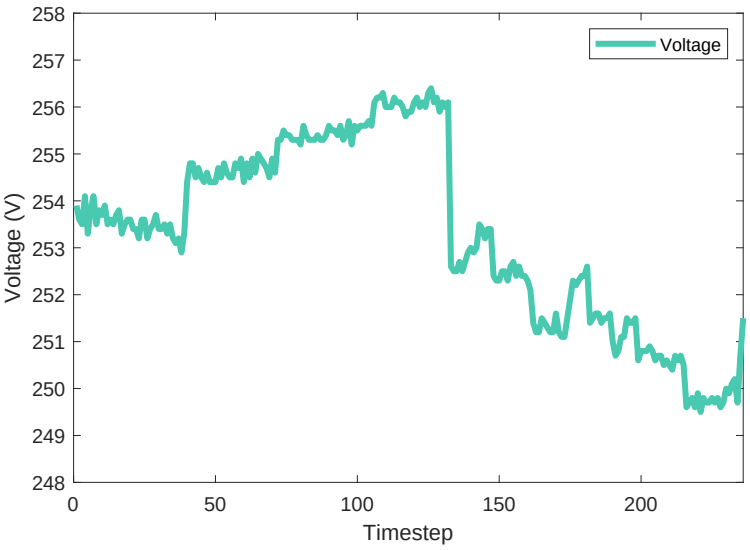

Figure 3.19: Voltage profile of KCM feeder in response to reactive power modulation.

A similar trial is conducted for reactive power sensitivity, where the measured waveforms for the reactive power modulation and resultant voltage profile are presented in Figure 3.18 and Figure 3.19, respectively. As seen in Figure 3.18, the reac-

Table 3.4: Voltage sensitivity calculations at the KCM as a function of reactive power

cosPhi Setpoint	Average Power (kVAR)	Average Voltage (V)	Interim Sensitivity (kVAR/V)
1	0.30	253.43	-
0.9	1.22	254.59	0.79
0.8	1.82	255.34	0.82
0.7	2.44	256.01	0.92
-0.98	-0.53	252.67	-
-0.9	-1.16	251.57	0.57
-0.8	-1.72	250.76	0.70
-0.7	-2.28	250.13	0.90
		Average Sensitivity	**0.78**

tive power is modulated by manipulating the power factor (cosPhi) of the inverters in increments of +/- 0.1, while the active power is held constant at approximately 8 kW to negate the factor of variable irradiance. The aforementioned waveforms again show a strong correlation, and the calculations presented in Table 3.4 show that the average sensitivity of the KCM feeder to reactive power injections is 0.78 kVAR/V. This means that the KCM feeder is more sensitive to reactive power modulation than active power. It is worthwhile to note that Table 3.4 shows a slightly irregular setpoint of -0.98, which is set within the trial to begin the negative descent from a cosPhi pf -1 to -0.7. However, the SolarEdge 6000 SE inverters do not allow a cosPhi setpoint of -1 to be set, and thus, the maximum setpoint of -0.98 is observed within the table.

3.4.4.2 Agent Reactive Power Control

The ability of an agent to mitigate voltage violations locally via reactive power modulation is demonstrated in Figures 3.20 - 3.22. The upper bound for the voltage is set at 252 V, while measurements are taken at a sampling rate of 5 seconds. Figure 3.20 shows the active power generation of the SolarEdge inverters at bus 3, while Figure 3.21 shows the corresponding voltage profile at the PCC. As seen in Figure 3.21, the voltage is never permitted to rise above the 252 V mark due to the reactive power absorption of the inverters, which is shown in Figure 3.22. The agent modulates the reactive power output of the inverters using the sensitivity metrics determined in the previous subsection, and thus, increases the reactive power absorption rate when the voltage creeps towards the 252 V mark. It can also be seen that active power did not need to be curtailed during the experiment in order to mitigate the overvoltage violation. Thus, the ability of the agent to modulate reactive power is demonstrated to be an effective method of regulating voltage, thereby leading to the maximal harvesting of active power.

3.4.4.3 Agents Executing AWC Strategy

The final experiment demonstrates the ability of the agents to execute the modified AWC strategy to mitigate overvoltage violations at the KCM. Figure 3.23 shows two major instances of overvoltage violations at times 13:03:30 and 13:03:50, where Agent 1 observes voltages of 252.5 V and 253.6 V, respectively. In each instance, Agent 1 sends an *ok?* message to Agent 2, which receives the messages within the next second, evaluates the requests according to (3.10), and sets a target of $\Delta P = +5$ kW. After confirmation that the constraints have been satisfied, Agent 2 sends back an *good* message and begins to charge the BESS. The impact of

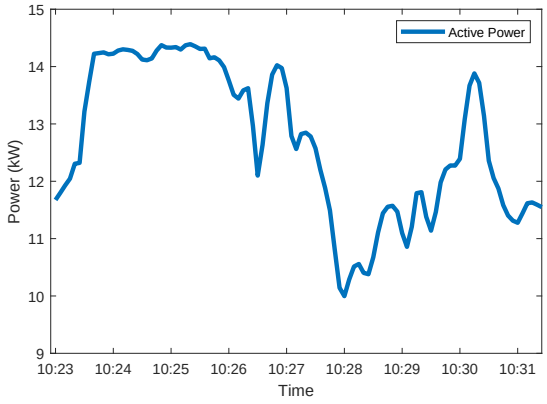

Figure 3.20: Active power generation of inverters during reactive power modulation.

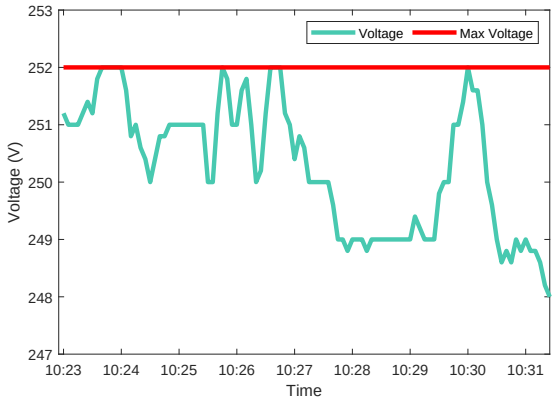

Figure 3.21: KCM voltage profile during reactive power modulation.

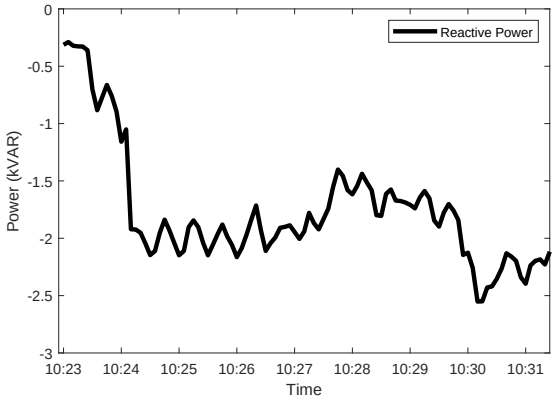

Figure 3.22: Reactive power modulation to mitigate voltage violations.

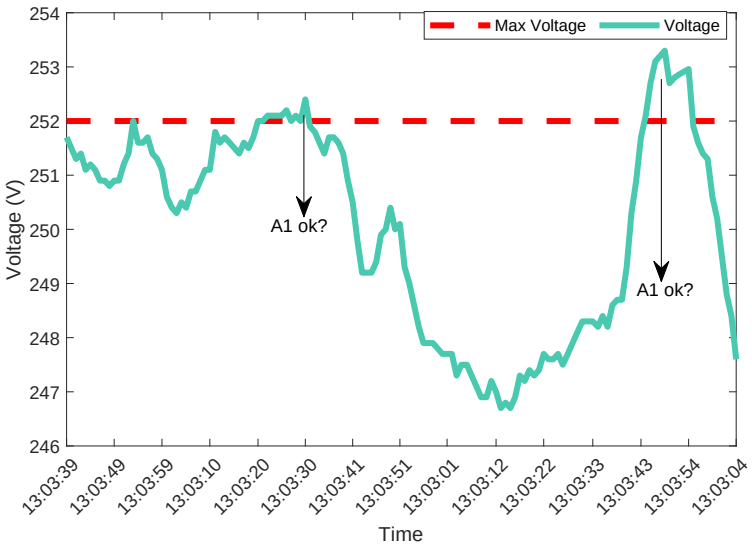

Figure 3.23: Voltage profile at bus 3 during coordinated control.

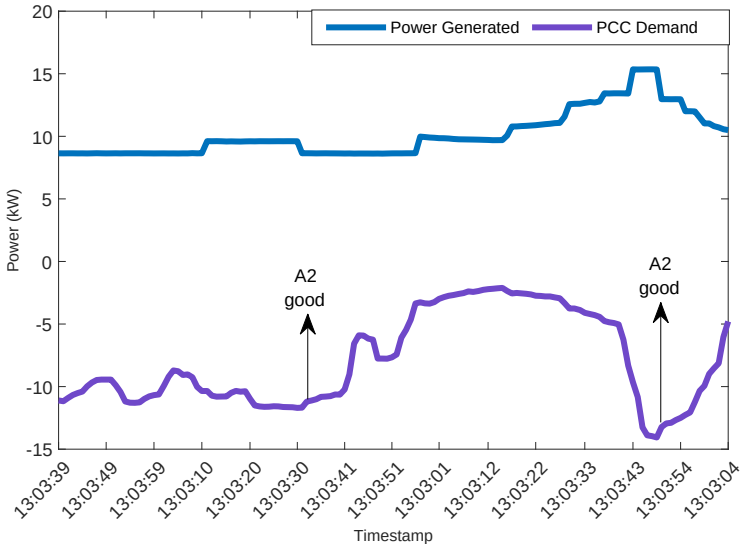

Figure 3.24: BESS charging mitigates voltage violation.

these control actions can be seen in Figure 3.24, which displays measurements of power demand at the PCC. After the *good* messages are sent back to Agent 1, the power demand of the microgrid increases by approximately 5 kW, which equals

the setpoint calculated by Agent 2. Figure 3.24 also shows the steady active power generated by Agent 3's SolarEdge inverters, confirming that maximum active power generation is harvested during the experiment while regulating the voltage within permissible limits. The end-to-end mitigation time for both instances of voltage regulation is 5 seconds.

3.5 Assumptions and Limitations

The following bulleted list summarizes some assumptions made by the implementation of the DCF as well as some of its limitations.

- **Assumption: Time synchronization:** It is assumed that the agents are time-synchronized, which means that the agents would share a common reference of time that is subject to drift or jitter within one millisecond. Synchronization that achieves this level of precision is delivered by the use of global positioning satellites [91], which were not available for this thesis. Thus, to validate the message latency of the proposed DCF, the benchmarks were conducted by distributing messages across 4 agent platforms, however, only the results where the agents were on the same agent platform were used in the evaluation, so as to ensure that the difference in clock timing between the agent platforms did not bias the result.

- **Assumption: Sensitivity factors are constant:** The proposed voltage regulation algorithm assumes that the sensitivity matrices remain constant during the time of study, however, feeder characteristics can change over time due to wear and tear, which may affect the aforementioned sensitivity matrices [92]. Sensitivity trials, as were done in this thesis, can be performed regularly to account for the differences over time.

- **Limitation: Agents have a common global objective, not local or personal:** Disparate agents operating different sets of DERs in different zones may not readily offer their assistance to neighboring agents without the promise of an incentive. Thus, the distributed voltage regulation algorithm proposed in this chapter is suitable for scenarios where the operation of agents is distributed, but their ownership is held by one entity, where incentives do not play a factor. This limitation will be further explored in the next chapter.

3.6 Chapter Summary

This chapter presents the design of a DDS-based DCF for MAS-based SDG applications that provides real-time and robust communication between agents, thereby increasing the efficacy of distributed control strategies. A SIL platform is developed to prototype the DCF, and benchmarks indicate that the DCF provides significantly reduced message latency when compared to other popular middlewares, while satisfying minimal latency requirements for SDG applications. The DCF is applied to the SDG application of distributed voltage regulation, which is formulated as a DisCSP and solved using the AWC technique. The DCF is used to increase the efficacy of the conventional AWC technique by providing support for discarding outdated messages, thereby enabling agents to rejoin the network after a disconnection and align their control actions to prevent energy loss. Both simulation and real-world tests show the effectiveness of the DCF under different operational parameters, thus demonstrating the ability to resolve voltage violations in a timely manner.

Chapter 4 - A Blockchain Based Transactive Energy System for Voltage Regulation in SDGs

While Chapter 3 utilized DDS-based middleware to perform distributed voltage regulation, it did not consider aspects of trust, accountability, and incentive for the agents. As such, this chapter introduces the design and development of a blockchain-based TES for distributed voltage regulation, which is centered around establishing distributed trust among the agents. To start with, this chapter summarizes the motivation of the proposed TES, which is to provide a decentralized platform that enables agents to bid for voltage regulation services in return for financial incentives, while also being able to ensure that all agent transactions are auditable and held accountable to standards of performance. Important consideration is also given to the ability of the TES to enable agents to resolve multiple voltage violations simultaneously via the ECNP control strategy. Subsequently, the blockchain architecture within the proposed TES is discussed in context of its implementation of the ECNP control strategy. Following this, two experiments are presented to demonstrate the efficacy of the proposed TES, and the chapter is finally concluded with a discussion of the major outcomes disseminated from this work.

4.1 Problem Description and Hypothesis

As seen in the previous chapter, performing voltage regulation in a distributed manner eliminates a central point of authority, which leads to improvements in latency and reliability. However, the work in the previous chapter, as well as much of the work that came before it, does not provide mechanisms of providing appropriate financial compensation to the agents in return for their services [19, 20, 93]. Nor does the previous work it discuss the issue of establishing *trust*, where the compensation would be fairly calculated and delivered, and agents may be penalized if the services provided are not satisfactory [94]. Instead, agents are assumed to be cooperative, unselfish, and willing to operate their DERs at an economic loss in order to resolve a voltage violation, which is unrealistic given that agents are primarily motivated by financial gain [79]. An example of this scenario is when an agent may ask another agent to curtail their active power to mitigate an overvoltage violation. Additionally, the case of multiple agents engaging in multiple, asynchronous negotiations to resolve voltage violations is not considered in all of the aforementioned work. Instead, an agent encountering a voltage violation initiates a "Call For Proposal" (CFP) and waits for other agents to respond. This method is similar to using a centralized dispatch technique since the responding agents are effectively "blocked" while waiting for a confirmation from the initiating agent. This means that agents cannot bid on multiple CFPs simultaneously to determine the optimal economic/operational decision for themselves [95], and must resort to bidding sequentially.

These shortcomings are addressed in this chapter by the proposal of a blockchain-based TES that provides a competitive marketplace wherein agents can rationally bid for voltage regulation services. Agents suffering from voltage violations may initiate a CFP and solicit bids for voltage regulation services from neighboring

agents, where the final bid price is generated considering the price of both active and reactive power contributions (P/Q). All agent interactions and negotiations are proposed to be handled by the ECNP control strategy, which is specifically designed to support multiple, asynchronous negotiations between agents [95]. Thus, a voltage regulation service contract is awarded to an agent based on the bid price and agent *credit score*, which reflects the agent's trustworthiness in resolving voltage violations. The role of the blockchain is instrumental in i) automating the ECNP process between agents by implementing it as a smart contract, ii) enforcing service contracts between agents by confirming that the correct P/Q control action was taken by the agent to resolve the voltage violation, and iii) autonomously and impartially maintaining the agent credit score. The proposed system is implemented using the HLF blockchain platform.

As such, this chapter hypothesizes that the proposed TES is able to provide an auditable, trustless mechanism to facilitate distributed voltage regulation services between agents, while being able to resolve multiple voltage violations in less bidding cycles than comparative approaches due to its ability to resolve multiple voltage violations simultaneously.

4.2 Design of TES for the Application of Distributed Voltage Regulation

4.2.1 High-level Design of Proposed TES

To illustrate how blockchain technology is integrated within the physical SDG, a cyber-physical representation of the SDG is depicted in Figure 4.1. As shown in the Figure, Layer 1 represents the power flow within the physical SDG, and Layer 2 represents the virtual blockchain network that delivers zonal measurements from

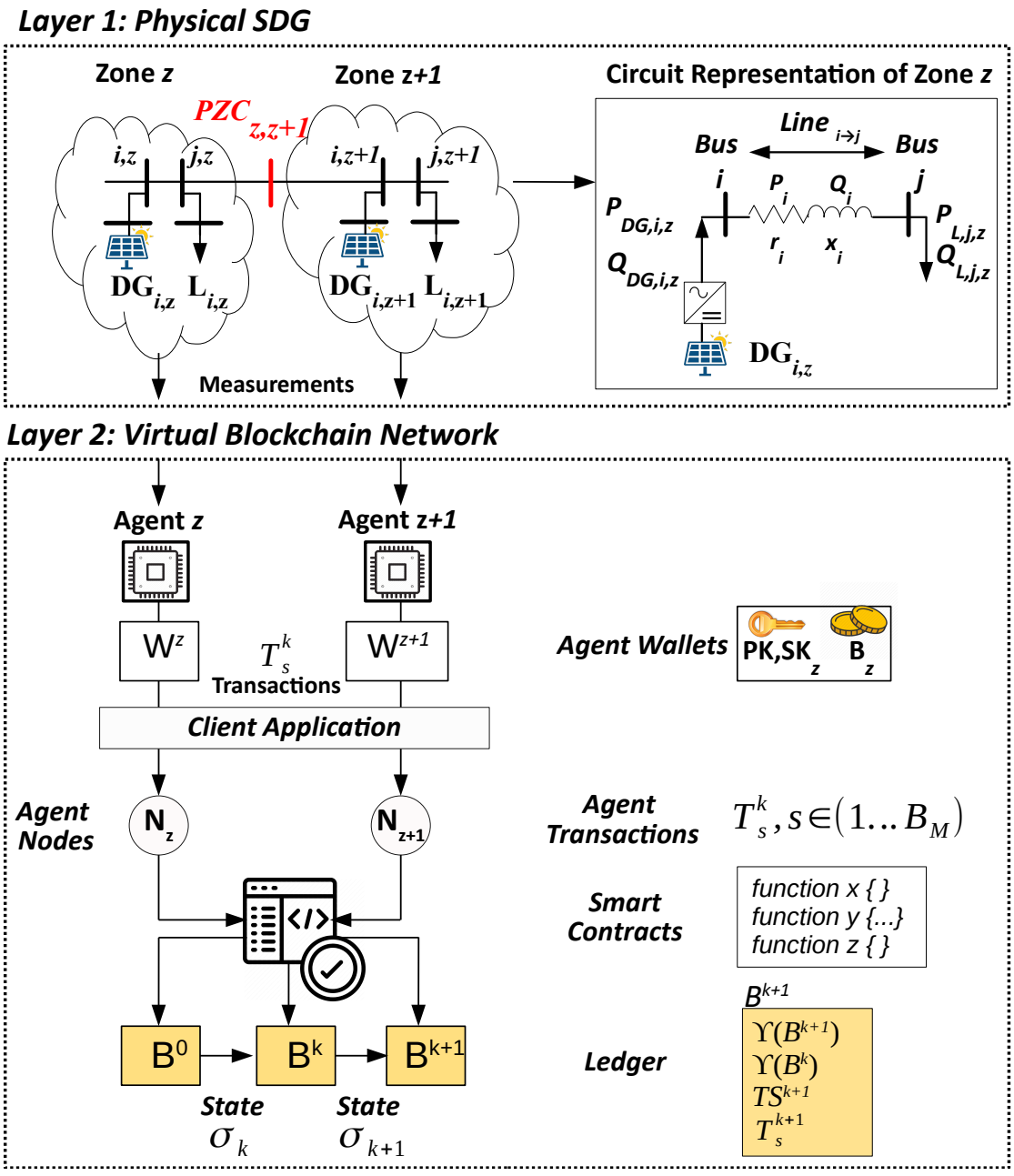

Figure 4.1: A cyber-physical representation of the proposed blockchain-based TES.

the SDG to the agents, manages all communication and bidding, and announces the final contract assignments. The mathematical formulation of the power flow

and voltage profile in Layer 1 remains the same as presented in Chapter 3, however, it is worth providing a recap of the equations for the convenience of the readers. Thus, in general, the P/Q power flow within any zone z between bus i, z and bus j, z, as well the voltage at bus i, z can be represented as follows [90]:

$$P_{i,z}(t) = P_{j,z}(t) + \sum_{n=i,z}^{n=j,z} \big(P_{L,n}(t) - P_{DG,n}(t)\big) \tag{4.1}$$

$$Q_{i,z}(t) = Q_{j,z}(t) + \sum_{n=i,z}^{n=j,z} \big(Q_{L,n}(t) - Q_{DG,n}(t)\big) \tag{4.2}$$

$$V_{i,z}^2(t) = V_{j,z}^2(t) - 2\sum_{n=i,z}^{n=j,z} \big(r_n P_n(t) + x_n Q_n(t)\big) \tag{4.3}$$

Equations (4.1)-(4.3) show that the zonal voltage profile is heavily influenced by the P/Q power flow in the zone. Based on (3), the impact of P/Q modulation by a DG at bus j, z on the voltage of bus i, z can be formulated as:

$$\Delta V_{i,z}(t) = \frac{1}{V_{i,z}(t-1)} \left[V_{j,z}(t-1)\Delta V_{j,z}(t) + \Delta P_{DG,j,z}(t) \sum_{n=j,z}^{j,z} r_n + \Delta Q_{DG,j,z}(t) \sum_{n=j,z}^{j,z} x_n \right] \tag{4.4}$$

Rearranging, the formulation for $\Delta P_{DG,j,z}(t)$ and $\Delta Q_{DG,j,z}(t)$ can be derived as:

$$\Delta P_{DG,j,z}(t) = \frac{\Delta V_{j,z}(t) V_{j,z}(t-1)}{V_{i,z}(t-1)/SP_{i,j,z} + \sum_{n=j,z}^{j,z} r_n} \tag{4.5}$$

$$\Delta Q_{DG,j,z}(t) = \frac{\Delta V_{j,z}(t) V_{j,z}(t-1)}{V_{i,z}(t-1)/SQ_{i,j,z} + \sum_{n=j,z}^{j,z} x_n} \tag{4.6}$$

where, $\{SP_{i,j,z}, SQ_{i,j,z}\}$ represents the sensitivity factor by which a change in P or Q at bus j, z impacts the voltage at bus i, z, as described by the following relationship:

$$SP_{i,j,z} = \frac{\partial V_{i,z}}{\partial P_{j,z}}, SQ_{i,j,z} = \frac{\partial V_{i,z}}{\partial Q_{j,z}} \tag{4.7}$$

The expressions for $\{SP_{i,j,z}, SQ_{i,j,z}\}$ can be formulated as follows .

$$SP_{i,j,z} = \frac{\partial V_{i,z}}{\partial P_{j,z}} = \frac{\sum\limits_{n=j,z}^{j,z} r_n}{V_{i,z}(t-1)}, SQ_{i,j,z} = \frac{\partial V_{i,z}}{\partial Q_{j,z}} = \frac{\sum\limits_{n=j,z}^{j,z} x_n}{V_{i,z}(t-1)} \tag{4.8}$$

Thus, an agent regulating zone z within an ADN can provide zonal voltage support by determining the precise values for its control actions of $\Delta P_{DG,j,z}$ and $\Delta Q_{DG,j,z}$ using (4.4)-(4.8). These equations are crucial in the determining if an agent executed the correct control action to resolve a particular voltage violation, as will be seen in the experimental results discussed in Section 4.2.4.

On the other hand, the blockchain network depicted in Layer 2 is accessed by an agent via its assigned node. The node exposes a client application wherein agents may submit transactions (T_s^k) to the ledger, which are automatically triggered by smart contracts. In the case of the application of distributed voltage regulation, the design of the smart contract and ledger play crucial roles in ensuring an appropriate level of trust between agents, where agents must rely on each other to maintain a non-partisan, auditable metric to establish trustworthiness over time, as well as ensuring that a voltage violation was resolved using the correct agent control action [94]. Thus, the ledger is designated as the component that serves as the single point of truth for all agents, where all agent transactions are verified in consensus before being finalized, while the smart contract provides automation for agent negotiation and enforcement of service contracts. As such, each agent governing a virtual zone of operation is assigned a node within the blockchain network, and contributes to the maintenance of the ledger by participating in the consensus process. The ledger stores measurements of voltage at the PZC, $V_{PZC,z,z+1}$, as well as the P/Q measurements of agent DGs.

To govern inter-agent communication, a smart contract is deployed to initiate CFPs and assign service contracts to the agent that responds with the best bid. The service contract includes a service level agreement (SLA) that outlines i) the magnitude of voltage deviation to be corrected, ii) the price of the bid, and iii) the bid expiration time. After CFP assignment, the smart contract validates that the

voltage violation was resolved by checking the latest measurements for $V_{PZC,z,z+1}$ on the ledger. Further, to establish a metric that reflects an agents trustworthiness and effectiveness over time, a credit score is stored on the ledger and updated by the smart contract at the end of every service contract. The credit score is updated in proportion to the voltage deviation to be corrected, and also includes penalty factors that significantly hamper an agent's credit score when an agent is unsuccessful in resolving a voltage violation it was assigned. Lastly, since smart contracts can be called asynchronously by all agents, agents are able to bid for multiple CFPs simultaneously. The smart contract implements the ECNP control strategy for this purpose, as will be discussed in the next subsection.

4.2.2 The Extended Contract Net Protocol

The ECNP, introduced in [95], is based on the original contract net protocol (CNP) that defines agents as task managers, A_M, or task contractors, A_C, where managers are task providers and contractors are task workers. The CNP implementation includes three stages that are defined as announcement, bidding, and assignment, in which an A_M announces a CFP, requests bids from A_C, and assigns a service contract to the best bid, respectively. An A_C may also "subcontract" a CFP to another A_C, thereby becoming the A_M for the subcontract. The CNP forces an A_C to bid for CFPs *sequentially* because once the A_C bids for the CFP, it must commit its resources and wait for a confirmation before bidding on other CFPs [95].

The ECNP mitigates this issue by providing two rounds each for bidding and assignment, which are *PreBidding* and *FinalBidding*, as well as *PreAssignment* and *FinalAssignment*, respectively. The prefixes "Pre" and "Final" are used as temporary and final states for the CFP, where the agent can submit multiple bids for each CFP in each round. To provide further clarity, a state transition diagram

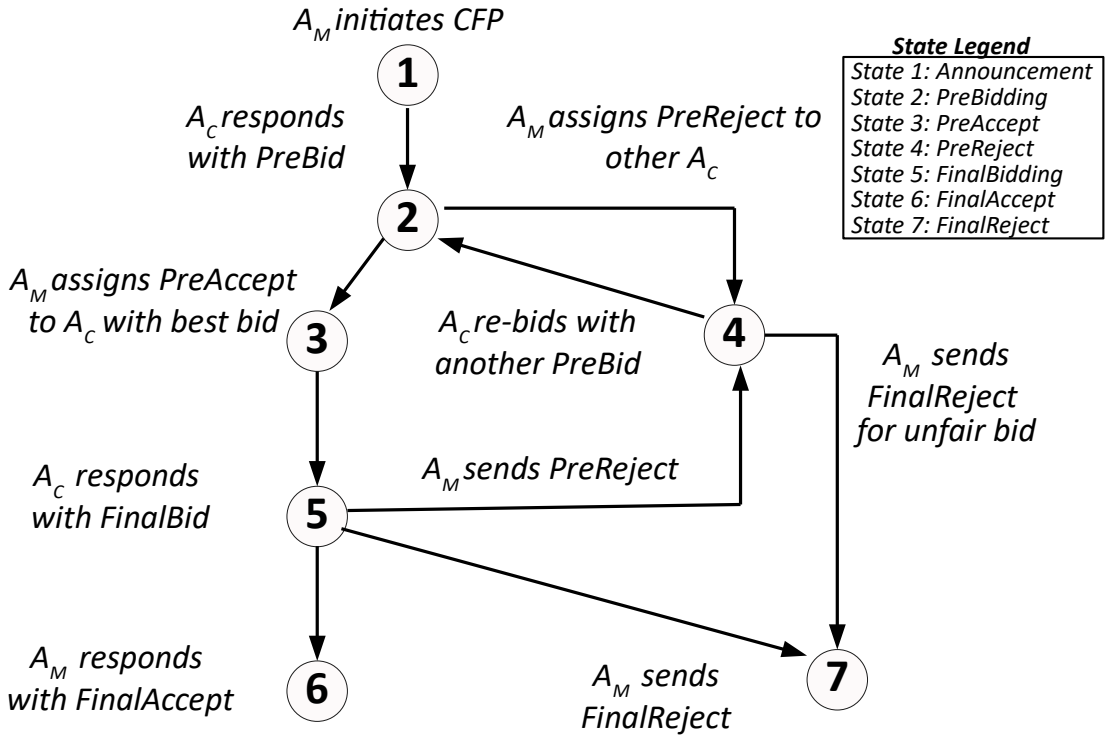

Figure 4.2: State transition diagram of the proposed ECNP process.

of the ECNP process is provided in Figure 4.2. State 2 in the diagram signifies the beginning of the PreBidding round, where all A_C submit tentative PreBids to the A_M, and the A_C with the best bid is temporarily given a *PreAccept* message (state 3), while all other A_C are given *PreReject* messages (state 4). Henceforth, the term $A_{C,W}$ will be used for the PreBid winners and the term $A_{C,L}$ will be used for the PreBid losers.

At this point, the $A_{C,W}$ may submit a definitive, FinalBid to the A_M (state 5), while $A_{C,L}$ may update their PreBids (state 2). If the FinalBid of $A_{C,W}$ is still better than the PreBids of other $A_{C,L}$, the A_M sends a *FinalAccept* message to $A_{C,W}$ and grants it a service contract at state 6. Additionally, the A_M sends a *FinalReject* message to $A_{C,L}$, as shown in state 7. However, if the FinalBid from

$A_{C,W}$ is less than the PreBids of $A_{C,L}$, the A_M sends a *PreReject* message to $A_{C,W}$, and the PreBidding round starts again, as shown from the transition from state 5 to state 4 to state 2. It is worth mentioning that if the $A_{C,W}$ submits a FinalBid that is of significantly less value than its previously submitted FinalBid, the $A_{C,W}$ is sent a *FinalReject* message and is not permitted to bid for the CFP again, as seen from the transition from state 5 to state 4 to state 7. This rule prevents agents from "gaming the system" by submitting very lucrative bids during the PreBidding round to secure the *PreAccept*, and then devaluing the FinalBid to secure a high profit margin. Lastly, if an agent is only evaluating one CFP at a time, the ECNP process can proceed directly to the FinalBidding round to avoid a redundant PreBidding round.

Mapping the ECNP to the application of distributed voltage regulation, it follows that agents that detect a voltage violation in their zone would become an A_M, and issue a CFP to its neighboring agents, A_C, where A_C would bid on the CFP. Agents would utilize the proposed blockchain-based system's smart contract to handle all aspects of the agent negotiation process, including CFP initiation, bidding, and final assignment. The implementation details of the ECNP as a smart contract will be explored in the next subsection.

4.2.3 Implementation of Proposed TES

4.2.3.1 Blockchain Design Principles Applied to Proposed TES

A permissioned blockchain architecture is chosen for the proposed application because the identity of the agents must be qualified before admittance into the network. Also, the use of permissioned blockchains reduces the transaction latency and computational burden of the consensus process, as discussed in Chapter 2.

From the perspective of blockchain scalability, it is important to define *on-chain* tasks, which are executed by agents triggering smart contracts that use data on the ledger, and *off-chain* tasks, which are tasks executed outside of the blockchain network [96].The minimization of on-chain tasks reduces the computation burden of the consensus mechanism as well as the execution time of the smart contract [97]. Thus, the only data required by smart contracts are defined in (4.4), which are: voltage measurements of each zone's PZC, P/Q output of each DG, and a matrix that stores the sensitivity factors $SP_{i,j,z}$ and $SQ_{i,j,z}$ [94]. To handle agent negotiation and contract enforcement, the smart contract would also need the ledger to store all bids and CFPs, as well as the credit score of each agent. All other task execution where ledger data is not needed can be conducted *off-chain*, which will be discussed in the next subsection.

4.2.4 Agent Coordination Process to Resolve Voltage Violations

The agent coordination process to resolve voltage violations is depicted in Figure 4.3, where the workflow of the tasks executed by both A_M and A_C are shown. The legend within the figure indicates whether the tasks are executed on-chain or off-chain, so as to clearly demarcate the role of the blockchain within the proposed system. The coordination process is summarized as follows:

First: An agent obtains the zonal voltage profile by collecting measurements from local smart meters and its DGs, and then performs local state estimation as in [87]. If a voltage violation exists, the agent initiates a CFP to its neighboring agents, while also evaluating if its DGs can resolve the violation locally by using (3.8). In the former case, the agent needs to calculate the target voltage at its PZC with neighboring zones that would resolve its own violation. The target voltage can be

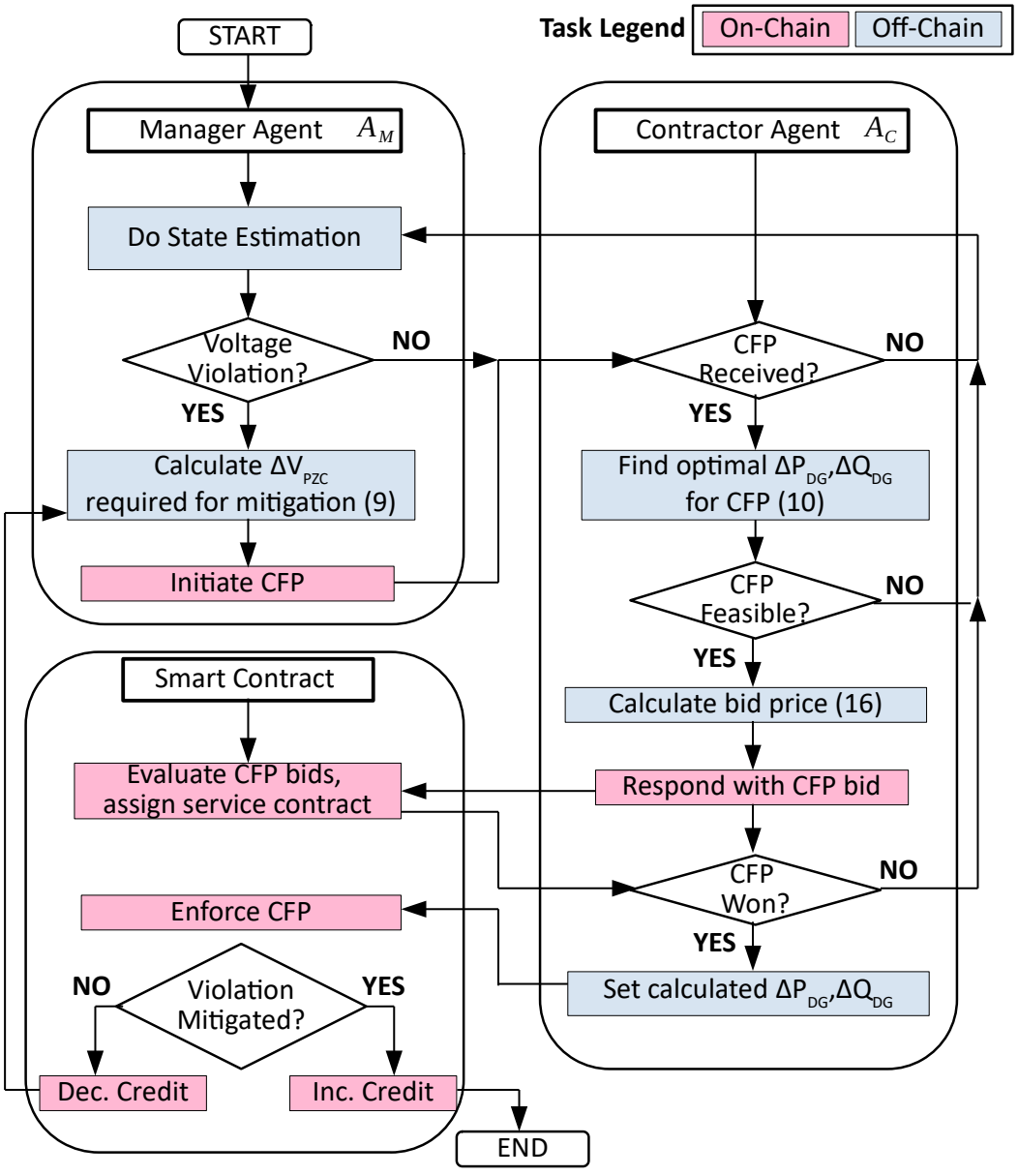

Figure 4.3: Workflow of the proposed agent coordination process.

calculated as per the following equation, noting that $V_{PZC,z,z+1}$ will henceforth be

abbreviated to $V_{PZC,z}$ to avoid redundancy.

$$\Delta V_{PZC,z}(t) = \begin{cases} \frac{\partial V_{PZC,z}}{\partial V_{i,z}} \times (V_{ub} - V_{i,z}(t-1)) & , \forall\, V_{i,z} > V_{ub} \\ \frac{\partial V_{PZC,z}}{\partial V_{i,z}} \times (V_{i,z}(t-1) - V_{lb}) & , \forall\, V_{i,z} < V_{lb} \end{cases} \tag{4.9}$$

Subsequently, $\Delta V_{PZC,z}(t)$ is packaged into a CFP and issued to neighboring agents using the smart contract, which stores the CFP on the ledger.

Second: In response to a CFP, the A_C must determine the CFP's feasibility before deciding to bid on it. The feasibility check is formulated as an optimization problem, where the agent attempts to minimize the cost of resolving a voltage violation as a function of its output active/reactive power. The optimization problem is executed off-chain, and solved by the agent only after a CFP has been issued to it. The objective function of the optimization problem is formulated as:

$$\textbf{Min: } \xi_z(t) = PR_P(t)(P_{DG,m,z}(t)\Delta t) + PR_Q(t)(Q_{DG,m,z}(t)\Delta t) \tag{4.10}$$

where $\xi_z(t)$ is cost of the agent resolving a voltage violation, subscript m is the index of the DG in zone z, Δt is the timestep, PR_P is the price of active power that is assumed to be set by the DSO, and PR_Q is the price of reactive power set arbitrarily by the agent. The agent solves (4.10) to calculate the P/Q setpoints for each of its DGs to resolve the voltage violation. The objective function in (4.10) is constrained by the target voltage identified in the CFP:

$$\Delta V_{PZC,z}(t) = \Delta V_{PZC,z}(t) - \epsilon \tag{4.11}$$

where ϵ is a tolerance factor used to relax the requirement of the agent to reach $\Delta V_{PZC,z}$ exactly. Additionally, (4.10) is also constrained by the requirement to obey the min/max current and voltage limits within the zone:

$$I_{n,z}(t) \leq I_{n,z}^{CAP} \quad \forall\, n \in F^z \tag{4.12}$$

$$V_{lb} \leq V_{i,z}(t) \leq V_{ub} \quad \forall\, i \in M^z \tag{4.13}$$

Lastly, (4.10) is constrained by the maximum operational ratings of its DGs:

$$P_{DG,m,z} \leq P^{MAX}_{DG,m,z}(t) \tag{4.14}$$

$$P_{DG,m,z}(t) \leq Q^{MAX}_{DG,m,z}(t) \tag{4.15}$$

Recall that the agent does not bid at the marginal cost in (4.10). For the agent to receive some profit, the marginal cost is adjusted with a markup factor, α, resulting in a final bid price, PR_{BID}, that is computed as:

$$PR_{BID} = \alpha_z \xi_z(t) \tag{4.16}$$

Recall, that the agent credit score is also considered when evaluating bids for CFPs since it reflects the trustworthiness of an agent. Thus, the markup factor should be a function of the credit score to avoid an agent bidding too high when its credit score is low. The range of markup factor is determined according to the following heuristic, where the credit score is denoted as G.

$$\alpha_z(G_z) = \begin{cases} 0.6 - 1.0 & , G_z < 0.99 \\ 1.0 - 1.1 & , 0.99 \leq G_z \leq 1.2 \\ 1.1 - 1.5 & , G_z > 1.2 \end{cases} \tag{4.17}$$

Thus, the agent responds to the CFP with the bid price computed in (4.16) using the smart contract, which stores the bid response to the ledger.

Third: Upon receiving responses for the CFP, the smart contract executes the ECNP as discussed in Section 4.2.2. An example of the inter-agent messaging during the ECNP is described below, where the PreBidding and FinalBidding rounds, as well as the PreAssignment and FinalAssignment rounds, have been combined

into a single Bidding and Assignment round, respectively, for the sake of avoiding redundancy.

1) Announcement: A_M encounters a voltage violation and issues CFPs targeted at its neighboring agents that are stored on the ledger in the following format:

$$\{A_M, CFP_{ID}, \Delta V_{PZC,z}, \kappa\} \tag{4.18}$$

where A_M is the ID of the manager agent in zone z, CFP_{ID} is the ID of the CFP, and κ is the timeout period of the CFP.

2) Bidding: A_C receive notifications that a CFP was assigned to them, and find the $\Delta V_{PZC,z}$ required for the CFP. Equation (4.10) is used to check for a feasible solution. If feasible, the agent computes a final bid price using (4.16), and stores the bid price on the ledger in the following format:

$$\{A_C, CFP_{ID}, PR_{BID}\} \tag{4.19}$$

where A_C is the ID of the contractor agent in zone z.

3) Assignment: The smart contract collects all bid prices and multiplies them with the inverse of the credit score to calculate the final value of the bid. The lowest final value is granted the service contract. The smart contract notifies all A_C by issuing a message encoded as:

$$\{A_M, CFP_{ID}, ST_{ID}, DEC\} \tag{4.20}$$

where ST_{ID} signifies which stage the negotiation is in, where the values can be 'P' for PreBidding stage, and 'F' for FinalBidding stage, while DEC is a binary decision variable, where the values can be 1 for assignment, and 0 for rejection.

Fourth: The proposed system adds an additional *enforcement* stage to the ECNP

that checks the ledger to determine whether the agent resolved the voltage violation as per the SLA of the service contract. If the SLA is met, the smart contract updates the credit score of the A_C as a function of the $\Delta V_{PZC,z}$:

$$G_z(t) = G_z(t-1) + \gamma|\Delta V_{PZC,z}| \tag{4.21}$$

where G_z is the credit score for an agent and γ is an arbitrary scaling factor that is multiplied by -1 if the agent fails in resolving the violation, thereby significantly worsening the agent credit score.

4.2.5 Summary of Blockchain Implementation

To relate the proposed system's implementation back to the generalized system description presented in Figure 4.1, a summary diagram is shown in Figure 4.4. The on-chain data is shown within the blocks of the ledger, while a description of the smart contract functions is found below:

initAccount(): This function requires the agent to authenticate its identity using SK_Z. Upon successful authentication, the function assigns the agent a unique ID, and sets the account balance to zero.

createCFP(): This function is called by an A_M when it encounters a voltage violation. The CFP is stored on the ledger as $\{A_M, CFP_{ID}, \Delta V_{PZC,z}, \kappa\}$, and signed by the SK_Z of the A_M to establish its provenance.

replyCFP(): This function is called by all A_C that are interested in responding to the CFP with a bid price. On the first call of the function, the smart contract initializes an empty array of bids that are assigned to the CFP_{ID}. Subsequently, all bids from A_C are checked to ensure i) the price of the bid is less than the balance of A_M and ii) if the recorded timestamp of the bid is within the timeout period of the CFP (κ). If any of these conditions are false, the bid is rejected, and a notification

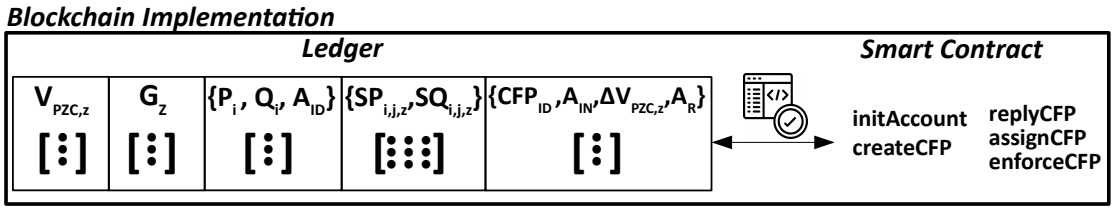

Figure 4.4: Blockchain implementation of the proposed TES.

is sent to the agent with an error message. If both conditions are true, the bid is appended to the array of bids for the CFP_{ID} on the ledger.

assignCFP(): The smart contract multiplies the inverse of the credit score of each A_C with its corresponding bid price, and sorts the cumulative value by ascending order. The lowest value is assigned either a *PreAccept* or *PreReject*, depending on which state the ECNP is in. It is worthwhile to note that the smart contract keeps track of the state of the CFP in accordance to the state transition diagram in Figure 4.2.

enforceCFP(): This function determines whether the SLA of the service contract has been met by the A_C. The function uses (4.5)-(4.6) to calculate the anticipated control actions of the agent DGs, which are verified against measurements on the ledger. The $\Delta V_{PZC,z}$ is also compared to the requirement posted within the CFP, and if both comparisons are true, the function increments the credit score of the A_C using (4.21). Else, the credit score of A_R is penalized using (4.21).

4.3 Experimental Results

Experiments are conducted on a modified 69 bus system shown in Figure 4.5, and the settings of the DGs used by the agents are shown in Table 4.5. Since reference prices for voltage regulation services have not been defined within distribution systems, the prices for both active and reactive power have been adapted from [98].

Table 4.5: Settings of Agent DGs within 69 bus system.

$\mathbf{DG_{m,z}}$	**Bus**	$\mathbf{Q_{MAX}}$ **(MVAR)**	$\mathbf{PR_Q}$ **(\$ /MVARh)**	$\mathbf{G_z}$
1,1 & 2,1	35,46	1.33	100	1.2
2,2	52	2.50	80	0.95
1,3 & 2,3	55,65	1.33	50	1.05
1,4	69	2.0	100	1.2
1,5	27	1.0	100	1.2

The credit scores for each agent have been set to facilitate wide margins during the bidding process that generate more choices for agents to respond to CFPs. The upper and lower bounds for voltage within the system have been set as 1.05 p.u. and 0.95 p.u., respectively. The scaling factor for credit score, γ, has been set to 10 arbitrarily. The power flow for the 69 bus system is solved by MATLAB, while the earlier discussed smart contract is implemented on the HLF platform [99] that executes pBFT consensus. A REST API, as in [100], is used to facilitate external information exchanges between HLF and MATLAB, such that each zonal agent can trigger smart contract functions to submit, assign, reply to, and enforce a CFP. A block diagram of the system implementation can be seen in Figure 4.6, where MATLAB is used to solve the power flow and deliver the zonal voltage profile to each agent, where each agent is implemented within a MATLAB script. The agents then use the REST API to submit transaction proposals to the HLF ledger by calling specific smart contract functions. The transaction proposals are finalized after the consensus process is executed, and the results are delivered back to the agents, who subsequently wait for the next time step in the simulation.

The load and generation profiles of the system under study have been adapted from [101] and can be seen in Figure 4.7. The corresponding controlled (C) and

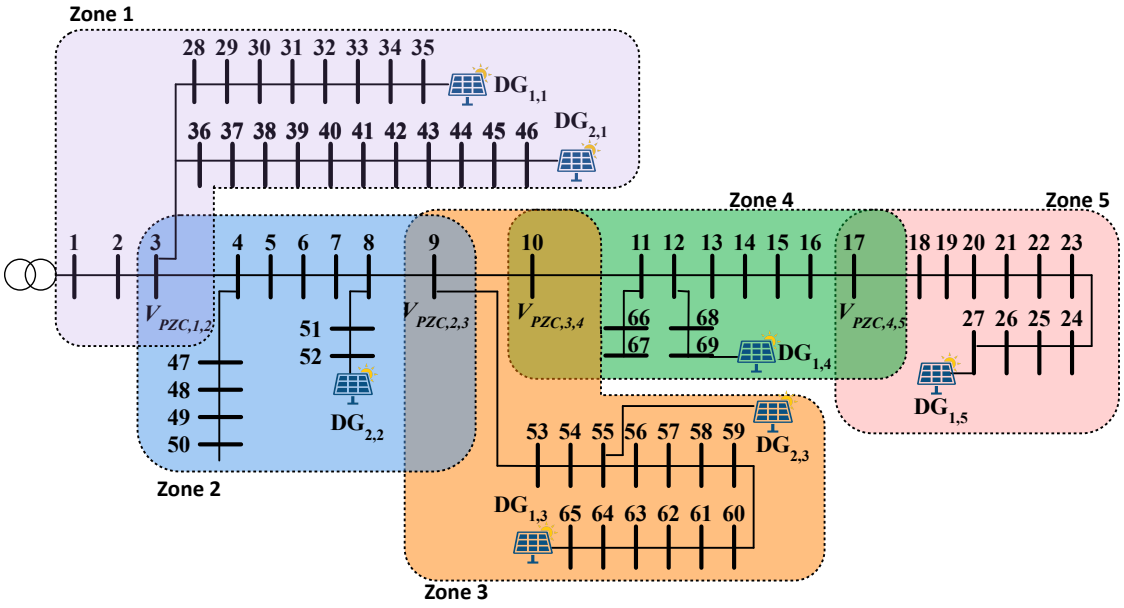

Figure 4.5: Zonal representation of 69 bus system.

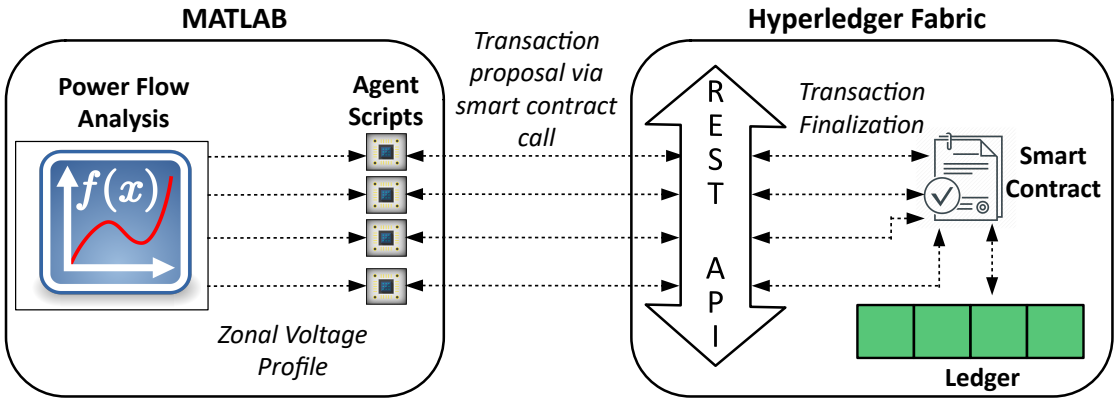

Figure 4.6: Block diagram of system implementation using MATLAB/Hyperledger Fabric.

uncontrolled (UC) voltage profile for bus 27 is shown in Figure 4.8, while the reactive power dispatch of agent DGs is shown in Figure 4.9. As seen in Figure 4.8, there is an overvoltage violation and undervoltage violation that occur at 12:00 and 19:00, respectively. Each violation will be discussed as a separate experiment below, with

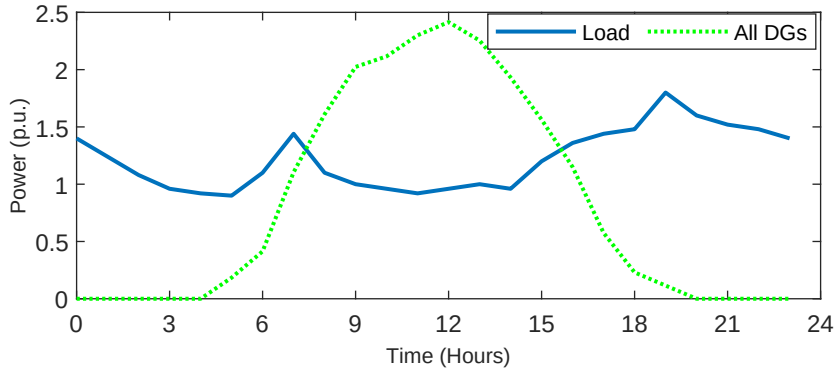

Figure 4.7: Normalized load/generation profile for system under study.

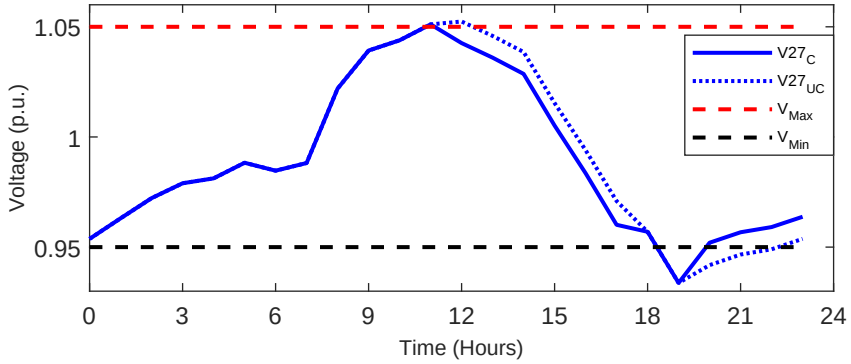

Figure 4.8: Controlled and uncontrolled voltage profile for bus 27.

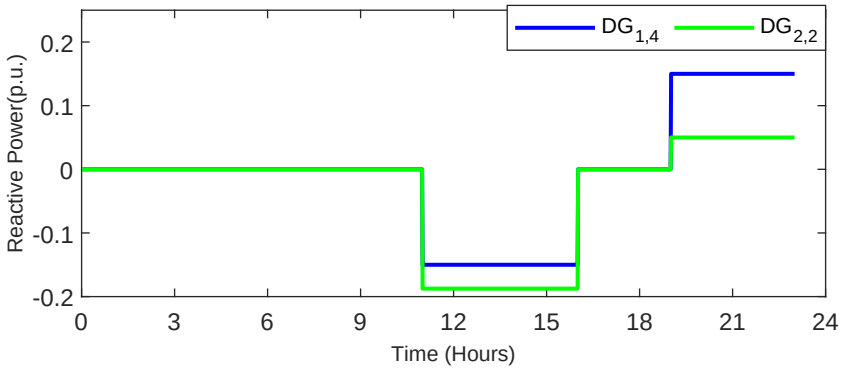

Figure 4.9: Reactive power modulation for $DG_{1,4}$ and $DG_{2,2}$.

the agent message log from the ECNP procedure being shown in Figure 4.10 and Figure 4.12, respectively. Note that the timeout period, κ, has been removed from the messages to avoid redundancy and is assumed to be set at a constant of 1 minute.

4.3.1 Experiment 1: Overvoltage Violation in 3 Zones

Excess DG generation at 12:00 causes three simultaneous voltage violations at bus 27 in Zone 1 (V=1.0511 p.u.), bus 65 in Zone 3 (V=1.0541 p.u.), and bus 46 in Zone 5 (V=1.0511 p.u.). As seen in Figure 4.10, Agents 1, 3, and 5 trigger the announcement stage of the ECNP procedure by generating CFPs with IDs 1, 2, and 3 using the *createCFP* function of the smart contract. The CFPs contain the ΔV_{PZC} required at each of the agent's neighboring zones to mitigate the voltage violations using (4.9). Simultaneously, these agents also execute (4.10) to determine if it would be cheaper to mitigate the violation locally by curtailing their active power, where the active power price at 12:00 is 549.3 \$/MWh. In response to Agent 5's CFP_{ID} 1, Agent 4 uses (4.10) to determine a solution set of $\{\Delta P = 0, \Delta Q = -0.667$ MVAR$\}$ that results in a marginal bid price of \$63.3. Since the credit score of Agent 4 is relatively high at 1.2, it marks up the bid by a factor of 1.1 using (4.17) for a PreBid price of \$69.6. Similarly, Agent 2 processes Agent 3's CFP_{ID} 2 by computing a solution set of $\{\Delta P = -0.267$ MW,$\Delta Q = -1.37$ MVAR$\}$ that results in a marginal bid of \$283.2 and a marked up PreBid of \$311.5. Agent 2 also receives Agent 3's CFP_{ID} 2 and generates a solution set of $\{\Delta P = -0.4$ MW,$\Delta Q = -2.50$ MVAR$\}$. Since Agent 2's credit score is relatively low at 0.95, it chooses a markup factor of 1, thus responding with a PreBid of \$422.8. Agent 2 follows the same process to respond to Agent 1's CFP_{ID} 3 by generating a solution set of $\{\Delta P = -1.33$ MW,$\Delta Q = -2.50$ MVAR$\}$ and a PreBid of \$932.4. All PreBids are submitted by

the responding agents by calling the *replyCFP* function.

Subsequently, the PreBids are evaluated by Agents 1, 3, and 5 during the PreAssignment stage. Agent 5 computes a solution set of $\{\Delta P = -0.133$ MW$\}$ for its own CFP_{ID} 1, which translates to a cost of \$73.2 and is more expensive than Agent 4's bid. Thus, Agent 5 sends Agent 4 a *PreAccept* message for CFP_{ID} 1. On the other hand, Agent 3 evaluates the bids for CFP_{ID} 2 and determines that Agent 4's bid of \$311.5 is less expensive than Agent 2's bid of \$422.8, thereby sending a *PreAccept* message to Agent 4 and a *PreReject* message to Agent 2 for CFP_{ID} 2. Similarly, Agent 1 sends Agent 2 a *PreReject* message for CFP_{ID} 3 because the cost for its solution set of $\{\Delta P = -0.273$ KW$\}$ is \$146.9, which is less expensive than Agent 2's bid of \$93.2. The result of the PreAssignment stage is that Agent 4 has won both its bids and Agent 2 has lost both of its bids. All bid assignments are executed by initiating agents calling the *assignCFP* function.

As the FinalBidding stage begins, Agent 2 improves its bids by using the lower range of the markup factor to discount its bids by a factor of 0.6, resulting in a FinalBid of \$281.3 for CFP_{ID} 2 and \$530.5 for CFP_{ID} 3. Other agents do not change their bids, since they have received PreAccept messages. In consequence, the FinalAssignment stage results in *FinalAccept* messages for Agent 1 for CFP_{ID} 3 and for Agent 4 for CFP_{ID} 1, while Agent 2 gets a *FinalReject* message for CFP_{ID} 3. However, due to its lower bid price for CFP_{ID} 2 in the FinalBidding stage, Agent 2 receives a *PreAccept* message and Agent 4 receives a *PreReject* message. This again triggers a FinalBidding round, in which the agents choose to not change their bid amounts, resulting in the FinalAssignment stage in which Agent 2 receives a *FinalAccept* message and Agent 4 gets a *FinalReject* message. All winning agents dispatch their DGs as per the agreed upon terms within the CFP, which can be seen in the reactive power modulation plot in Figure 4.9. The CFPs are enforced

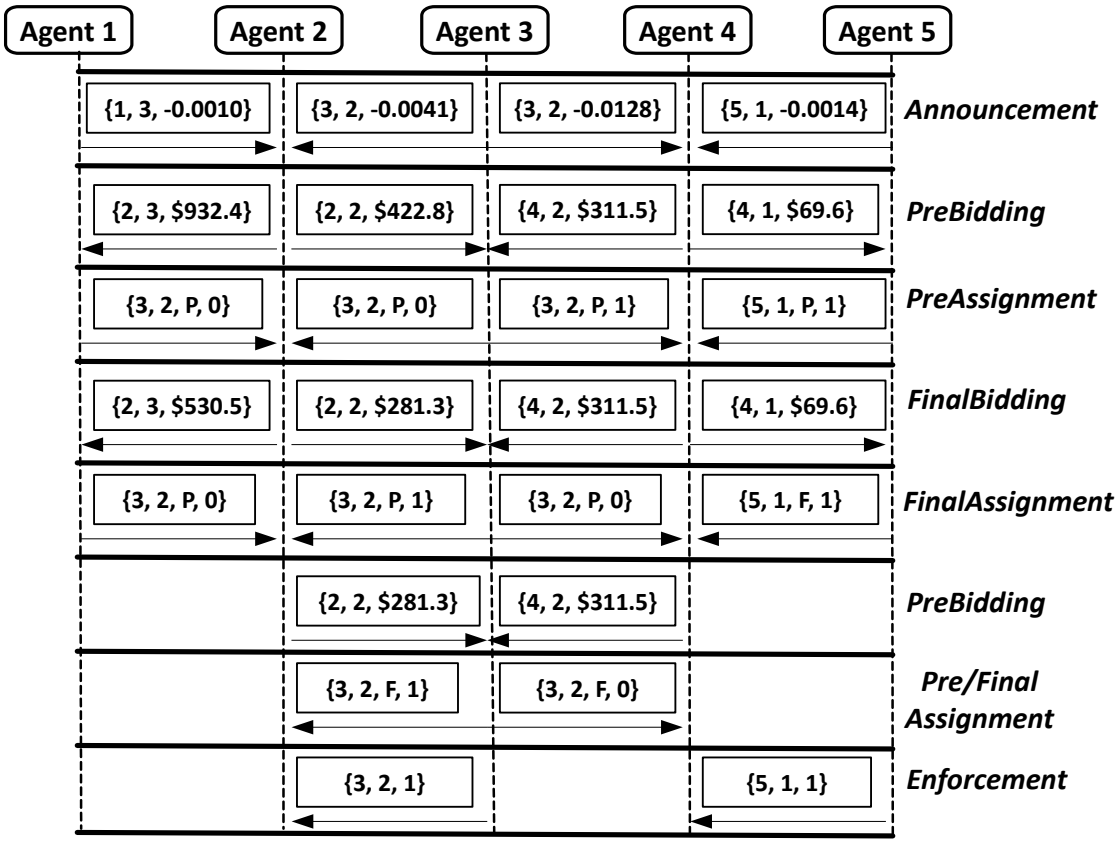

Figure 4.10: Agent message log for overvoltage violation at 12:00.

by the smart contract by checking the measurements posted by Agent DGs on the ledger to confirm that the agreed upon ΔV_{PZC} was indeed achieved. Subsequently, the CFP is closed, and the smart contract updates the credit scores of Agent 2 and Agent 4 as per (4.21). The credit score for Agent 2 and Agent 4 increase from 0.95 to 0.991, and 1.2 to 1.328, respectively. The enforcement of the CFP is triggered via the *enforceCFP* function, which auto-executes after the time expiry stated in the CFP.

When comparing the ECNP procedure to the standard CNP procedure, recall that the CNP procedure does not permit an agent to bid on two CFPs simultaneously. In some scenarios, namely, when the number of voltage violations exceeds the

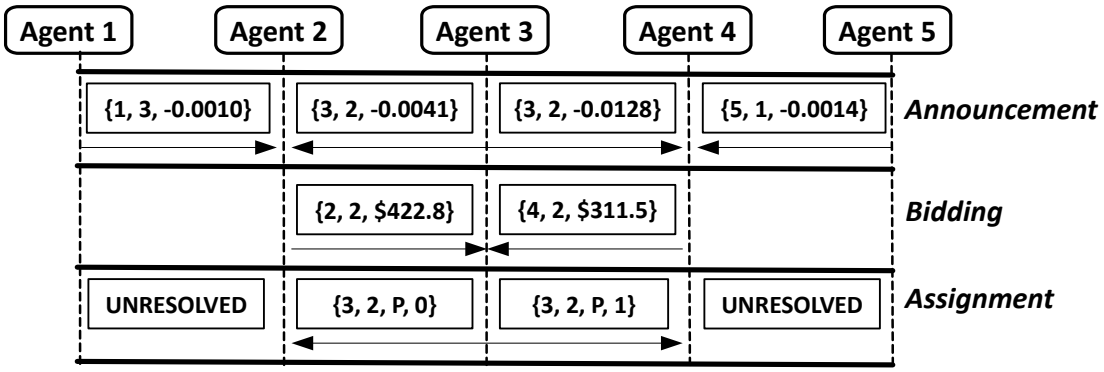

Figure 4.11: Example bidding scenario if CNP control strategy is used.

number of agents that have the ability to resolve them, this restriction will result in unresolved voltage violations until the next bidding cycle. An example of this scenario is shown in Figure 4.11, where the bidding protocol follows the original CNP process of a single round for announcement, bidding, and assignment, and is used in context of the overvoltage violation just discussed. If both Agents 2 and 4 choose to bid on CFP_{ID} 2 from Agent 3, Agent 1 and Agent 5 would not receive any responses to their CFPs, which would result in unresolved voltage violations.

4.3.2 Experiment 2: Undervoltage Violation in 2 Adjacent Zones

At 19:00, Zones 4 and 5 suffer from undervoltage violations at bus 17 (V=0.9337) and bus 27 (V=0.9479), respectively. Agent 5 executes (4.10) to determine if it can resolve the violation locally, however, the solution is infeasible because of the limited reactive power capability of Agent 5's DG, which can operate at a maximum of 1.0 MVAR when 1.5 MVAR is needed. Similarly, Agent 4 requires a ΔQ injection of 6.13 MVAR, but its DG can only operate at a maximum of 2.0 MVAR. Since the undervoltage violations cannot be prevented by Agents 4 and 5 using the capabilities of their DGs, the ECNP process must be executed to facilitate additional bids for

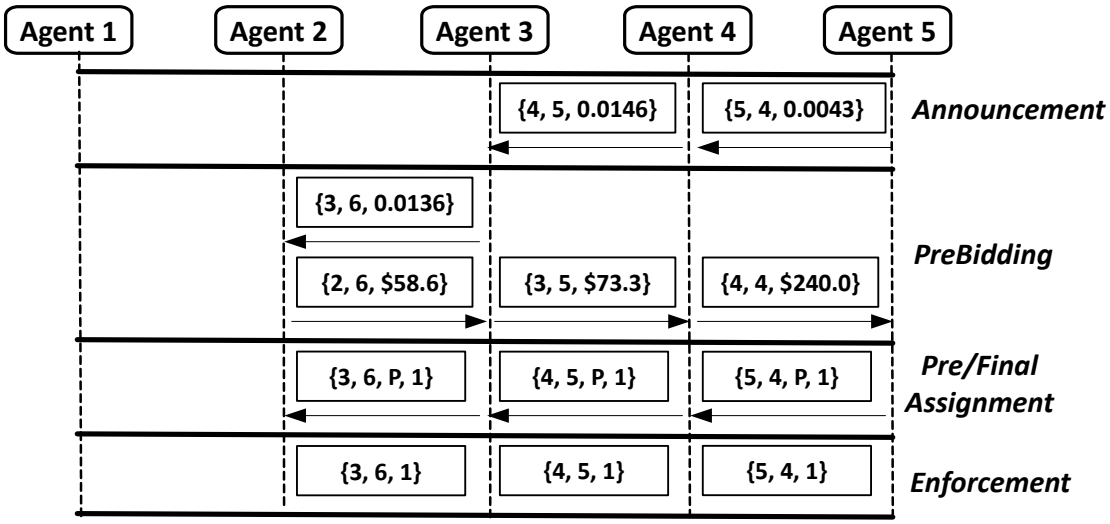

Figure 4.12: Agent message log for undervoltage violation at 19:00.

reactive power support in order to mitigate the voltage violations. As such, both Agents 5 and Agent 4 calculate the ΔV_{PZC} needed to mitigate the violations, which are ΔV=0.0043 at bus 17 and ΔV=0.0043 at bus 10, respectively. As seen in Figure 4.12, the CFPs are generated as CFP_{ID} 4 to Agent 4 and CFP_{ID} 5 to Agent 3, respectively. It is worth noting that Agent 4 is essentially "subcontracting" the CFP to Agent 3 while still having a violation in its own zone. This process is repeated by Agent 3 in response to CFP_{ID} 5, where the required ΔV_{PZC} generates an infeasible solution, and another subcontracted CFP_{ID} 6 is sent to Agent 2.

In response to CFP_{ID} 6, Agent 2 calculates a solution of $\{\Delta Q = 0.65$ MVAR$\}$, which results in a marginal bid price of \$53.3. Due to its increase in credit score from the last round, Agent 2 marks up the bid by 1.1 using (4.17), and responds with a PreBid of \$58.6. Similarly, Agent 3 responds to CFP_{ID} 5 with a marked up PreBid of \$73.4, which is generated by solution of $\{\Delta Q = 1.33$ MVAR$\}$ and a marginal bid of \$66.7. Meanwhile, Agent 4 responds to CFP_{ID} 4 with a marked up PreBid of \$240.0, which is generated by a solution of $\{\Delta Q = 2.0$ MVAR$\}$ and a

marginal bid of $200.0. Since there is precisely one bid for each agent, the smart contract considers the bids as final, and all bids are accepted as offered. Agents 2, 3, 4, and 5 subsequently dispatch their DGs as agreed upon, as shown by the reactive power injections in Figure 4.9. The smart contract subsequently checks the voltage measurements on the ledger to enforce the CFP and ensure that the voltage violations were mitigated. After the verification is complete, the smart contract updates the credit score of Agent 2 from 0.991 to 1.127, of Agent 3 from 1.05 to 1.196, and of Agent 4 from 1.328 to 1.371.

4.4 Assumptions and Limitations

The following bulleted list summarizes some assumptions made by the implementation of the TES as well as some of its limitations.

- **Assumption: Measurements used directly from DER inverters:** In this chapter, the smart contract validates voltage regulation smart contracts from voltage measurements at the PZC of each zone, which are provided by power quality meters, as well as P/Q measurements from the inverters themselves. In practice, however, it is not clear whether inverter measurements can be relied upon for validation purposes since they could be altered by the inverter manufacturer, or, whether meter disaggregation techniques need to be used to determine the P/Q contribution of each DER, as proposed in [102].

- **Limitation: Proposed algorithm suitable only for sustained voltage violations:** The proposed algorithm assumes that the voltage violations occur over an extended period of time, in the range of minutes, or hours, and thus, do not require fast-responses within milliseconds that is more common in power quality applications such as voltage flicker [103]. Multiple negotia-

tions, especially over a blockchain-based system, introduce latency within the system, and is therefore not suitable for applications requiring extremely fast response.

- **Limitation: Determination of reactive power prices was arbitrary:** Since reactive power pricing within distribution systems does not exist in practice, its determination was arbitrarily done within the experimental results for this chapter. Further feasibility studies are required to determine the ranges of reactive power pricing that would be profitable for agents, while still ensuring that voltage violations can be mitigated in a timely manner.

4.5 Chapter Summary

This chapter presents a blockchain-based TES that implements the ECNP control strategy to enable agents to resolve multiple voltage violations in parallel within a competitive marketplace. The ECNP is implemented as a smart contract, which automates the agent bidding and negotiation process, and facilitates the submission of power and voltage measurements to the blockchain ledger. The smart contract also enforces the voltage regulation service contracts by validating the power and voltage measurements on the ledger against the contract details. The proposed system is implemented on the permissioned blockchain HLF platform. Simulation results on a 69 bus system validate the proposed system's ability to resolve multiple violations simultaneously via the ECNP process. The proposed system is also compared to the original CNP process, where it is shown that the ECNP can mitigate voltage violations in less bidding cycles and deliver voltage stability within SDGs more quickly than the CNP process.

Chapter 5 - A Blockchain Based Residential Energy Trading System To Reduce Peak Demand

While chapters 3 and 4 focus on the SDG application of distributed voltage regulation, this chapter focuses on the residential application of energy trading among homeowners. Thus, this chapter develops a blockchain-based RETS that facilitates energy trades between the DERs of homeowners and enables the reduction of peak demand within a residential community. The chapter begins with a summary of the problem description and hypothesis, which describes the impact of uncontrolled DER operation by homeowners on the peak demand of the community, and the techno-economic effect that the proposed RETS may have in lowering the aforementioned peak demand. Subsequently, the concept of residential energy marketplaces is described, which provides design details that include the development of novel bidding strategies for homeowner DERs, as well as the design of the underlying blockchain-based implementation of the RETS. Next, the chapter presents experimental results from both simulated and real-world settings that illustrate the efficacy of the proposed RETS in reducing peak demand, minimizing CAPEX for DSOs, and providing acceptable transaction latency for the SDG application of residential energy trading and demand response. Finally, the chapter is concluded with a discussion of the results, as well as a summary of the major outcomes of this work.

5.1 Problem Description and Hypothesis

Homeowners investing in DERs are interested in reducing their energy bills [104], customizing their tariff structures according to their preferences to maximize the use of renewable energy, and observing transparent billing practices that guarantee the provenance of renewable energy sources [105]. Homeowners typically use home energy management systems (HEMS) to achieve these objectives, where homeowners specify energy preferences related to the operation of their DERs, and the HEMS generates a dispatch schedule for the DERs as a result [106]. Thus, the presence of a HEMS transforms a home into a *smart home*, which is capable of autonomously controlling the DERs of the homeowner to achieve their aforementioned requirements. However, a significant limitation of HEMS' is that they typically provide local control of a single home, and they do not have observability of the entire residential community [107]. This leads to uncoordinated operation of DERs within the community, which may result in major increases in peak demand and overloading of transformers when EVs and BESSs are charging coincidentally [30]. Thus, new mechanisms are needed to facilitate the coordination of DERs at the community level, while also taking the local transformer capacity into account. Since this scenario involves the presence of homeowners and the DSO, each with potentially conflicting objectives, the mechanism must provide a framework that enables trust, transparency, and impartiality [108].

To those ends, this chapter presents a blockchain implementation for a RETS that enables the reduction of peak demand within a community. Bidding strategies for EVs, STs, and BESSs are explicitly modeled based on homeowner preferences that characterize how DERs can be either "helpful" or "selfish", which reflect the willingness of the homeowner to alter the operational schedule of their DERs to reduce peak demand. Since BESSs are the only bi-directional DER in this work, a

fuzzy logic-based bidding strategy is proposed to handle this additional complexity, which considers parameters such as the time of day, net load, and SoC. The proposed system also enables DSOs to set demand caps on the community to limit the allowable peak demand. Simulated experiments are executed to demonstrate the proposed system's ability to reduce peak demand when the market is dominated by helpful BESSs, as well as when DSOs place demand caps on the community. The results of the simulated experiments further inform a financial assessment on ten DSOs in Ontario, Canada, which quantifies the average CAPEX savings for the DSOs by avoiding upgrades to transformer capacity as a result of the reduction in peak demand. Lastly, the proposed system is implemented on the HLF platform and deployed to the KCM, where the execution time of the proposed smart contract is benchmarked across 12 nodes, and its ability to reduce demand and minimize energy imports from the DSO is highlighted.

To summarize, the hypothesis of this chapter is that the proposed RETS is able to provide a significant reduction in the peak demand of a residential community, while also providing adequate transaction latency to satisfy the timing requirements of RETS, which typically operate in 5 minute market intervals [109].

5.2 Modeling of DERs Within a Smart Home

This section introduces the mathematical modeling of DERs within a smart home, including BESSs, EVs, PVs, and STs. The modeling of these DERs will allow baseline load profiles for a community of smart homes to be generated, such that the peak demand of the community can be quantified. To that end, the section derives several load metrics to evaluate the efficacy of the proposed system, including the total peak demand, the required CAPEX of the DSO to support the peak demand, load factor, renewable energy utilization, and total energy cost. Therefore, in gen-

eral, a set of smart homes, denoted by subscript m, possess any combination of DERs, denoted by subscript n. The variable k signifies discrete time.

5.2.1 Modeling of BESSs and EVs

A BESS is modeled as a bi-directional DER, where the power output of the BESS ($P_{BESS,m,n}$) is constrained by the maximum and minimum limits of its onboard inverter, and the SoC of the BESS ($SoC_{BESS,m,n}$), which should remain within the recommended limit of the manufacturer. The aforementioned constraints can be seen in (5.1)-(5.2), while the equation for the SoC of the BESS is derived in (5.3).

$$P^{MIN}_{BESS,m,n} \leq P_{BESS,m,n}(k) \leq P^{MAX}_{BESS,m,n} \tag{5.1}$$

$$SoC^{MIN}_{BESS,m,n} \leq SoC_{BESS,m,n}(k) \leq SoC^{MAX}_{BESS,m,n} \tag{5.2}$$

$$SoC_{BESS,m,n}(k) = SoC_{BESS,m,n}(k-1) + \Big(\chi_{m,n} \cdot \eta^{CH}_{m,n} - (1-\chi_{m,n})\eta^{DIS}_{m,n}\Big) P_{BESS,m,n}(k-1) \tag{5.3}$$

where, $\{P^{MIN}_{BESS}, P^{MAX}_{BESS}\}$ are the minimum and maximum power limits, $P_{BESS}(k)$ is the instantaneous power requirement, $\{SoC^{MIN}_{BESS}, SoC^{MAX}_{BESS}\}$ are the minimum and maximum SoC limits, $SoC_{BESS}(k)$ is the current SoC, χ is a binary variable that represents 1 for charging mode and 0 otherwise, and $\{\eta^{CH}, \eta^{DIS}\}$ are the charging and discharging efficiencies, respectively.

On the other hand, an EV is modeled as a unidirectional load, as seen in (5.4).

$$SoC_{EV,m,n}(k) = SoC_{EV,m,n}(k-1) + \Big(\chi_{m,n} \cdot \eta^{CH}_{m,n}\Big) P_{EV,m,n}(k-1) \tag{5.4}$$

The EV is subject to the same constraints as in (5.1)-(5.2), in addition to a constraint that specifies that the SoC of the EV should be greater or equal than a desired level of SoC before a target departure time, as seen in (5.5). Generally, this

constraint forces a homeowner to charge the EV to a minimum amount before the departure time to ensure that the EV has enough SoC for its trip [110].

$$SoC_{EV,m,n}(k_{Dep}) \geq SoC^{Des}_{EV,m,n}(k_{Dep}) \tag{5.5}$$

where k_{Dep} is the time of departure for an EV, $SoC_{EV}(k_{Dep})$ is the SoC at the time of departure, and $SoC^{Des}_{EV}(k_{Dep})$ is the desired SoC to be reached before the time of departure. It is worth noting that the modeling for the discharging of the EV is not covered within this thesis, where the modeling is a function of the daily driving distance of the vehicle (in kilometers - km) and the energy consumption per distance traveled (kWh/km) [111]. As in [111], it is assumed that the SoC of the EV depletes at a linear rate throughout the day, and begins to charge when it arrives at home.

5.2.2 Modeling of PVs

The direct current (DC) power generated from a PV array can be found as follows [112],

$$P^{DC}_{PV,m,n} = P^{RT}_{PV,m,n} IRR(k) F_T(T_{m.n})(k) \tag{5.6}$$

where, P^{DC}_{PV} is the DC power generated by the PV array, P^{RT}_{PV} is the nameplate rating of the PV array, IRR is the current level of irradiance in kW/m^2, T is the current temperature in °C, and F_T is an interpolated temperature factor that can be found in [112]. The alternating current (AC) power output of the PV system can then be found as follows,

$$P_{PV,m,n}(k) = P^{DC}_{PV,m,n}(k) \psi_{m,n} \tag{5.7}$$

where, $P_{PV,m,n}$ is the final AC output power of the PV system, and $\psi_{m,n}$ is the inverter efficiency that can be interpolated using methods and data found in [112].

5.2.3 Modeling of STs

The modeling of the ST depends on the dynamics of the indoor temperature of the home, which is presented below [113].

$$T_{in,m}(k) = T_{in,m}(k-1) + \beta\Delta k\Big(P_{ST,m}(k-1) - \lambda(T_{in,m}(k-1) - T_{out,m}(k-1))\Big) \quad (5.8)$$

where T_{in} is the indoor temperature (°C), Δk is the period of time between timesteps k and $k-1$, β is the inverse of the heat capacity (°C/Joules), P_{ST} is the heating power of the ST (kW), λ is the heat loss coefficient (kW/°C), and T_{out} is the outdoor temperature (°C). The equation describing the energy consumption of the ST (E_{ST}) as a function of the indoor, outdoor, and setpoint temperatures ($T_{set,m}$) is [114]:

$$\beta E_{ST,m}(k) = \lambda\beta\Delta k T_{out,m}(k) - T_{set,m}(k) - (\lambda\beta\Delta k - 1)T_{in,m}(k) \quad (5.9)$$

Rearranging, the energy consumption of the ST of a home can be formulated as:

$$E_{ST,m}(k) = \lambda\Delta k T_{out,m}(k) - T_{set,m}(k)/\beta - (\lambda\Delta k - 1/\beta)T_{in,m}(k) \quad (5.10)$$

5.2.4 Community Modeling and Derivation of Load Metrics

In general, a residential community, denoted by subscript i, is composed of a number of smart homes (N_m) and associated DERs (N_n). Thus, the peak demand of any single community, i, can be represented as:

$$P_{PEAK,i} = \max_{\forall k \in D}\left(\sum_{a=1}^{N_m}\sum_{b=1}^{N_n} P_{DER,m,n}(k) + L_m(k)\right) \quad (5.11)$$

where, D is a set of k timesteps that represent a period of time, $P_{DER,m,n}$ is the generalized form of any of the aforementioned DERs, and L_m represents critical house loads that are uninterruptible, such as lighting and appliances. To avoid

overloading the local transformer that serves the community, $P_{PEAK,i}$ must be less than the transformer capacity, denoted by $T_{CAP,i}$. If $P_{PEAK,i}$ exceeds $T_{CAP,i}$, the presiding DSO most invest in CAPEX to replace or upgrade $T_{CAP,i}$ as seen in the following equation,

$$CAPEX_i = \begin{cases} PT_{CAP,i}^{NEW} - PT_{CAP,i}^{OLD} & , P_{PEAK,i} > T_{CAP,i} \\ PT_{CAP,i}^{OLD} & , P_{PEAK,i} < T_{CAP,i} \end{cases} \tag{5.12}$$

where, PT_{CAP}^{NEW} is the price of the new transformer with upgraded capacity, and PT_{CAP}^{OLD} is the price of a transformer with the same capacity. The CAPEX calculation assumes that the transformer will be replaced at one point during its lifetime. Thus, if $P_{PEAK,i}$ does not exceed $T_{CAP,i}$, the DSO will still bear the cost of a single replacement, but will save the cost of upgrading its capacity.

Thus, the specific problem that the proposed system seeks to mitigate is to reduce the peak demand of a community by facilitating a RETS, whereby homeowners may elect to bid and trade energy during discrete intervals of the day. Each homeowner may have different strategies that would affect the price and quantity of the bid per DER, and the ability of the proposed system to utilize these bidding strategies to reduce the peak demand of the community is a key contribution of the proposed RETS. Along with the reduction of peak demand (kW) and the resultant CAPEX savings ($ CAD), several other load metrics can be utilized to evaluate the efficacy of the RETS, including total energy consumption (kWH), community cost ($), renewable energy utilization (%), and load factor (%) [115]. These load metrics will be described below.

By facilitating an energy marketplace that seeks to match local energy demand with local energy supply, there is potential to reduce the aggregate energy consumption

of a community, which may also decrease its total energy cost as well. Thus, the equations for community energy consumption, E_{COMM}, and community energy cost, E_{COST}, are formulated below:

$$E_{COMM,i} = \left(\sum_{k=1}^{\forall k \in D} \sum_{a=1}^{N_m} \sum_{b=1}^{N_n} P_{DER,m,n}(k) + L_m(k) \right) \tag{5.13}$$

$$E_{COST,i} = \left(\sum_{k=1}^{\forall k \in D} \sum_{a=1}^{N_m} \sum_{b=1}^{N_n} \left(P_{DER,m,n}(k) + L_m(k) \right) * MCP(k) \right) \tag{5.14}$$

where $MCP(k)$ is the market clearing price, or the cost of energy at timestep k, measured in \$/kWh.

Since the form of energy supply in residential marketplaces is primarily from renewables, there is also a need to measure if the renewable energy is indeed being utilized by the community, or if it is being exported to the main grid. Thus, the formula for the net energy export of a community, E_{EXP}, is described below, which sums the total energy consumption of the community *only when it is less than zero*:

$$E_{EXP,i} = \begin{cases} \sum_{k=1}^{\forall k \in D} E_{COMM,i}(k) & , E_{COMM,i}(k) < 0 \\ 0 & , E_{COMM,i}(k) >= 0 \end{cases} \tag{5.15}$$

Additionally, the formula for the total renewable energy generation of the community, E_{REN}, is as follows:

$$E_{REN,i} = \left(\sum_{k=1}^{\forall k \in D} \sum_{a=1}^{N_m} \sum_{b=1}^{N_n} \left(P_{PV,m,n}(k) + P_{BESS,m,n}(k) \right) \right) \tag{5.16}$$

Thus, the total renewable energy utilization can then be derived as:

$$E_{UTIL,i} = \frac{E_{REN,i} - E_{EXP,i}}{E_{REN,i}} \tag{5.17}$$

Lastly, since the peak demand of the community may be reduced by the marketplace, this may result in an increase for the overall load factor of the community. The load factor, P_{LF}, can be determined by taking the total community energy consumption during a period of time, D, and dividing it by the product of the peak demand and the number of timesteps in D, as described below:

$$P_{LF,i} = \frac{E_{COMM,i}}{P_{PEAK,i} * |D|} \tag{5.18}$$

where $|D|$ represents the cardinality of the set D, which is equivalent to the total number of timesteps in the set.

5.3 Overview of Residential Community Energy Marketplaces

A common method used to calculate the market clearing price (MCP) of electricity markets is the double auction method [116]. In a double auction, an auctioneer receives energy bids from market participants for each discrete market interval during the day, where an energy bid is represented by a corresponding quantity and price. The auctioneer first divides the bids into generation and load bids, and then sorts the generation bids by ascending price and the load bids by descending price, thus generating a supply curve and a demand curve, respectively. The intersection between the two curves is computed as the MCP of the market interval. Generation bids that are lower than, or equal to the MCP are granted, while load bids that are higher than, or equal to the MCP are also granted. The implementation of the

double auction method results in the merit-order effect, where the most expensive load bids are satisfied by the most inexpensive generation bids [110].

Figure 5.1 shows the double auction method that is adapted for a residential community marketplace, where generator bids can be submitted by PVs or BESSs, while load bids can be submitted by BESSs, STs, and EVs. As discussed earlier, critical loads are those house loads that cannot be interrupted, and thus, they are slotted at the highest price on the load curve. The presiding DSO is able to submit energy bids during the market interval, referred to as grid bids, and is also able to set a demand cap that limits the total community demand within the interval. As seen in Figure 5.1, a potential scenario has the demand cap placed at a vertical bid of 0.6 kWh with a corresponding price that tends towards infinity, which results in an MCP of \$0.13/kWh (MCP 1), and further results in only the critical bids being granted. As more DER penetration enters the market, the merit-order effect occurs, and more load bids are granted as a result of the MCP being lowered, as seen by MCP 2 (\$0.12/kWh) and MCP 3 (\$0.07/kWh).

5.3.1 Bidding Strategies for STs and EVs

Since a bidding curve represents a collection of energy bids that map the bid's energy quantity to a price that a homeowner is willing to pay for that quantity, a homeowner may face difficulty in determining precise values for their bid curve. Thus, the bidding curves proposed in this chapter aim to provide an intuitive, indirect method of mapping the bid quantity to the bid price by reflecting the bid quantity as a function of the DER's operational attributes. Consequently, the bid curve reflects the willingness of a homeowner to alter their DER's operational schedule, thereby adjusting its bid quantity, based on the *value* of the service it provides [110]. In the case of STs, the item of value is the flexibility of thermal

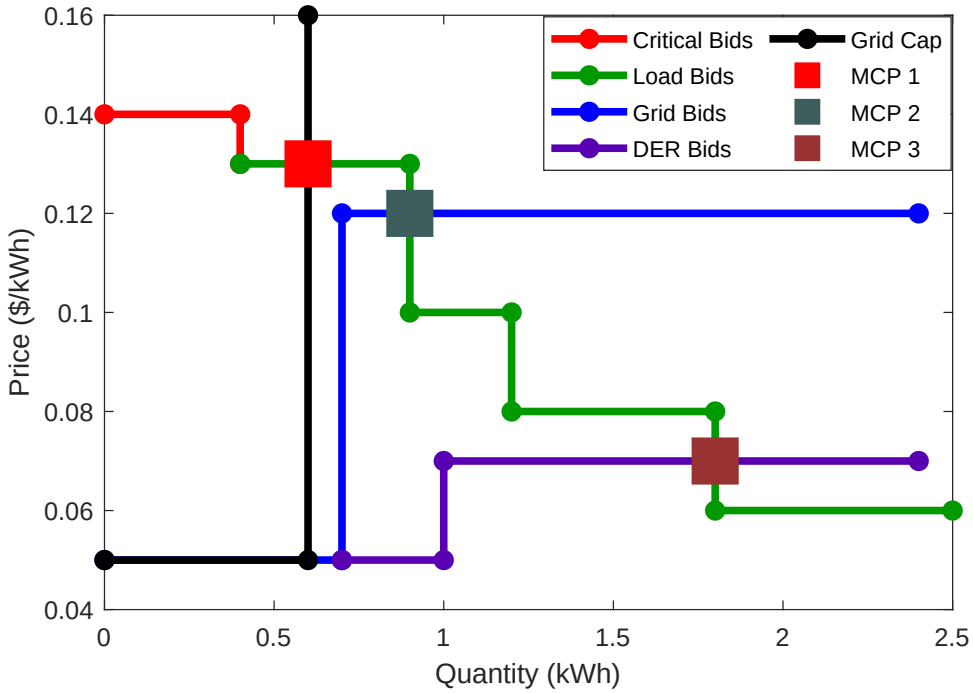

Figure 5.1: Community marketplace representation.

comfort, while in the case of EVs, the item of value is the flexibility of reaching the desired SoC before a target departure time [108]. Each point along these bid curves indirectly reflects the quantity of energy required by the DER at a price point that the homeowner is willing to pay for it, thus aligning with the bid curves depicted in Figure 5.1. Thus, this chapter considers the formulation of *selfish* and *helpful* bidding strategies, where helpful homeowners are much more willing to disrupt a DER's operating schedule in comparison to selfish homeowners. As a result, helpful DER owners generate more flexible bid curves than selfish DER owners, and therefore, helpful DER bid curves tend to have greater potential in reducing peak demand. It is worth mentioning that the classification of bidding strategies as selfish and helpful have been used widely, as in [117] and [118].

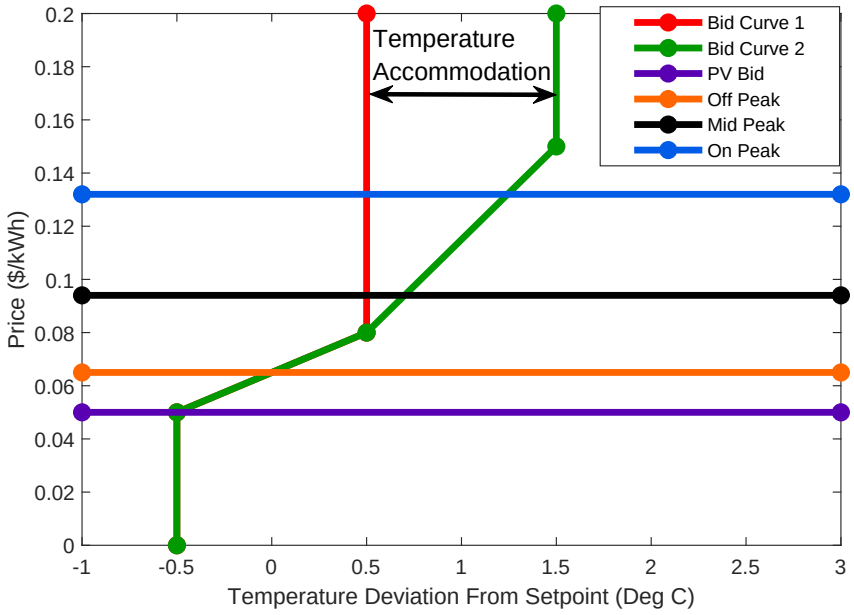

Figure 5.2: Example bid curves of STs.

For instance, Figure 5.2 depicts two separate bidding curves for STs, where the bid curves symbolize the incremental price a ST is willing to pay as a function of thermal discomfort, which can be measured by the temperature deviation from its desired setpoint [108]. Also depicted in Figure 5.2 are generation bids that follow the electricity pricing defined by typical time of use (TOU) rate plans offered by DSOs [119], where higher rates are charged during on-peak and mid-peak hours, and lower rates are charged at the off-peak hours. A sample bid of PV energy is also shown in Figure 5.2. Thus, the intersection of the ST bid curve with each of the generation bids represents the price that the ST is willing to pay per unit of temperature deviation from the setpoint, per provider of energy. As such, Bid Curve 1 can tolerate a maximum temperature deviation of +0.5 °C, from which point, the vertical line at +0.5 °C signifies that the ST will pay *any* price for its bid to be accepted and for thermal comfort to be restored. On the other hand, Bid Curve 2

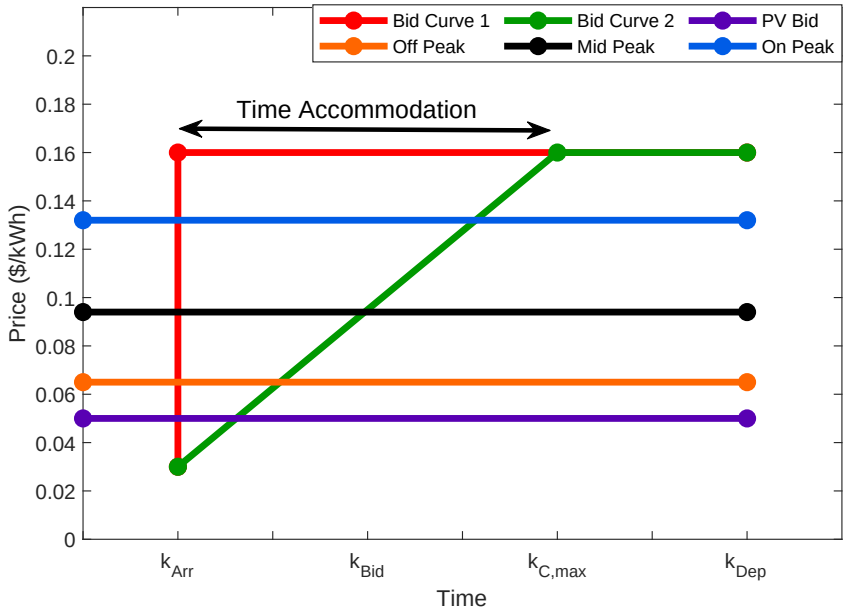

Figure 5.3: Example bid curves of EVs.

has much more flexibility, since it can tolerate a maximum temperature deviation of +1.5 °C. The difference in maximum acceptable temperature deviation between Bid Curve 1 and Bid Curve 2 is representative of how much more accommodating, or helpful, Bid Curve 2 can be in reducing peak demand. Thus, Bid Curve 2 is characterized as being more helpful than Bid Curve 1.

Similarly, bidding curves for EVs are depicted in Figure 5.3, where k_{Arr} is the arrival time of the EV, k_{Bid} is the time when the homeowner makes a bid for the EV, $k_{C,max}$ is the maximum time the EV can wait before it must charge at full power to reach a desired SoC based on the time of departure, and k_{Dep} is the time of departure of the EV. As seen in Figure 5.3, the vertical line of Bid Curve 1 at k_{Arr} indicates that at the time of arrival, the EV is willing to pay any electricity price to start charging, and that there is absolutely no flexibility or time accommodation it considers in its bidding strategy. On the other hand, Bid Curve 2 is more flexible,

and is willing to bid in the market by steadily increasing its bid price until $k_{C,max}$. At this point, the two bid curves converge, thus representing that the EVs would need maximum charging power to reach the desired SoC before k_{Dep}. Thus, it follows that the Bid Curve 2 is more helpful than Bid Curve 1 because of its willingness to provide more accommodation in terms of time.

As such, it follows that the lack of flexibility for selfish DERs inhibit their ability to participate in initiatives to reduce the peak demand of the community, as will be demonstrated in the experimental results.

5.3.2 Fuzzy Bidding Strategy for BESSs

As shown in Figures 5.2 and 5.3, the bidding curve for the STs and EVs can be formulated by a single input and a single output. However, the BESS is bi-directional in nature, and its bidding strategy must accommodate a wider range of input parameters, such as the need to retain enough SoC to provide power to critical house loads, while also being watchful of market prices to reduce its operating cost. The addition of complex input parameters requires precise numerical limits to be in place to generate a bidding curve for the BESS, which can be difficult to obtain [120]. Alternatively, fuzzy logic can be used to classify the input parameters into a set of imprecise variables, which are then evaluated against plain-language rules to generate specific outputs. The classification process involves the usage of a fuzzy membership function, which specifies the degree by which an input/output parameter belongs to specific variable, and is quantified between the range of 0 (no membership) to 1 (full membership). Since the membership function allows partial membership, the input parameters can be easily tuned, and thus, fuzzy logic is a viable option to overcome uncertainty in defining precise limits within a system [120].

As such, a fuzzy bidding strategy is proposed for BESSs in this chapter, where the block diagram of the bidding strategy can be seen in Figure 5.4. The proposed fuzzy bidding strategy has three discrete inputs, which are the time of day, the net load of the house, as well as SoC of the BESS. These discrete input variables are then fuzzified to their corresponding fuzzy variables using input membership functions, which are depicted in Figure 5.5. For the net load, the membership function defines three fuzzy variables, which are surplus (generation of home exceeds demand), deficit (demand exceeds generation), and neutral (minimal level of surplus or deficit). For the BESS SoC, the membership function also defines three fuzzy variables, which are low, medium, and high. The shape of these two membership functions are triangular, which reflect the degree of membership by which the discrete input variable belongs to the fuzzy variables. It is worthwhile to mention that the membership function for the time of day is not depicted because there is no uncertainty as to when the off/mid/on peak times are, and thus, the resultant membership function is simply binary.

After the fuzzification process classifies the input parameters into a set of fuzzy variables, the fuzzy rule set evaluates the variables and generates a set of fuzzy outputs. The fuzzy rule set depicted in Figure 5.4 aligns with the earlier mentioned methodology of classifying homeowners as selfish and helpful. In this case, a selfish BESS is motivated by financial opportunity, thereby charging at off-peak periods when the market price tends to be lower, and discharging at on-peak periods to gain maximum revenue. On the other hand, a helpful BESS is motivated by self-consumption, charging only when there is excess PV energy available during the day, and discharging during the evening off-peak period when other DERs would be drawing power to take advantage of off-peak prices. The aforementioned description of the strategies is reflected by the fuzzy rule set, where the helpful BESS seeks

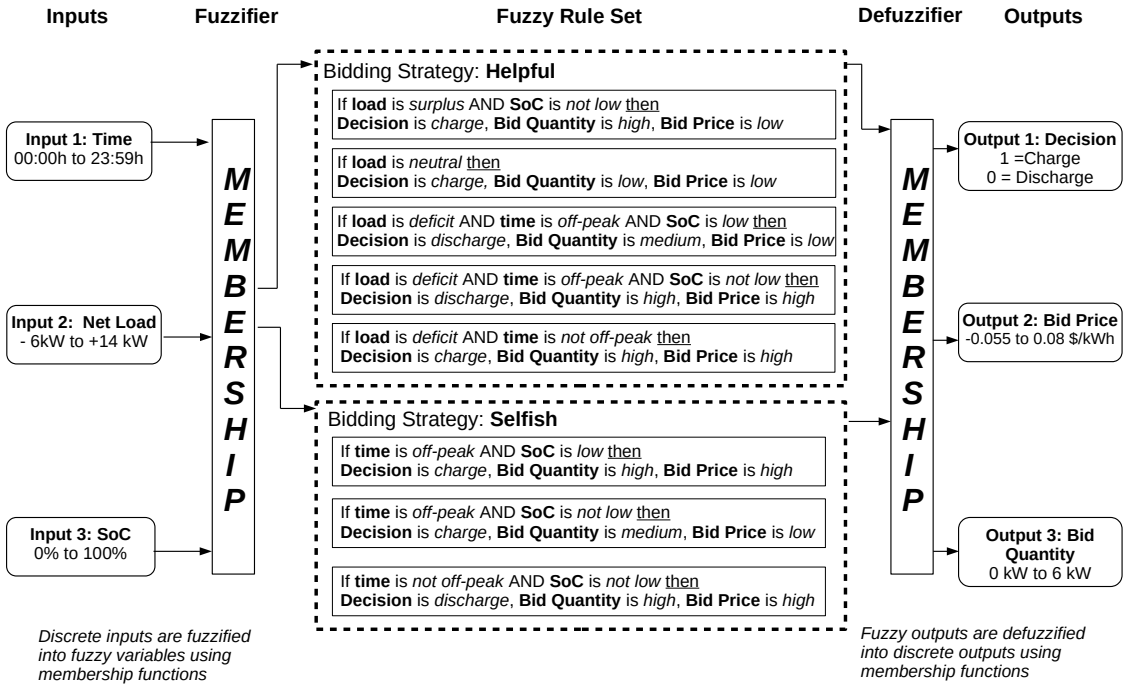

Figure 5.4: Block diagram of proposed fuzzy logic-based BESS bidding strategy.

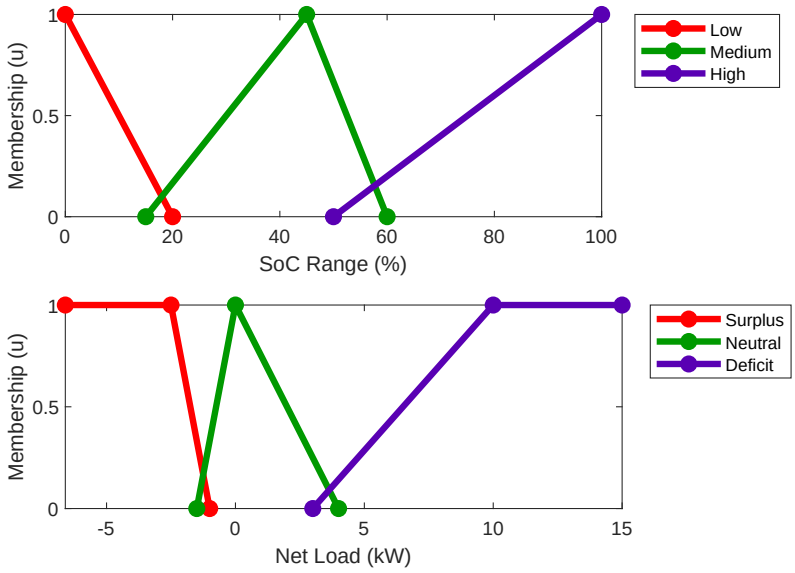

Figure 5.5: Input fuzzy membership functions.

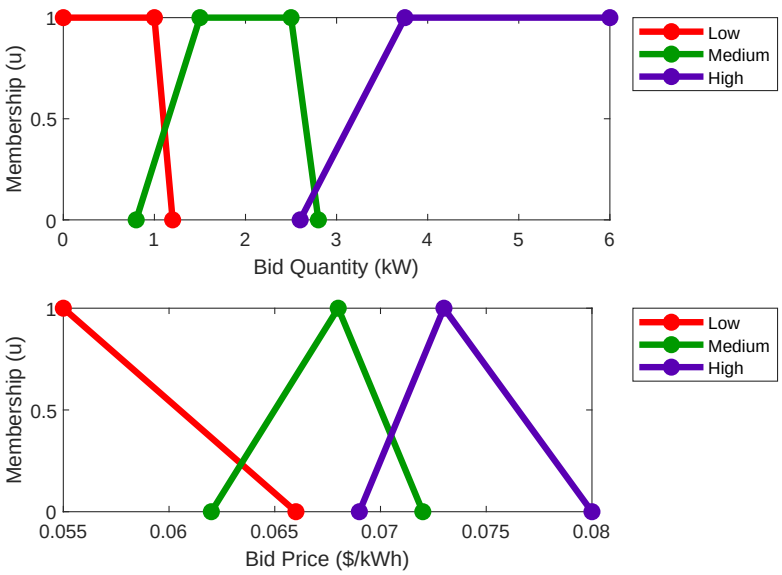

Figure 5.6: Output fuzzy membership functions.

to charge when the net load of its home is not at a deficit or when there are off-peak periods, and will vary the quantity of its bid depending on the net load. The strategy attempts to ensure that the BESS retains enough SoC throughout the day such that it can discharge in the evening off-peak period. On the other hand, the selfish BESS always discharges in off-peak periods as long as its SoC is not low, while keeping the bid price and bid quantity high to maximize revenue.

Once the fuzzy rule set evaluates the input fuzzy variables, it generates output fuzzy variables that must be defuzzified into discrete outputs using output membership functions. These discrete outputs are the charging decision, the bid price, and the bid quantity. The output membership functions that describe these variables can be seen in Figure 5.6. The charging decision variable has binary outputs, which are either to charge (1) or discharge (0), while on the other hand, both the bid price and bid quantity define variables of low, medium, and high. Combined together,

these discrete outputs completely describe the bidding strategy of the BESS with numerical values of what the bid price and quantity should be for a specific time interval during the day. It is worthwhile to mention that the membership functions seen in Figures 5.5 and 5.6 were tuned using trial and error methods with the objective of finding the best possible configuration to maximize the reduction of peak demand, as will be seen in the experimental results later on in the chapter.

5.4 Design of Permissioned Blockchain System

The proposed system is developed using HLF, which is a permissioned blockchain development platform that enables the peers within a blockchain network to be segregated into private channels [121]. Each channel is assigned a separate ledger and smart contracts, where the data on the ledger is kept hidden from other channels, thus leading to increased data privacy for the peers [122]. In this chapter, each community is designated its own channel, as can be seen in the architectural block diagram of the proposed system in Figure 5.7. The ledger stores three items, including data structures that represent a market interval, bids, and DER measurements. The market interval is represented by an interval ID, denoted by M_{ID}, the MCP for the interval, symbolized by MCP_{ID}, and the interval time expiry, denoted by TXP^{k}_{ID}. The bids, denoted as BID^{p}_{a}, are indexed according to the M_{ID}, where the $^{p}_{a}$ notation represents the identity of the homeowner. Each bid has a corresponding bid price and quantity, which are denoted as $\{PR^{p}_{a}, Q^{p}_{a}\}$, respectively, and are associated with a DER, symbolized by $DER_{m,n}$. Each bid also has a unique timestamp, denoted by TS^{k}. Measurements from each DER are also stored to the ledger, denoted by E^{p}_{a}, along with the corresponding market interval, DER, and timestamp. The smart contract provides functions that autonomously administer the marketplace, including homeowner account initialization, creating a

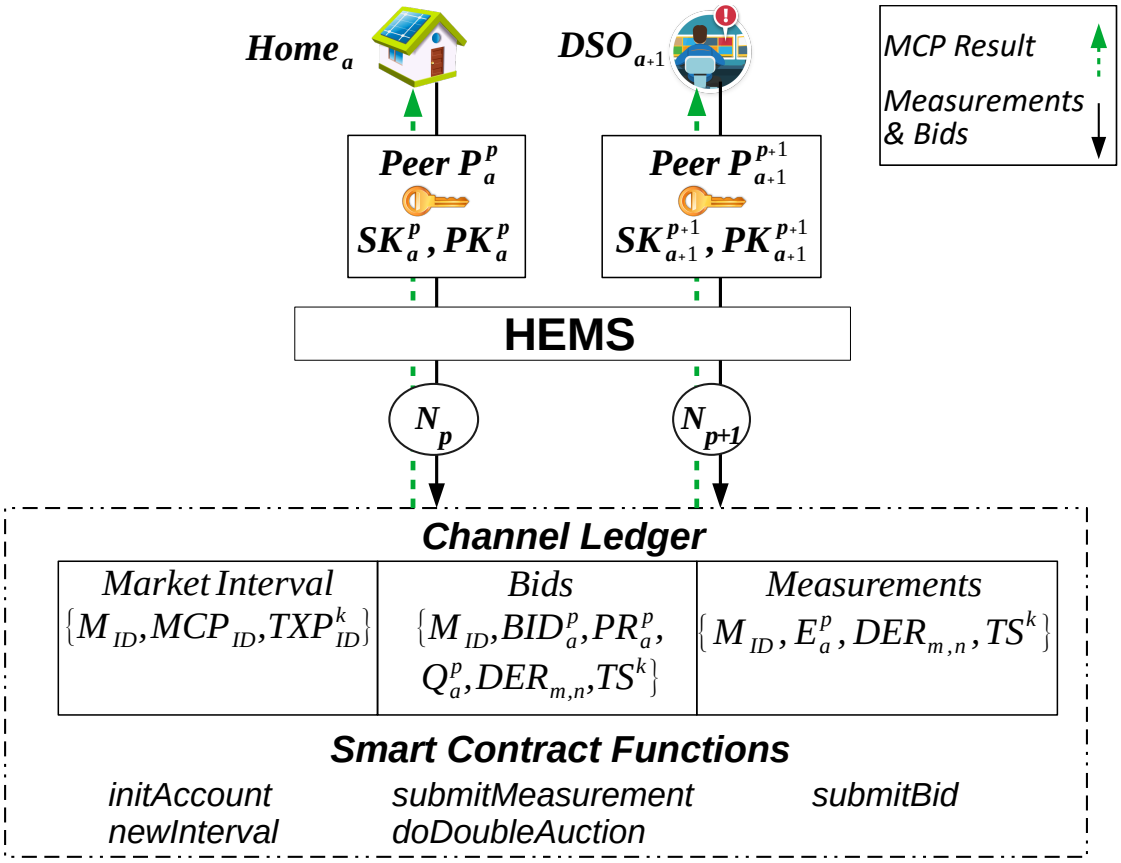

Figure 5.7: Architectural block diagram of proposed blockchain system.

new market interval, submitting bids/measurements, as well as executing the double auction to find the MCP for the market interval. Also, the presiding DSO may submit generator bids, referred to as grid bids, or demand caps for each market interval, where the demand cap is denoted by G_{CAP}. It is assumed that homeowners interact with the proposed blockchain system via the user-interface of an HEMS.

In order to provide more clarity on the implementation of the smart contract, a description of each function is provided below. Additionally, the pseudo-code that describes every function of the smart contract is provided in Algorithm 1.

initAccount(): This function initializes an account for the homeowner by generating its public/private keys ($\{SK_a^p, PK_a^p\}$), and setting the account balance to zero (B_a^p).

newInterval(): This function creates a new M_{ID} at TS^k, initializes an empty list of bids ($[BID_a^p]$) for the M_{ID}, and assigns the time expiry for the M_{ID} after a fixed time interval (TXP_{ID}^k).

submitBid(): This function is called by homeowner P_a^p, which accepts inputs of M_{ID}, PR_a^p, Q_a^p, $DER_{m,n}$, and TS^k. The function validates the incoming bid by checking if i) the homeowner has sufficient B_a^p in their wallet to make a bid for PR_a^p, and ii) if the time of the bid TS^k has not exceeded the time expiry TXP_{ID}^k. If both conditions are true, the bid is added to list of bids within M_{ID}.

doDoubleAuction(): This function executes a double auction by sorting the bids into supply and demand curves, and applying G_{CAP} if supplied. Subsequently, the MCP_{ID} is computed by finding the intersection of the curves and is broadcasted to the HEMS, which actuates the DER in accordance to the MCP.

submitMeasurement(): This function stores an energy measurement, E_a^p, on the ledger, indexed by M_{ID}, $DER_{m,n}$ and TS^k.

Algorithm 1 Proposed Smart Contract Implementation

function initAccount()

Input: Peer ID (P_a^p)

Generate SK_a^p, PK_a^p, initialize $B_a^p \leftarrow 0$

Output: $\{SK_a^p, PK_a^p, B_a^p\}$

function newInterval()

Create new market interval with time expiry, M_{ID} at TS^k

Create empty list on ledger to hold energy bids, $[BID_a^p]$

Output: $\{M_{ID}, TS^k, [BID_a^p]\}$

function submitBid()

Input: $\{M_{ID}, PR_a^p, Q_a^p, DER_{m,n}, TS^k\}$

Generate bid structure for BID_a^p based on inputs

if $PR_a^p \leq B_a^p$ && $TS^k \leq TXP_{ID}^k$

then append BID_a^p to list of bids $[BID_a^p]$

function doDoubleAuction()

Input: $\{M_{ID}, [BID_a^p], G_{CAP}\}$

Separate all bids into generation (G_{ID}) or load (L_{ID})

Sort G_{ID} by ascending price, L_{ID} by descending price

Apply G_{CAP} if supplied

Intersection of G_{ID} and $L_{ID} \rightarrow MCP_{ID}$.

Send notification to homeowner's HEMS for DER actuation.

Output: MCP_{ID}

function submitMeasurement()

Input: $\{M_{ID}, E_a^p, DER_{m,n}, TS^k\}$

Store E_a^p to ledger, indexed by $\{M_{ID}, DER_{m,n}, TS^k\}$

Additionally, to clearly depict the workflow and demarcate the information ex-

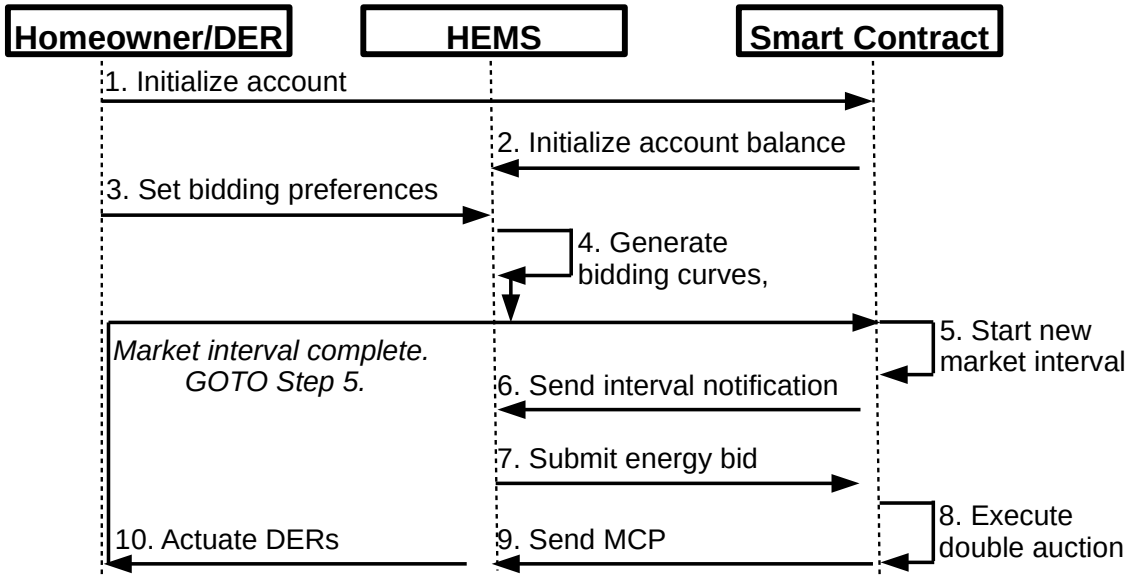

Figure 5.8: Sequence diagram of data flow across proposed system.

changes between a homeowner, HEMS, and the proposed smart contract of the blockchain-based system, a sequence diagram is shown in Figure 5.8. After registering on the blockchain network and initializing an account (steps 1-2), the homeowner configures individual preferences for their DERs as discussed in Chapter 5.3. Then, the HEMS uses the homeowner's preferences to generate bidding curves for the homeowner for each DER (steps 3-4). The smart contract then auto-creates a new market interval, and sends a notification to the HEMS to respond with a bid (steps 5-6). The smart contract collects valid energy bids from the HEMS, waits until the time expiry for the market interval has passed, calculates the MCP, and broadcasts the MCP back to the HEMS. The HEMS then actuates the DER of the homeowner according to the MCP (steps 7-10). That is, if the bid is a generation bid and its bid price is greater than equal to the MCP, or, in the case of the load bid, the bid price is lower than or equal to the MCP, the bid is granted and the DER is turned on. Its power flow is regulated by the HEMS to the precise quan-

tity of energy the DER bid for. Otherwise, the DER is turned off for the market interval. After the market interval closes, a new market interval is started after a configurable period of time, and steps 5-10 are repeated indefinitely.

5.5 Experimental Results

This section presents the results of the proposed RETS in both simulated and real-world settings. First, the experimental methodology will be provided, which describes the equipment used to conduct the experiment, the SLD of the KCM that the experiments were conducted at, the experimental variables, as well as the experimental methods. Following this, the results of the simulated experiments will be provided, followed by the results of the real-world experiments.

5.5.1 Experimental Methodology

5.5.1.1 Experimental Equipment

The simulated experiments revolve around the modeling, simulation, and control of an 8 home, all-electric residential community. The nameplate ratings of the DERs used within the simulated experiments can be found in Table 5.6. On the other hand, real-world experiments are executed at the KCM. A single line diagram of the microgrid is provided in Figure 5.9, while the nameplate ratings of its DERs are provided in Table 5.6. There are 4 individual buildings at the KCM, which are the solar hut, wind hut, as well as Smart Homes A and B. The solar hut is equipped with 30 kW of PV, although only 12 kW were connected at the time of the experiment. The wind hut contains 20 kW of wind power capacity, a 75 kWh BESS, as well as a 6 kW electric load (E-Load). Downstream of the solar and wind huts, smart home A has a Level 2 charging station used for charging an on-premises EV (Nissan

Table 5.6: Nameplate Ratings of DERs Used in Experiments.

DER	Nameplate (Simulated)	Nameplate (Real-World)
PV	5 kW	SolarEdge 6000H, 2 x 6 kW
BESS	6 kW, 25 kWh	-
EV	6 kW, 45 kWh	Nissan Leaf 6 kW, 45 kWh
ST	0-2 kW	6 kW (E-Load)

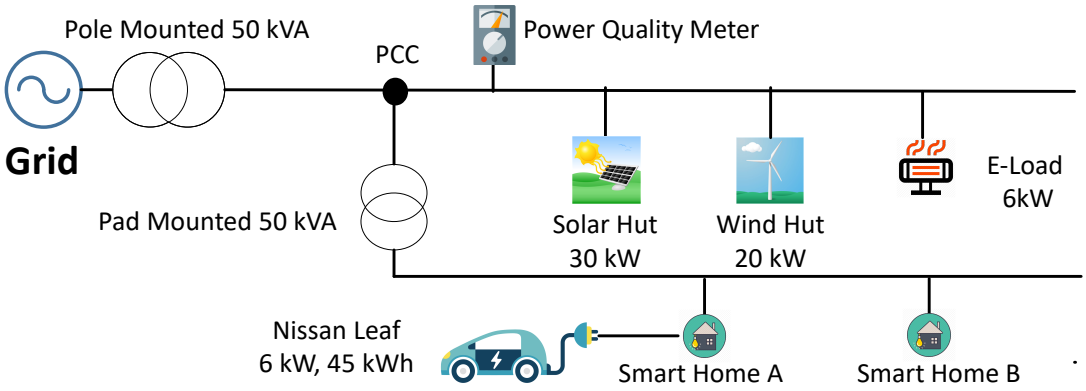

Figure 5.9: Single line diagram of the KCM used for validating the RETS.

Leaf), while smart home B has a 5 kW PV array. Each building is equipped with a gateway device (either a Raspberry Pi or desktop machine), that communicates with the blockchain network via a REST API. The model of the Raspberry Pi's used within the experiments is the Raspberry Pi B+, which has a 700 MHz processor and 512 MB RAM, while the desktop machine has a 2.2 GHz processor with 8 GB RAM that is running Ubuntu 16.04 operating system and HLF version 1.4.

5.5.1.2 Experimental Variables

For the simulated experiments, two independent sets of data are used, which include a summer data set (July 20-27, 2016), as well a winter dataset (Feb 1-Feb 8,

2016). The data includes measurements from sensors at the KCM, which provide observations for irradiance, indoor temperature, power generation/consumption of all controllable DERs, as well as the power consumption of typical critical loads for the home, including lighting, dishwasher, fridge, stove, among other standard appliances. In terms of the bidding prices, the following list identifies the specific parameters used to generate energy bids for each DER, depending on if the configuration of their DER preferences are selfish or helpful.

- Grid: TOU prices of 2018, plus regulatory and delivery charges. Off-peak bids at \$0.09435/kWh, mid-peak bids at \$0.1259/kWh, and on-peak bids at \$0.1673/kWh
- PV: Static bidding at \$0.05/kWh
- ST: Maximum bidding price of \$0.1673/kWh, curve based on following configurations:
  - Helpful: Between 0°C and 4°C setpoint deviation allowed.
  - Selfish: Between 0°C and 1°C setpoint deviation allowed.
- EV: Maximum bidding price of \$0.1673/kWh, curve based on following configurations:
  - Helpful: Bidding ranges between \$0.05/kWh - \$0.09435/kWh (arrival to departure)
  - Selfish: Bidding ranges between \$0.05/kWh - \$0.1673/kWh (arrival to departure)
- BESS: Maximum bidding price of \$0.12/kWh, curve based on following configurations:

– Helpful: Charging at $0.06/kWh, Discharging at $0.08/kWh

– Selfish: Charging at $0.10/kWh, Discharging at $0.12/kWh

5.5.1.3 Experimental Methods

The simulated experiments are conducted on a testbench desktop application that is developed as a part of this work, where a workflow diagram of the testbench is depicted in Figure 5.10. First, the bidding preferences for each DER of each homeowner are configured as selfish or helpful. Second, weather data (indoor/outdoor temperature and irradiance) and electricity prices are separated into 5 minute market intervals and loaded into the testbench. Third, the load profile of the community is generated by equations Eqs (5.1)-(5.10) for every discrete market interval, and the bidding strategies for all DERs are then executed to generate bids for the market interval. The bids are evaluated by the proposed smart contract to generate the MCP for the market interval, and the MCP is fed back into the community model to determine the energy consumption/generation for each DER. When all market intervals have been evaluated, the testbench exports the resultant load profile of the community to a data file to calculate the load metrics described in Eqs (5.11)-(5.18).

The real-world experiments are conducted at the KCM in a similar manner to the simulated experiments. The configuration of the bidding strategies and the pricing remains the same, however, the measurements and bids generated from the DERs are collected by the RETS in real-time. Each DER is governed by a gateway device, which is connected to the RETS by a REST API, that is developed to submit bids and measurements to the blockchain ledger, as well as to monitor the result of the MCP calculation. Once the smart contract finds the MCP, a notification is received by the gateway device of the building, and the relevant DER is dispatched

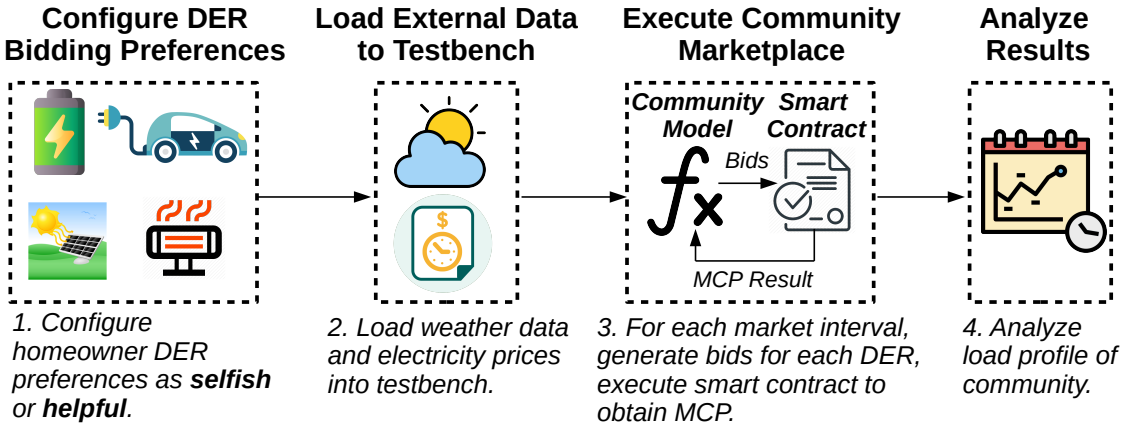

Figure 5.10: Workflow of testbench used to evaluate experimental results.

accordingly.

5.5.2 Results From Simulated Experiments

5.5.2.1 Experiment 1: Benchmarking of Proposed System

The objective of the first experiment is to benchmark the proposed system's scalability by observing its transaction latency as a function of increasing nodes. The benchmarking is performed as per the monte carlo-based methodology defined in [123], where eight client applications are launched simultaneously, which invoke the *submitBid* and *doDoubleAuction* methods of the smart contracts for 1000 iterations. The consensus mechanism used for the benchmark is pBFT. The number of nodes participating in the pBFT consensus process is varied from 2 to 12 in order to determine their effect on the overall execution time of the aforementioned functions. It is important to reiterate that the number of nodes does not equal the number of homeowners engaging in energy trading within the proposed system. As explained in Chapter 2, multiple peers, or in this case, homeowners, can be assigned to a single node, and interact with the node using a client application.

Thus, the number of active client applications is the true measure of the number of homeowners engaging in the trading process.

To facilitate the benchmarking of the trading process, the ledger is loaded with 1000 bids from 8 different client applications using the *submitBid* function, and the MCP is calculated for the 1000 bids for 1000 iterations using the *doDoubleAuction* function. The consensus execution time, otherwise referred to as the transaction latency, is calculated by recording the timestamp at the transaction proposal stage and subtracting it from the timestamp recorded as soon as the transaction is committed to the ledger. The block size and block speed are retained from the default settings as 10 transactions per block, and 2 seconds, respectively.

The benchmarking results can be seen in Figure 5.11, where the *submitBid* function has little latency differential from 2 nodes (3.62 s) to 12 nodes (5.72 s). This is in contrast to the *doDoubleAuction* function, where the latency differential almost triples from 3.5 s at 2 nodes to 11.4 s at 12 nodes. At 12 nodes, the latency of the *doDoubleAuction* function is roughly double of the *submitBid* function, which is to be expected, since the computational complexity of the former is greater than the latter. Nonetheless, even at 12 nodes, the proposed system demonstrates good scalability, where the total transaction time of both functions at 12 nodes is 17.12 s, which is sufficient to execute RETS, where typical market intervals operate in the time resolution of minutes [109].

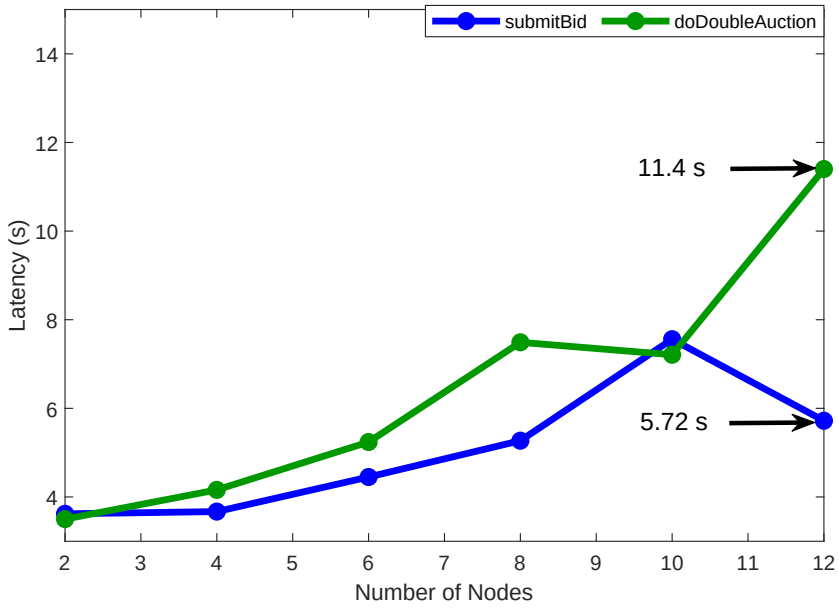

Figure 5.11: Transaction latency of proposed RETS as a function of increasing nodes.

5.5.2.2 Experiment 2: Impact of Helpful Bidding Strategies on Peak Demand

The objective of this experiment is to determine the impact of helpful bidding strategies on the peak demand of the community. To begin with, the impact of the helpful BESS bidding strategy will be determined. First, a baseline is established, whereby each homeowner within the 8-home community is configured to have a selfish strategy for their BESS, EV, and ST, as depicted in Figure 5.10. Subsequently, the strategy distribution of the BESSs is incremented by one helpful BESS at a time, with community load profiles being generated from a distribution of 8 selfish BESSs and 0 helpful BESSs, to 0 selfish BESSs and 8 helpful BESSs. This type of sensitivity analysis is useful in isolating the impact of the BESS bidding strategy on the peak demand of the community. While the strategy distribution

of the BESS bidding strategy is being manipulated, observations are also recorded for the net cost for the community ($), the total energy consumption (kWH), the load factor (%), as well as the renewable energy utilization.

The results of the aforementioned sensitivity analysis for the summer data set can be seen in Figure 5.12 and Figure 5.13. As seen in the figures, increasing the amount of helpful BESSs has a direct impact on reducing the community peak load, as well as the community cost. The peak load reduces from 101.7 kW when there are 8 selfish BESSs, to 53.3 kW when there are 8 helpful BESSs, which is a decrease of 62%. Similarly, the community cost decreases from $252.1 to $240.8, which is a decrease of 4.76%. To highlight the full impact of the helpful BESSs, the load profiles of two scenarios are plotted in Figure 5.14, where the first load profile is the baseline load profile where all DERs are configured as selfish, and the second load profile has a configuration of 8 helpful BESSs. As seen in Figure 5.14, the daily peak reduction is significant due to the presence of helpful BESSs.

Furthermore, Figure 5.15 shows the difference in behavior of helpful BESSs and selfish BESSs as a function of their power output. As seen in the figure, the daily peak demand aligns with the coincident charging of selfish BESSs, while during the same time frame, helpful BESSs tend to discharge (negative values for power output signify that the BESS is discharging). Thus, helpful BESSs play a dominant role in reduction of peak demand for the community, and contribute a maximum cumulative reduction of 40.8 kW, which is 85% of the total reduction observed during the time of the study.

Further load metrics are provided in Table 5.7, which indicate that the presence of helpful BESSs lead to significant increases in load factor (from 14% to 27%), and renewable energy utilization (69% to 93%). The increase in renewable energy utilization is primarily due to the fact that the helpful BESSs seek to charge with

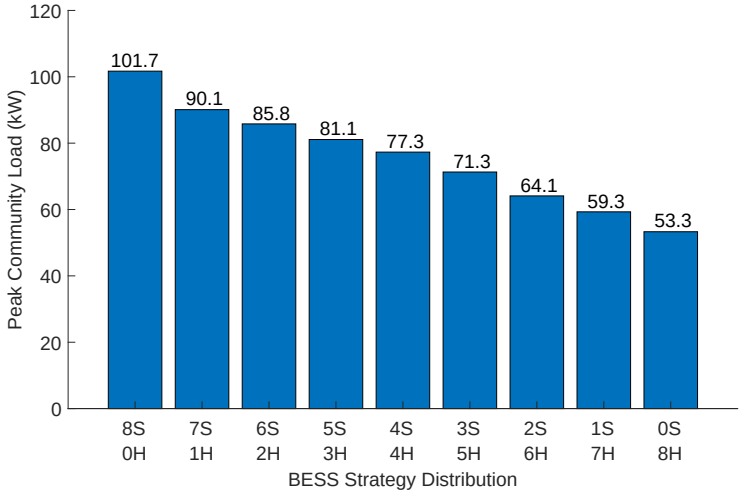

Figure 5.12: Impact of helpful BESSs on peak demand.

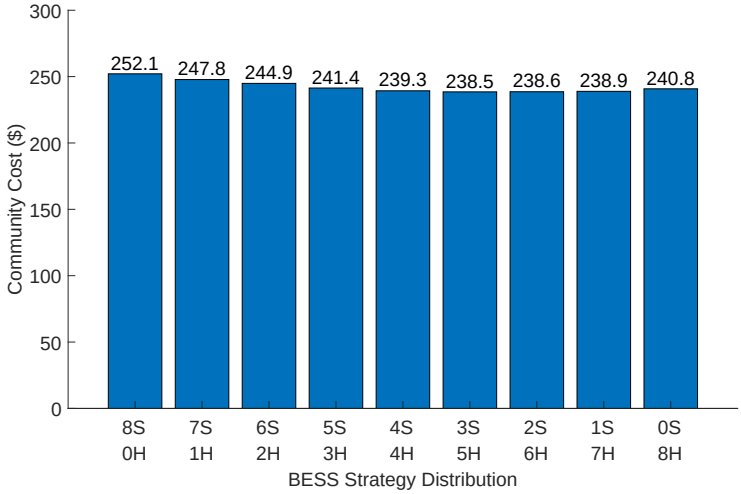

Figure 5.13: Impact of helpful BESSs on community cost.

any excess renewable power available throughout the day-time, when PV power is abundant. The increase in load factor is again impacted significantly by the helpful BESSs that discharge at off-peak hours, where the consumption of EVs would be at their highest. There is also a reduction in weekly energy consumption between the two scenarios, which is observed to be 54.9 kWh, or 2.23%.

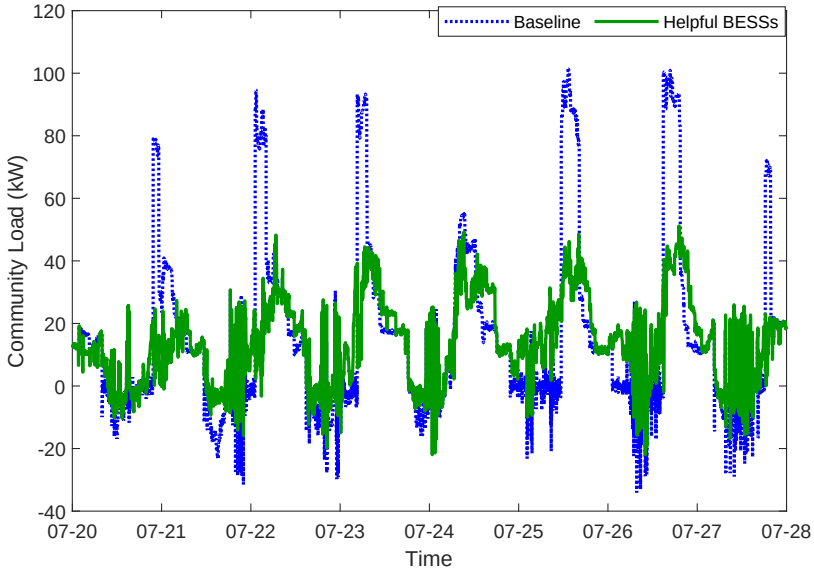

Figure 5.14: Load profile comparison of a community between baseline and helpful BESSs for summer dataset.

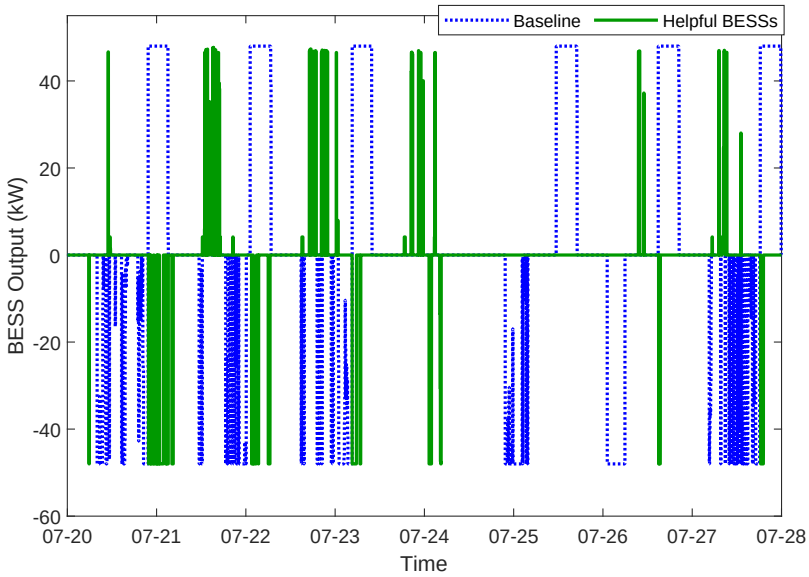

Figure 5.15: Power output of selfish and helpful BESSs.

Table 5.7: Comparison of load metrics for baseline and helpful scenarios for summer dataset.

Metric	Baseline	8 Helpful BESSs
Weekly Energy Consumption (kWh)	2411.0	2356.1
Peak Load (kW)	101.7	53.3
Load Factor (%)	14	27
Renewable Energy Utilization (%)	69	93

It is worthwhile to mention that the STs also have a role to play in the reduction of the peak load. By closely following the MCP, STs are able to pre-cool their homes when the MCP is lower and reduce their consumption by adjusting their cooling needs when the MCP is high. This can be seen in Figure 5.16, where the MCP hovers around the \$0.05/kWh mark from the period of 8:00 to 16:00. The MCP is driven to this mark because of the excess generation of inexpensive PV energy during the day. During this time frame, the STs increase their electrical consumption to pre-cool their homes. On the other hand, the spiking of the MCP to \$0.12/kWh after 17:00 causes the STs to decrease their electrical consumption.

The experiment is repeated for the winter dataset, with the weekly load profile comparison presented in Figure 5.17, and the load metric comparison presented in Table 5.8. As seen in the table, against the baseline scenario, the presence of 8 helpful BESSs results in a peak reduction from 114.4 kW to 62.5 kW, which is a reduction of 45%. There is also a noticeable increase in load factor, from 25% to 41%, which represents an increase of 64%. Further, there is a significant decrease in overall energy consumption, from 4820.3 kWh, to 4258.7 kWh, which is a decrease of 11.6%. There is negligible improvement in the renewable energy utilization, primarily because the utilization is already quite high at 93%.

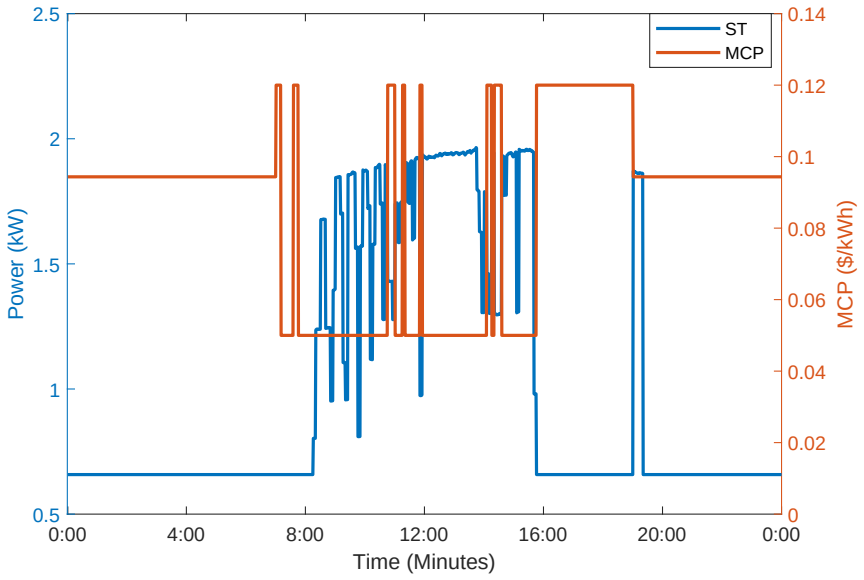

Figure 5.16: Power consumption of helpful STs that follow the MCP.

Recalling that the peak demand reduction from the summer dataset is 52%, it can be observed that the helpful bidding strategy does not perform as well in the winter as it does in the summer. This can be explained by the fact that there is much less PV energy available in the winter when compared to the summer, and as such, helpful BESSs are not able to charge completely during the daytime. This means that the helpful BESSs cannot discharge as effectively during the evening when the peak loading occurs. This is illustrated in Figure 5.18, where the figure shows the SoC of selfish and helpful BESSs, and it can be seen that the selfish BESSs are able to reach 100% SoC on a daily basis, while helpful BESSs are not.

Nevertheless, a winter peak demand of 62.5 kW translates into a peak apparent load of 69.5 kVA, assuming a typical residential power factor of 0.9 [30]. This means that DSOs would need to replace all 50 kVA distribution transformers with 75 kVA transformers to support the peak demand. This results in CAPEX savings

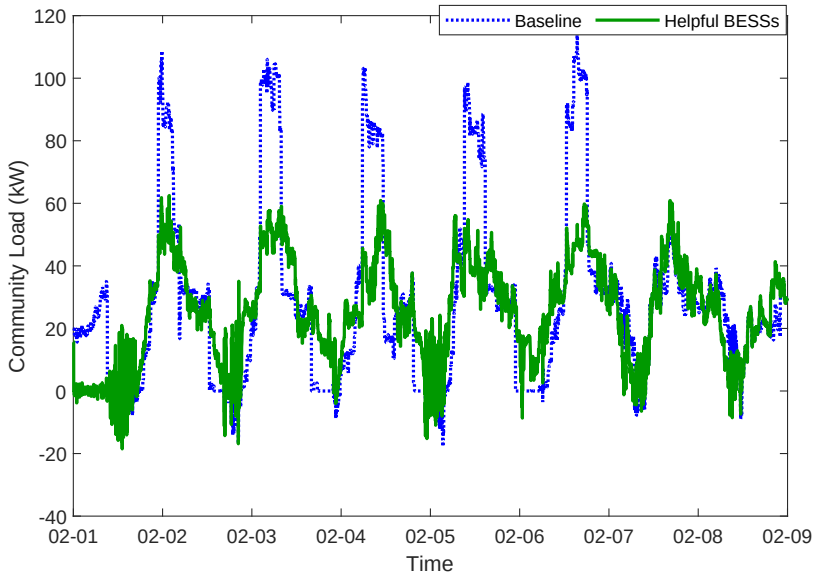

Figure 5.17: Load profile comparison of a community between baseline and helpful BESSs for winter dataset.

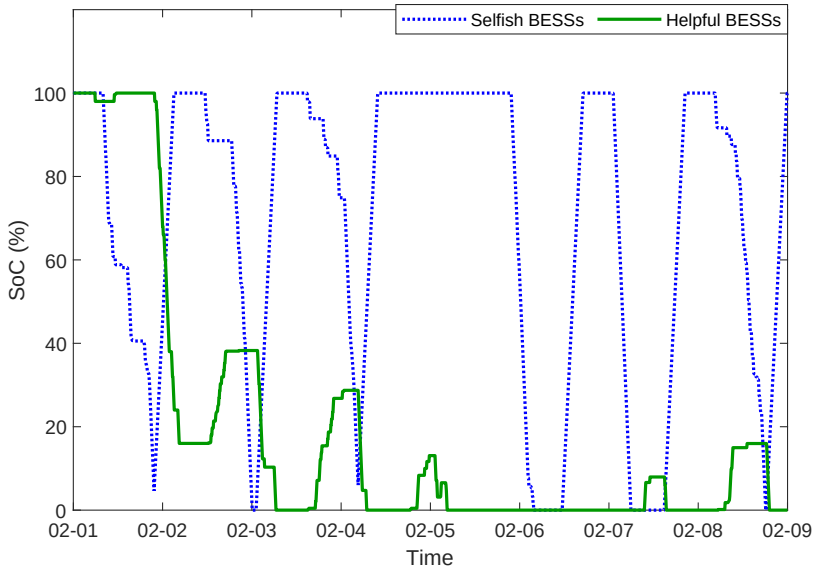

Figure 5.18: SoC comparison between helpful and selfish BESSs for winter dataset.

Table 5.8: Comparison of load metrics for baseline and helpful scenarios for winter dataset.

Metric	Baseline	8 Helpful BESSs
Weekly Energy Consumption (kWh)	4820.3	4258.7
Peak Load (kW)	114.4	62.5
Load Factor (%)	25	41
Renewable Energy Utilization (%)	93	95

for DSOs as compared to the baseline scenario, where the peak demand is recorded as 101.7 kW (113 kVA), and the capacity of the transformer would need to be upgraded to 125 kVA. The overall CAPEX savings for a DSO is approximately $2,340 per transformer according to the transformer prices found in [124]. Thus, the resultant CAPEX savings generated by the proposed RETS for 10 DSOs in Ontario, Canada, can be found using (5.12), where the results of this financial assessment are presented in Table 5.9. As seen in the table, the proposed RETS is able to provide an average of $56.8M, or 31.6%, of CAPEX savings for each DSO.

Table 5.9: CAPEX savings for DSOs with a reduced peak demand of 62.5 kW.

DSO	Transformer Replacements	Baseline CAPEX ($)	RETS CAPEX ($)	CAPEX Saved ($)
Alectra Utiliites	102,260	756.5 M	517.2 M	239.3 M
Toronto Hydro	54,081	400.1 M	273.5 M	126.6 M
Hydro Ottawa	42,348	313.3 M	214.2 M	99.1 M
London Hydro	13,535	100.1 M	68.5 M	31.7 M
Kitchener-Wilmot	9,583	70.9 M	48.5 M	22.4 M
Waterloo North	7,354	54.4 M	37.2 M	17.2 M
EnWin Utilities	5,963	44.1 M	30.2 M	17.2 M
Halton Hills Hydro	3,622	26.8 M	18.3 M	8.5 M
Essex Powerlines	2,774	20.5 M	14.0 M	8.5 M
Lakefront Utilities	1,104	8.2 M	5.6 M	2.6 M
Averages	24,262	179.5 M	122.7 M	56.8 M

5.5.2.3 Experiment 3: Impact of Demand Caps on Peak Demand

The objective of this experiment is to determine the impact of DSO-provided demand caps on the peak demand of the community. As such, two types of demand caps are experimented with, which are quantity demand caps (Q-caps), as well as price demand caps (P-caps). For Q-caps, the quantity of the cap is set to 40 kW, while the price is set to the TOU price for every market interval during the simulation. For the P-Cap, the quantity is again capped at 40 kW, however, the price of the cap is twice as much as the TOU price. The bidding preferences for the community remain the same as used in the previous experiment, where 8 helpful BESSs are used.

Table 5.10: Comparison of load metrics for demand cap scenarios for summer dataset.

Metric	8 Helpful BESSs	40 Q-Cap	40 P-Cap
Weekly Energy Consumption (kWh)	2356.1	2356.1	1493.9
Peak Load (kW)	53.3	49.6	41.7
Load Factor (%)	27	28	21
Renewable Energy Utilization (%)	93	93	93
Community Cost ($)	231.4	231.4	299.7

The impact of demand caps can be seen in Figure 5.19, while relevant load metrics are provided in Table 5.10. As seen in the figure, although both the Q-Cap and P-Cap are able to reduce the peak demand on all days of the week, their maximum peak is still above 40 kW (49.6 kW for the Q-Cap, 41.71 kW for the P-Cap). Several reasons cause this behavior. First, critical loads represent 17 kW, or 42.8% of the P-Cap peak load, and these critical loads must be served regardless of high the MCP is. Second, there is a limit to how helpful the DERs can be with respect to the theoretical limits of their bidding curves. To illustrate this, a plot of the SoC of the EVs is presented for both Q-Cap and P-Cap scenarios in Figure 5.20. As seen in the figure, the plot of the P-Cap shows that the EV never gains a full charge during the week because of the doubling of the MCP, whereas, an EV in the Q-cap scenario retains a full charge at the start of every day. It is also worthwhile to mention that the community energy costs in the P-Cap scenario rise significantly from $231.43 to $299.72, which is an increase of 22.7%, also due to the rise in MCP.

For the sake of completion, a similar analysis is done for the winter dataset. The weekly load profile is provided in Figure 5.21, while the accompanying load metrics are provided in Table 5.11. In this case, the P-Cap is able to reduce the community

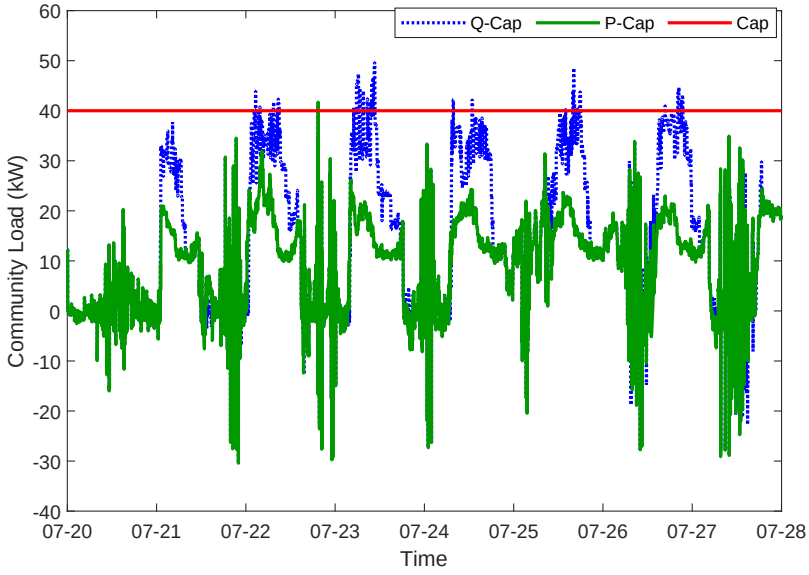

Figure 5.19: Peak reduction of community after demand caps are applied.

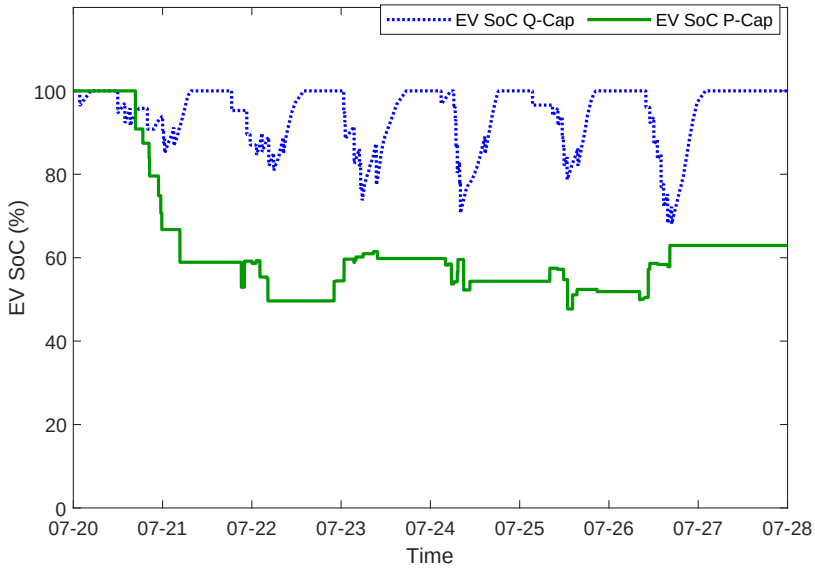

Figure 5.20: SoC of EVs when demand cap is enforced.

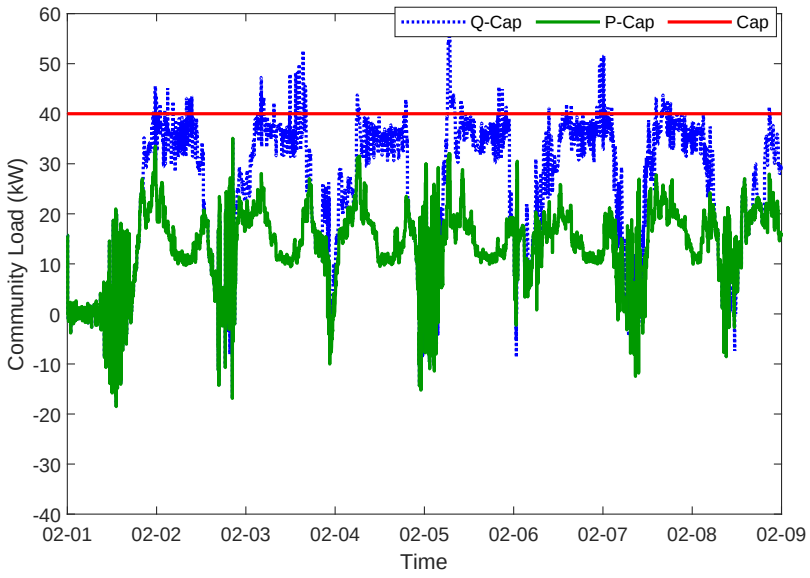

Figure 5.21: Peak reduction of community after demand caps are applied for winter dataset.

peak load from 62.5 kW to 35.1 kW, which is a reduction of 43.8%. However, the community cost also rises from $462.58 to $529.7, which is an increase of 12.7%.

From the CAPEX savings point of view, the ability of the proposed RETS to drive the peak demand down to a maximum of 41.7 kW (46.3 kVA) means that DSOs would not need to upgrade their existing 50 kVA distribution transformers. Deducting the cost of replacing the 50 kVA transformers once during their expected lifetime, the computed CAPEX saving is $7398 per transformer as per the transformer pricing in [124]. Thus, the resultant CAPEX savings are presented in Table 5.12, where the proposed RETS is able to provide an average of $102.5 M (or 57.1%) of CAPEX savings for the DSOs under study.

Table 5.11: Comparison of load metrics for demand cap scenarios for winter dataset.

Metric	8 Helpful BESSs	40 Q-Cap	40 P-Cap
Weekly Energy Consumption (kWh)	4258.8	4192.6	2303.6
Peak Load (kW)	62.5	56.0	35.1
Load Factor (%)	41	45	39
Renewable Energy Utilization (%)	96	95	94
Community Cost ($)	462.6	457.2	529.7

Table 5.12: CAPEX savings for DSOs with a reduced peak demand of 41.7 kW.

DSO	Transformer Replacements	Baseline CAPEX ($)	RETS CAPEX ($)	CAPEX Saved ($)
Alectra Utiliites	102,260	756.5 M	324.4 M	432.1 M
Toronto Hydro	54,081	400.1 M	171.2 M	228.5 M
Hydro Ottawa	42,348	313.3 M	134.3 M	179.0 M
London Hydro	13,535	100.1 M	42.9 M	57.2 M
Kitchener-Wilmot	9,583	70.9 M	30.4 M	40.5 M
Waterloo North	7,354	54.4 M	23.3 M	31.1 M
EnWin Utilities	5,963	44.1 M	18.9 M	25.2 M
Halton Hills Hydro	3,622	26.8 M	11.5 M	15.3 M
Essex Powerlines	2,774	20.5 M	8.8 M	11.7 M
Lakefront Utilities	1,104	8.2 M	3.5 M	4.7 M
Averages	24,262	179.5 M	76.9 M	102.5 M

5.5.3 Results From Real-World Experiments

5.5.3.1 Experiment 4: Energy Trading at KCM

The execution of the real-world experiments involves the participation of the PV of the solar hut, the EV of Smart Home A, the E-Load of the wind hut, as well as the critical loads of Smart Home B. The objective of this case study is to demonstrate energy trading between the three aforementioned DERs. Figures 5.22 - 5.24 show the results of 3 consecutive bidding cycles, while Figure 5.25 shows the individual load profile of all three DERs, including measurements from the PCC of the microgrid to the main distribution grid. The sign of the PCC measurements indicates whether the microgrid is exporting (negative) or importing (positive) power from the main grid. All bids from the DERs are submitted using the *submitBid* function, while the MCP is found by executing the *doDoubleAuction* function, which is triggered for every 2 minute market interval.

A description of all three bids is as follows:

- Bid #1 Market Interval: 11:51:10 to 11:53:10
  - **Bid Details:** As seen in Figure 5.22, the E-Load bids at \$0.10/5 kWh, while PV bids at \$0.05/10 kWh. The EV is assumed to have just arrived home and is on standby power (1.4 kW), which is counted as a critical load. With the critical loads of Smart House B being roughly 1.6 kW, the resultant critical load bid is \$0.1/3 kWh.
  - **Result:** All bids are accepted at an MCP of \$0.05/kWh. The PV of the KCM is able to satisfy its entire load.
- Bid #2 Market Interval: 11:53:10 to 11:55:10

- **Bid Details:** As seen in Figure 5.23, the EV requires charging and bids at \$0.15/5 kWh, which outbids the bid of the E-Load at \$0.10/6 kWh. The critical load bid is unchanged.
- **Result:** The PV of the KCM cannot satisfy the total demand bid into the market. The MCP for this market interval is calculated at \$0.1/kWh, which grants the bids of critical loads and EV, while denying the bid of the E-Load.

- Bid #3 Market Interval: 11:55:10 to 11:57:10
  - **Bid Details:** As seen in Figure 5.24, The E-Load upgrades its bid to \$0.20/6 kWh, while the critical load and EV bids are unchanged.
  - **Result:** The upgraded E-Load bid pushes the MCP to \$0.16/kWh, which matches the TOU bid price of the grid. This results in the KCM importing roughly 1 kWh from the main grid to satisfy all three loads.

A time series graph of the experiment is provided in Figure 5.25, which reflects the load profile of the DERs during all three bidding cycles. The PV output remains constant throughout the experiment, while the measurement at the PCC fluctuates as a result of the EV and E-Load being turned on and off. Prior to the first bidding cycle, the E-Load is off, while the EV draws 1.4 kW of standby power. At this point, the KCM is still exporting approximately 1.5 kW of its PV generation, which can be determined by taking the difference from the total PV generation (10 kW) and the total demand at the PCC (-8.5 kW). With the result of the first bidding cycle dictating that only the E-Load is turned on, the E-Load begins to consume its full bid quantity of 6 kW, which can be seen in Figure 5.25 since there is a corresponding spike of 6 kW in the plots of the PCC and E-Load.

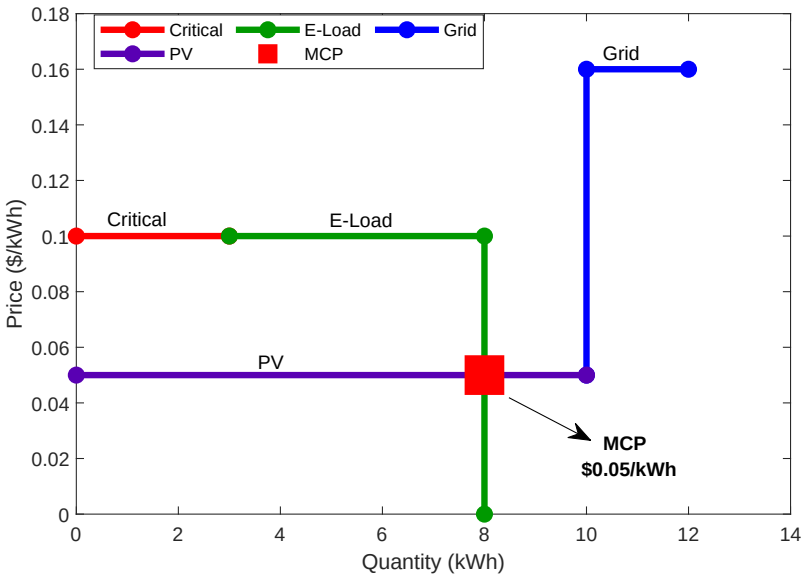

Figure 5.22: Bid #1: PV energy satisfies entire KCM demand.

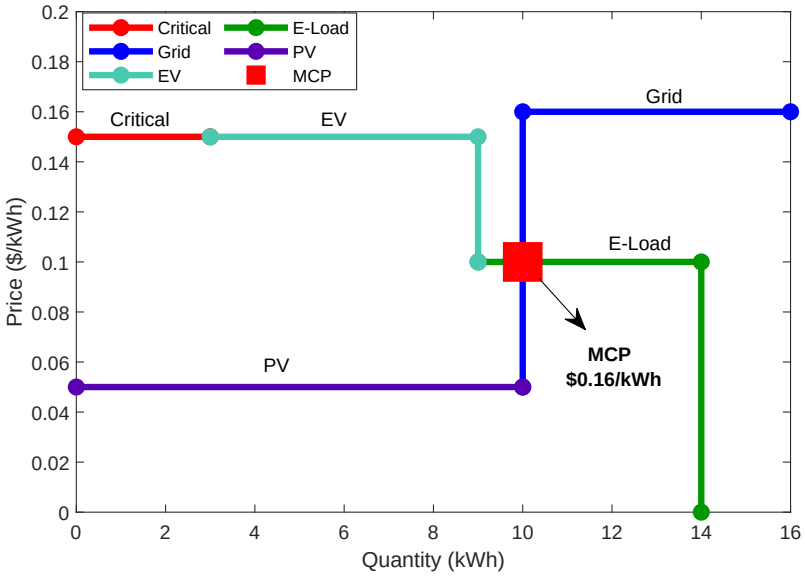

Figure 5.23: Bid #2: E-Load is turned off due to being outbid by the EV.

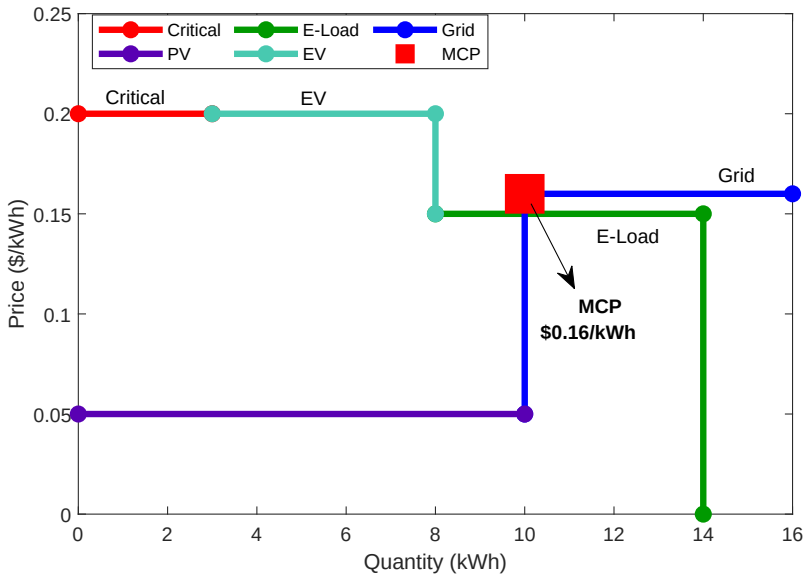

Figure 5.24: Bid #3: KCM requires grid import due to high bids from EV and E-Load.

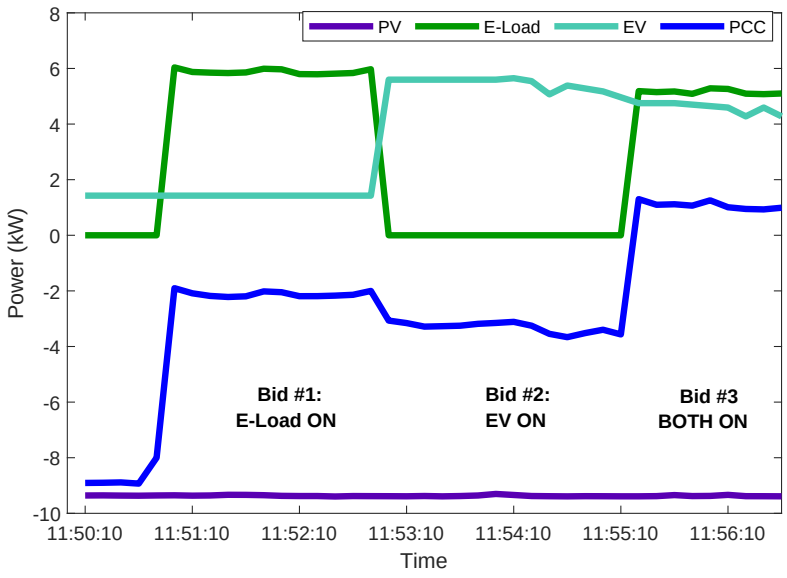

Figure 5.25: Load profile of DERs during all three bids.

In the second bidding cycle, the EV outbids the E-Load, which results in the EV being allowed to consume its full bid quantity of 6 kW, while the E-Load is turned off. This can be seen in Figure 5.25, where the plot of the E-Load reports zero consumption, and the plot of the EV shows its power consumption nearing 6 kW. Finally, in the third bidding cycle, both the EV and E-Load win their bids and are turned on. This results in the plot of the PCC turning positive for the first time in Figure 5.25, indicating that the KCM is importing approximately 1 kW from the main grid to satisfy its loading requirement.

5.5.3.2 Experiment 5: Implementation of Demand Cap at KCM

The objective of the final experiment is to demonstrate the impact of demand caps at the KCM, where a time-series plot of the load profile of the KCM can be seen in Figure 5.26. At the beginning of the experiment, observed at a timestamp of 14:35:30, both the EV and the E-Load are idle and are consuming no power. Both the EV and E-Load subsequently bid into the marketplace and win their initial bids at 14:36:00, with the loading of the KCM peaking to 10 kW as a result. The first instance of a demand cap is signaled at 14:36:30, where the cap is set at a threshold of 5 kW. In this case, the EV outbids the E-Load, and the E-Load turns off, resulting in the KCM net load being approximately 4 kW. The second instance of a demand cap is executed at 14:37:20 and set to 0 kW, which results in the EV being turned off as well. This results in the KCM ultimately having a negative load, and which signifies that the KCM is exporting power back to the main grid. Thus, the impact of demand caps can conclusively be seen in Figure 5.26, which demonstrates its ability to limit the total demand of the KCM.

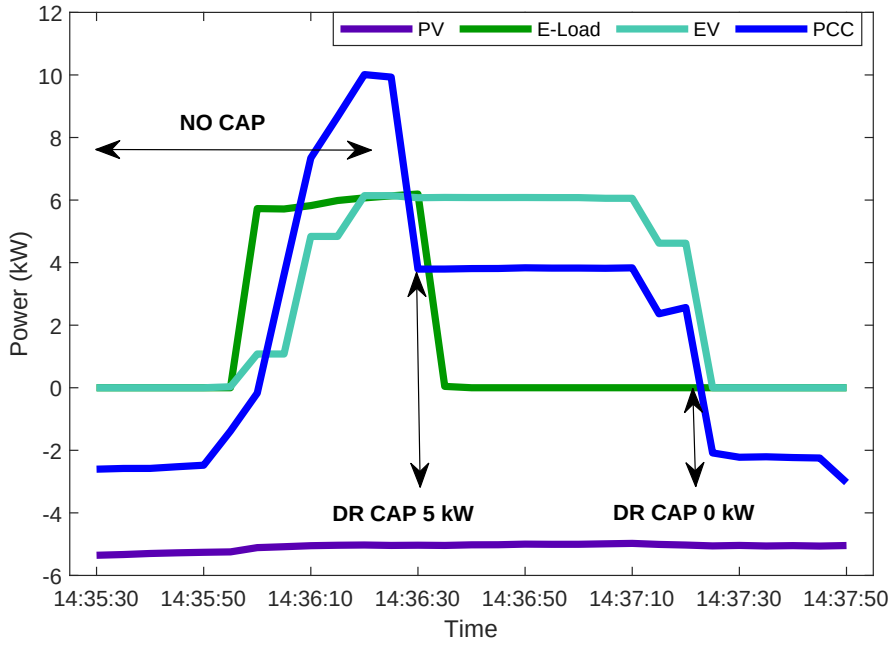

Figure 5.26: Plot of demand caps altering load profile of the KCM.

5.6 Assumptions and Limitations

The following bulleted list summarizes some assumptions made by the implementation of the TES as well as some of its limitations.

- **Assumption: Transformer rating must never be exceeded:** The condition for the potential replacement of a transformer is that the peak demand of the community may never exceed the transformer capacity rating. However, in practice, short-term overloading of the transformer is permissible, in some cases, with up to 50% of its rated capacity [125]. While short-term overloading will reduce the life of the transformer, it does provide some level of tolerance that should be factored into the financial assessment.

- **Limitation: Experiments conducted on original TOU schedules:** It is reasonable to assume that DSOs would alter TOU schedules after finding that homeowner behavior would create a new peak after 19:00, when conventionally, those hours would be classified as off-peak hours. The limitation of this work is that the TOU schedules used to simulate the RETS are based on conventional TOU schedules, when, in practice, TOU timings would be varied to determine their relative impact on the peak demand of the community.

- **Limitation: Financial assessment does not consider upstream distribution system:** The portion of the SDG that is upstream from the neighborhood transformer, including feeder capacity and substations, was not considered in the avoided CAPEX calculation. Indeed, the avoided CAPEX could be much more significant if additional capacity needs to be added to either the substation or the many feeders within the SDG as a result of the increase in peak demand. This limitation can be mitigated by obtaining a model of each of the DSOs and performing load-flow analysis to determine if any capacity constraints are violated.

5.7 Chapter Summary

This chapter presents a blockchain-based RETS that enables homeowners to trade energy and reduce peak demand. A fuzzy bidding strategy is developed for BESSs to distinguish their operation as selfish or helpful, thus enabling helpful BESSs to alter their schedule to reduce peak demand. Simulation results reveal that the proposed system reduces the peak load of an 8-home residential community by 62%, thus generating an average CAPEX savings of $102.5M for DSOs in Ontario. The proposed system is implemented on the HLF platform and deployed to the KCM,

where real-world experiments demonstrate how the KCM can reduce demand and minimize energy imports from the DSO. The execution time of the proposed RETS is benchmarked at 17.12 s, which is sufficient for RETS.

Chapter 6 - Conclusion and Future Work

The final chapter of this thesis seeks to summarize the findings of the distributed communication and control frameworks proposed in Chapters 3-5, and highlight the key contributions of this work. Additionally, since the thesis is heavily reliant on its contribution towards real-world experimentation, a section is devoted to challenges related to implementation and commercialization of the proposed frameworks. Finally, the chapter is rounded out by expanding and expand on the future directions that this research can follow.

6.1 Thesis Summary

This thesis develops three new distributed communication and control frameworks for SDG applications using modern technologies such as the IoT and blockchains. The proposed frameworks are designed to address key challenges within SDGs that are brought on by the rapid proliferation of agent-owned DERs, which revolve mainly around the unintended negative consequences that occur when DERs are operated in an uncoordinated manner. The concepts of distributed communication and control of DERs are instrumental in achieving a level of coordination that satisfy the economic and operational objectives of both DSOs and the agents. Utilizing the ethos of transactive energy as a basis for the design of distributed communication and control frameworks, the frameworks must provide i) robust, distributed

and real-time messaging capability; ii) auditable mechanisms that help enforce standards of performance when agents utilize DERs to provide ancillary services; and iii) techno-economic feasibility with respect to its scalability and cost-reduction potential. Thus, the proposed frameworks in this thesis utilize the scalable, real-time messaging capability of DDS to provide robust inter-agent messaging, while leveraging the distributed ledger of permissioned blockchains to provide a transparent and verifiable transaction history to eliminate any potential trust issues between agents and DSOs.

Chapter 3 proposes a DCF that is built on top of DDS middleware, with the objective of providing real-time inter-agent messaging that enables agents to coordinate their control actions despite experiencing intermittent connection issues that may result in the misaligned execution of distributed control strategies. A SIL platform is developed to enable the rapid prototyping of distributed control strategies that utilize the DCF in various SDG applications. In this particular chapter, the DCF is leveraged within the application of distributed voltage regulation, where agents execute the AWC control strategy to resolve voltage violations in real-time. Simulation results on a 39-bus test feeder demonstrate that the agents are able to execute the AWC successfully even when certain agents receive outdated messages after being disconnected from the network. Furthermore, the DCF is deployed to the KCM, which regularly suffers from extreme overvoltage violations due to its substantial PV generation. Real-world experimental results demonstrate the ability of the DCF to mitigate the aforementioned violations in real-time. Lastly, the DCF is benchmarked alongside other popular IoT middlewares, such as AMQP and MQTT, and is found to provide superior message latency and throughput, while also satisfying the minimum latency requirements of smart grid applications.

Chapter 4 presents a TES that utilizes a permissioned blockchain architecture

to facilitate a decentralized marketplace wherein agents may bid for voltage regulation service contracts. The main objective of the proposed TES is to eliminate trust issues between distributed agents that would otherwise have no mechanism to ensure that voltage violations are resolved at the correct time and at an agreed upon price. The presence of a decentralized marketplace also enables agents to bid for multiple voltage violations simultaneously, which can then be resolved in less bidding cycles when compared to similar approaches. Thus, the proposed TES implements a smart contract that maintains an auditable credit score for each agent to establish their trustworthiness and effectiveness in resolving voltage violations, and also implements the ECNP control strategy to enable agents to resolve multiple voltage violations in parallel. A novel incentive algorithm is also proposed to reward agents for successful mitigations of voltage violations, while also levying heavy penalties if the agents are unable to resolve any violations that they are assigned. Simulated experiments on a 69-bus feeder demonstrate the ability of the proposed TES to resolve voltage violations in less bidding cycles than the original CNP control strategy.

Chapter 5 presents a permissioned blockchain implementation of a RETS, with the objective of reducing the peak demand of a residential community. Novel bidding strategies of controllable DERs, such as EVs, BESSs, and STs, are developed to mimic realistic preferences of homeowners that govern the operation of these DERs. In particular, a fuzzy logic-based bidding strategy is developed for BESSs that takes its SoC, time of day, and net load into account before bidding into the proposed RETS. The bidding strategies are characterized as helpful or selfish, where a helpful strategy reflects the willingness of a homeowner to alter the operational schedule of their DERs to help reduce peak demand, while a selfish strategy maximizes the homeowner's individualistic objectives of convenience or cost reduction.

A smart contract is developed to facilitate the RETS in discrete market intervals, while also allowing DSOs to set demand caps to limit the allowable demand for an interval. Simulation results executed within an 8-home residential community show that the proposed RETS is able to reduce the peak demand of the community by 62%. Using this result, a financial assessment is carried out on 10 DSOs within Ontario, Canada, where it is determined that the reduction in peak demand would translate to an average of $102.5M in CAPEX savings for the DSOs due to the avoidance of transformer upgrades. The proposed RETS is also deployed to the KCM, where outdoor experiments demonstrate the ability of the RETS to minimize imports from the main grid, and obey demand caps set by the DSO. Lastly, the end to end execution of the smart contract is benchmarked using monte-carlo methods, and found to provide a transaction latency of 17 s, which is sufficient for the timing requirements of RETS.

6.2 Thesis Contributions

The following list highlights the contributions made by this thesis:

1. The development of a completely distributed communication framework for inter-agent messaging built on DDS. The design of the DCF is compliant with FIPA standards, while the configuration of its QoS profiles to prioritize critical agent messages, as well as prevent outdated messages from reaching agents who experience intermittent connection failures, enhances the efficacy of distributed control strategies that otherwise assume that messages always arrive in the exact order they are sent, which is unrealistic.

2. The development of a novel TES for distributed voltage regulation, which enables multiple voltage violations to be resolved simultaneously using the

ECNP control strategy, while facilitating a novel smart contract that audits agent performance and penalizes agents for the unsuccessful mitigation of voltage violations. The concept of enforcing penalties in an automated manner via smart contracts is an approach that has not been extended to the application of voltage regulation by previous work.

3. The design of bidding strategies that reflect the operational preferences of homeowners for BESSs, STs, and EVs, and the contextualization of these bidding strategies in terms of the impact they may have in reducing peak demand.

4. A techno-economic evaluation of a blockchain-based RETS that observes its scalability as a function of increasing nodes, as well as its ability to generate CAPEX savings for DSOs as a function of reduced peak demand.

5. The real-world implementation and deployment of all three proposed frameworks at a microgrid with significant amounts of renewable energy. The experimental results of this thesis present conclusive evidence in demonstrating the efficacy of the proposed frameworks for a variety of SDG applications, such as voltage regulation, energy trading, and demand response.

6.3 Challenges in Implementation and Commercialization

The following bulleted list summarizes the various challenges faced in the real-world experimentation of the proposed frameworks, with a view towards future commercialization.

- **Difficulty managing remote upgrades:** During the real-world experimentation of the RETS developed in Chapter 5, test cases where the SolarEdge

PV inverters needed to be curtailed for particular market intervals would fail and return an *unsupported function* error from the SolarEdge inverters. The error did not appear in the knowledge base of the SolarEdge company website. Upon contacting the SolarEdge technical team, it was found that they had disabled advanced grid control features for all single-phase inverters, and used a remote firmware upgrade to disable all applicable active SolarEdge inverters deployed in the field. This type of service interruption acts as a significant barrier to both research and development, as well as commercialization for use cases where local active and reactive power control is required in single-phase inverters. Any decision to push firmware upgrades from the manufacturers of DERs should be confirmed with customers prior to its deployment, such that any interruption to existing algorithms can be handled in advance.

- **Expensive software licenses:** The bulk of modeling and real-world implementation within this thesis was done in LabVIEW and MATLAB, both of which require expensive annual licenses to use. In contrast, the implementation of the communication frameworks based on AMQP and MQTT was based on Python, which is open-source and free of charge. Additionally, the blockchain implementation of HLF was also done in an open-source manner using NodeJS. Thus, to mitigate risk of expensive software licenses when potentially commercializing the frameworks proposed in this thesis, it may be a good idea to rewrite the proposed control algorithms in open-source languages such as Python or NodeJS.

- **Focusing on interoperability:** As more DERs continue to be adopted, there are significant issues for developers of energy control software in maintaining control modules, or drivers, to communicate with each type of device. To solve this issue, power system researchers are seeking to standardize the

data and services that DERs can provide, with standards such as IEC 61850 and SunSpec [126]. These standards ensure interoperability between DERs, such that the make/models of DERs can be switched seamlessly, therefore avoiding vendor lock. When looking forward to commercialization, this feature could reduce expensive and time consuming maintenance of software when DERs are changed.

6.4 Future Work

This subsection expands on the future work that may serve as a guide for further potential research directions. The future work is discussed in context of each of the proposed frameworks in this thesis, with the theme of cybsersecurity spanning across all three frameworks.

6.4.1 Impacts of Cybersecurity

With SDGs rapidly decentralizing and enlisting the support of DERs to enter the new paradigm of transactive energy, the importance of cybersecurity has never been more important. While previously, power system control and operations were governed by secure hardware and networks that were firmly in control of power system operators, the extension of the power system to include DER owners has introduced new vulnerabilities that could compromise the reliability of the overall system [127]. This thesis focuses on the role of disparate agents to coordinate the actions of DERs with DSOs, execute distributed algorithms, and disseminate incentives for services provided, however, this thesis does not particularly address the vulnerabilities of these data exchanges and their resulting impact on the overall SDG.

A major point of attack, for example, could be the agent platform itself, where the control logic of the agent is contained. If strict authentication protocols and firewalls are not present on the agent platform, a malicious agent could obtain access to the control logic, and begin to inject false data within the algorithm, which in the case of distributed voltage regulation algorithms that were presented in Chapter 3 and Chapter 4, could result in a voltage collapse. This scenario is especially relevant to IoT-based hardware, which are known to have light-weight hardware and thus may not have the computing power to reliably execute strict authentication procedures [128]. Another major point of attack is the integration points between the DSO network and the agent network, where the security protocols of the agent network may not be as robust as the network governed by the DSO. Since this thesis does not discuss fraud prevention or detection, it is difficult for DSOs to assess and validate the data being exchanged by agents. It is worthwhile to mention that blockchain-based systems utilize digital public/private keys to validate the identity of the agent and the authenticity of the agent's data, however, if the keys are located on the agent platform itself, a malicious agent may find an entry point within the system. In general, more work is required in building out a comprehensive cyber-attack mitigation strategy for SDGs, which may include a survey of vulnerable attack points that must be secured, attack identification, detection, and mitigation techniques, and protocols to follow when a cyber-attack is underway.

6.4.2 DDS-Based Distributed Communication Framework for Distributed Voltage Regulation

Building on the concerns related to cybersecurity as discussed in the previous subsection, the topic-based, publish-subscribe communication architecture is particularly vulnerable to attacks such as man-in-the-middle, or denial of service [129].

The security measures taken in the design of the DCF prevent eavesdropping from malicious agents, however, suitable attack prevention strategies that involve encryption may provide better security coverage [130]. The usage of encryption may also protect the integrity of the control message as it is distributed to many different agents [131]. Thus, one research direction for this work may be to further research security measures that are *native* to DDS, and leverage them within the design of the DCF as was done with the configuration of the QoS profiles to prevent the distribution of outdated messages. Aside from this, another step would be to utilize the developed SIL platform for ultra-critical SDG applications that have an extremely low threshold for latency and jitter, such as protection and control [132]. Will the message latency of the DCF be acceptable within this application when the number of agents exceed 1000, 10,000, or 1,000,000?

6.4.3 Blockchain-based TES for Distributed Voltage Regulation

As mentioned in Chapter 2, the pBFT consensus algorithm used in a permissioned blockchain architecture is useful in limiting the computational effort of consensus. However, its communication complexity of $O(n^2)$ may limit its efficacy as the number of agents grow within the network. In the context of cyber-physical SDGs, this can be countered by assigning an agent a larger spatial area of operation to reduce the total number of agents, but this may not be the most optimal solution if the spatial partitioning is not a function of size, but of the location of DERs. As such, it may be worthwhile to proceed in two directions. First, surveying the latest consensus protocols available in literature and determining their feasibility by evaluating their communication and computational complexity against the pBFT. Second, if suitable consensus protocols are not found, are there modifications that could be made to existing consensus protocols to increase their scalability?

6.4.4 Blockchain-based RETS

As demonstrated in Chapter 5, the effect of the demand cap significantly increases the community energy cost due to the increase in MCP. Considering the fact that DSOs would realize an average of $102.5M of CAPEX savings due to the presence of the demand cap, there is a need to provide compensation to homeowners that would incentivize them to participate in the RETS, thereby increasing its positive uptake. The design of incentive structures must, almost certainly, shield the homeowner from the additional cost they had to pay because of the rise in the MCP. Furthermore, the incentive structure should also enable homeowners to set minimum expectations for the compensation they feel that they deserve for providing flexibility to the DSO when demand response signals are sent.

Bibliography

[1] G. E. Asimakopoulou and N. D. Hatziargyriou, "Evaluation of economic benefits of der aggregation," IEEE Transactions on Sustainable Energy, vol. 9, no. 2, pp. 499–510, 2018.

[2] G. D. Zotti, S. A. Pourmousavi, J. M. Morales, H. Madsen, and N. K. Poulsen, "A control-based method to meet tso and dso ancillary services needs by flexible end-users," IEEE Transactions on Power Systems, vol. 35, no. 3, pp. 1868–1880, 2020.

[3] A. Cherukuri and J. Cortés, "Distributed coordination of ders with storage for dynamic economic dispatch," IEEE Transactions on Automatic Control, vol. 63, no. 3, pp. 835–842, 2018.

[4] M. K. Gray and W. G. Morsi, "Economic assessment of phase reconfiguration to mitigate the unbalance due to plug-in electric vehicles charging," Electric Power Systems Research, vol. 140, pp. 329 – 336, 2016. [Online]. Available: http://www.sciencedirect.com/science/article/pii/S0378779616302164

[5] M. Hasheminamin, V. G. Agelidis, V. Salehi, R. Teodorescu, and B. Hredzak, "Index-based assessment of voltage rise and reverse power flow phenomena in a distribution feeder under high pv penetration," IEEE Journal of Photovoltaics, vol. 5, no. 4, pp. 1158–1168, July 2015.

[6] D. Divan, R. Moghe, and A. Prasai, "Power electronics at the grid edge : The key to unlocking value from the smart grid," IEEE Power Electronics Magazine, vol. 1, no. 4, pp. 16–22, Dec 2014.

[7] T. Basso, S. Chakraborty, A. Hoke, and M. Coddington, "Ieee 1547 standards advancing grid modernization," 06 2015, pp. 1–5.

[8] R. Moghe, D. Tholomier, and D. Divan, "Distribution grid edge control: Field demonstrations," in 2016 IEEE Power and Energy Society General Meeting (PESGM), July 2016, pp. 1–5.

[9] Q. Hu, F. Li, X. Fang, and L. Bai, "A framework of residential demand aggregation with financial incentives," IEEE Transactions on Smart Grid, vol. 9, no. 1, pp. 497–505, Jan 2018.

[10] C. Patsonakis, S. Terzi, I. Moschos, D. Ioannidis, K. Votis, and D. Tzovaras, "Permissioned blockchains and virtual nodes for reinforcing trust between aggregators and prosumers in energy demand response scenarios," in 2019 IEEE International Conference on Environment and Electrical Engineering and 2019 IEEE Industrial and Commercial Power Systems Europe (EEEIC / I CPS Europe), June 2019, pp. 1–6.

[11] P. Vrba, V. Mařík, P. Siano, P. Leitão, G. Zhabelova, V. Vyatkin, and T. Strasser, "A review of agent and service-oriented concepts applied to intelligent energy systems," IEEE Transactions on Industrial Informatics, vol. 10, no. 3, pp. 1890–1903, Aug 2014.

[12] X. Dou, P. Xu, Q. Hu, W. Sheng, X. Quan, Z. Wu, and B. Xu, "A distributed voltage control strategy for multi-microgrid active distribution networks considering economy and response speed," IEEE Access, vol. 6, pp. 31 259–31 268, 2018.

[13] O. Abrishambaf, F. Lezama, P. Faria, and Z. Vale, "Towards transactive energy systems: An analysis on current trends," Energy Strategy Reviews, vol. 26, p. 100418, 2019. [Online]. Available: http://www.sciencedirect.com/science/article/pii/S2211467X19301105

[14] G. Yin, J. Wang, and F. Qiu, "Decentralized electricity market with transactive energy – a path forward," The Electricity Journal, 04 2019.

[15] C. P. Nguyen and A. J. Flueck, "Modeling of communication latency in smart grid," in 2011 IEEE Power and Energy Society General Meeting, 2011, pp. 1–7.

[16] H. S. V. S. K. Nunna and S. Doolla, "Demand response in smart distribution system with multiple microgrids," IEEE Transactions on Smart Grid, vol. 3, no. 4, pp. 1641–1649, Dec 2012.

[17] A. Abel Hafez, W. A. Omran, and Y. G. Hegazy, "A decentralized technique for autonomous service restoration in active radial distribution networks," IEEE Transactions on Smart Grid, vol. 9, no. 3, pp. 1911–1919, May 2018.

[18] K. Saxena and A. R. Abhyankar, "Agent-based decentralised load flow computation for smart management of distribution system," IET Generation, Transmission Distribution, vol. 11, no. 3, pp. 605–614, 2017.

[19] X. Zhou, E. Dall'Anese, L. Chen, and A. Simonetto, "An incentive-based online optimization framework for distribution grids," IEEE Transactions on Automatic Control, vol. 63, no. 7, pp. 2019–2031, July 2018.

[20] V. Kekatos, G. Wang, A. J. Conejo, and G. B. Giannakis, "Stochastic reactive power management in microgrids with renewables," IEEE Transactions on Power Systems, vol. 30, no. 6, pp. 3386–3395, Nov 2015.

[21] S. Su, Y. Hu, S. Wang, W. Wang, Y. Ota, K. Yamashita, M. Xia, X. Nie, L. Chen, and X. Mao, "Reactive power compensation using electric vehicles considering drivers' reasons," IET Generation, Transmission Distribution, vol. 12, no. 20, pp. 4407–4418, 2018.

[22] A. El-Mougy, I. Al-Shiab, and M. Ibnkahla, "Scalable personalized iot networks," Proceedings of the IEEE, vol. 107, no. 4, pp. 695–710, 2019.

[23] Y. Xiao, N. Zhang, W. Lou, and Y. T. Hou, "A survey of distributed consensus protocols for blockchain networks," IEEE Communications Surveys Tutorials, vol. 22, no. 2, pp. 1432–1465, 2020.

[24] T. Sato, Smart grid standards: specifications, requirements, and technologies. Wiley, 2015.

[25] D. Deka, S. Backhaus, and M. Chertkov, "Structure learning in power distribution networks," IEEE Transactions on Control of Network Systems, vol. 5, no. 3, pp. 1061–1074, Sep. 2018.

[26] A. I. Jones, B. E. Smith, and D. J. Ward, "Considerations for higher voltage distribution," IEEE Transactions on Power Delivery, vol. 7, no. 2, pp. 782–788, April 1992.

[27] A. Dubey and S. Santoso, "Electric vehicle charging on residential distribution systems: Impacts and mitigations," IEEE Access, vol. 3, pp. 1871–1893, 2015.

[28] Y. Liu, J. Bebic, B. Kroposki, J. de Bedout, and W. Ren, "Distribution system voltage performance analysis for high-penetration pv," in 2008 IEEE Energy 2030 Conference, 2008, pp. 1–8.

[29] M. Arif and A. Than Oo, "Net-zero emission residential building in temperate weather condition," Renewable Energy and Environmental Sustainability, vol. 2, p. 30, 01 2017.

[30] M. Gray and W. Morsi, "On the role of prosumers owning rooftop solar photovoltaic in reducing the impact on transformer's aging due to plug-in electric vehicles charging," Electric Power Systems Research, vol. 143, 11 2016.

[31] M. Joorabian, M. Ajodani, and M. Baghdadi, "A method for voltage regulation in distribution network equipped with oltc transformers and dg units," in 2010 Asia-Pacific Power and Energy Engineering Conference, March 2010, pp. 1–5.

[32] "Conditions of service for hydro one networks inc. distribution customers," Mar 2019. [Online]. Available: https://www.hydroone.com/business-services/commercial-industrial-generators-and-ldcs/power-quality/power-quality-definitions

[33] H. Mahboubi, F. Sharifi, A. G. Aghdam, and Y. Zhang, "Distributed control of multi-agent systems with limited communication range in the fixed obstacle environments," IEEE Access, vol. 7, pp. 118 259–118 268, 2019.

[34] A. Kantamneni, L. E. Brown, G. Parker, and W. W. Weaver, "Survey of multi-agent systems for microgrid control," Engineering Applications of Artificial Intelligence, vol. 45, pp. 192 – 203, 2015. [Online]. Available: http://www.sciencedirect.com/science/article/pii/S0952197615001529

[35] D. Camacho, R. Aler, C. Castro, and J. M. Molina, "Performance evaluation of zeus, jade, and skeletonagent frameworks," in IEEE International Conference on Systems, Man and Cybernetics, vol. 4, Oct 2002, pp. 6 pp. vol.4–.

[36] G. Fortino, A. Garro, and W. Russo, "Enhancing jade interoperability through the java-based interoperable mobile agent framework," in 2007 5th IEEE International Conference on Industrial Informatics, vol. 2, June 2007, pp. 1071–1077.

[37] S. Bashir, M. Rehman, H. F. Ahmad, A. Ali, and H. Suguri, "Distributed and scalable message transport service for high performance multi-agent systems," in 2004 International Networking and Communication Conference, 2004, pp. 152–157.

[38] R. B. Melton, "Gridwise transactive energy framework (draft version)," 11 2013. [Online]. Available: https://www.osti.gov/biblio/1123244

[39] M. Marjani, F. Nasaruddin, A. Gani, A. Karim, I. A. T. Hashem, A. Siddiqa, and I. Yaqoob, "Big iot data analytics: Architecture, opportunities, and open research challenges," IEEE Access, vol. 5, pp. 5247–5261, 2017.

[40] J. Dizdarevic, F. Carpio, A. Jukan, and X. Masip, "A survey of communication protocols for internet of things and related challenges of fog and cloud computing integration," ACM Computing Surveys, vol. 51, 04 2018.

[41] J. M. Schlesselman, G. Pardo-Castellote, and B. Farabaugh, "Omg data-distribution service (dds): architectural update," in IEEE MILCOM 2004. Military Communications Conference, 2004., vol. 2, Oct 2004, pp. 961–967 Vol. 2.

[42] T. Sultana and K. A. Wahid, "Choice of application layer protocols for next generation video surveillance using internet of video things," IEEE Access, vol. 7, pp. 41 607–41 624, 2019.

[43] N. Naik, "Choice of effective messaging protocols for iot systems: Mqtt, coap, amqp and http," in 2017 IEEE International Systems Engineering Symposium (ISSE), Oct 2017, pp. 1–7.

[44] Y. Xiao, N. Zhang, W. Lou, and Y. T. Hou, "A survey of distributed consensus protocols for blockchain networks," IEEE Communications Surveys Tutorials, vol. 22, no. 2, pp. 1432–1465, Jan. 2020.

[45] M. Belotti, N. Božić, G. Pujolle, and S. Secci, "A vademecum on blockchain technologies: When, which, and how," IEEE Communications Surveys Tutorials, vol. 21, no. 4, pp. 3796–3838, July 2019.

[46] J. Liu and Z. Liu, "A survey on security verification of blockchain smart contracts," IEEE Access, vol. 7, pp. 77 894–77 904, June 2019.

[47] R. Guo, H. Shi, Q. Zhao, and D. Zheng, "Secure attribute-based signature scheme with multiple authorities for blockchain in electronic health records systems," IEEE Access, vol. 6, pp. 11 676–11 686, Feb. 2018.

[48] D. Huang, X. Ma, and S. Zhang, "Performance analysis of the raft consensus algorithm for private blockchains," IEEE Transactions on Systems, Man, and Cybernetics: Systems, vol. 50, no. 1, pp. 172–181, 2020.

[49] M. M. Jalalzai and C. Busch, "Window based bft blockchain consensus," in 2018 IEEE International Conference on Internet of Things (iThings) and IEEE Green Computing and Communications (GreenCom) and IEEE Cyber, Physical and Social Computing (CPSCom) and IEEE Smart Data (SmartData), July 2018, pp. 971–979.

[50] W. Chan and A. Olmsted, "Ethereum transaction graph analysis," in 2017 12th International Conference for Internet Technology and Secured Transactions (ICITST), Dec 2017, pp. 498–500.

[51] M. H. Manshaei, M. Jadliwala, A. Maiti, and M. Fooladgar, "A game-theoretic analysis of shard-based permissionless blockchains," IEEE Access, vol. 6, pp. 78 100–78 112, 2018.

[52] K. J. O'Dwyer and D. Malone, "Bitcoin mining and its energy footprint," in 25th IET Irish Signals Systems Conference 2014 and 2014 China-Ireland International Conference on Information and Communications Technologies (ISSC 2014/CIICT 2014), June 2014, pp. 280–285.

[53] M. Cash and M. Bassiouni, "Two-tier permission-ed and permission-less blockchain for secure data sharing," in 2018 IEEE International Conference on Smart Cloud (SmartCloud), Sep. 2018, pp. 138–144.

[54] P. Thakkar, S. Nathan, and B. Viswanathan, "Performance benchmarking and optimizing hyperledger fabric blockchain platform," in 2018 IEEE 26th International Symposium on Modeling, Analysis, and Simulation of Computer and Telecommunication Systems (MASCOTS). IEEE, 2018, pp. 264–276.

[55] M. Sidorov, M. Tze Ong, R. Vikneswaran, J. Nakamura, R. Ohmura, and J. Huey Khor, "Ultralightweight mutual authentication rfid protocol for blockchain enabled supply chains," IEEE Access, vol. PP, pp. 1–1, 01 2019.

[56] Z. Zheng, S. Xie, H. Dai, X. Chen, and H. Wang, "An overview of blockchain technology: Architecture, consensus, and future trends," in 2017 IEEE International Congress on Big Data (BigData Congress), June 2017, pp. 557–564.

[57] Y. B. Bi, L. Jiang, X. J. Wang, and L. Z. Cui, "Mapping of iec 61850 to data distribute service for digital substation communication," in 2013 IEEE Power Energy Society General Meeting, 2013, pp. 1–5.

[58] B. AL-Madani and H. Ali, "Data distribution service (dds) based implementation of smart grid devices using ansi c12.19 standard," Procedia Computer Science, vol. 110, pp. 394–401, 12 2017.

[59] T. A. Youssef, M. E. Hariri, A. T. Elsayed, and O. A. Mohammed, "A dds-based energy management framework for small microgrid operation and control," IEEE Transactions on Industrial Informatics, vol. 14, no. 3, pp. 958–968, March 2018.

[60] T. A. Youssef, A. T. Elsayed, and O. A. Mohammed, "Data distribution service-based interoperability framework for smart grid testbed infrastructure," Energies, vol. 9, no. 3, 2016. [Online]. Available: http://www.mdpi.com/1996-1073/9/3/150

[61] M. H. Cintuglu, T. Youssef, and O. A. Mohammed, "Development and application of a real-time testbed for multiagent system interoperability: A case study on hierarchical microgrid control," IEEE Transactions on Smart Grid, vol. 9, no. 3, pp. 1759–1768, May 2018.

[62] H. F. Habib, M. M. Esfahani, and O. A. Mohammed, "Investigation of protection strategy for microgrid system using lithium-ion battery during islanding," IEEE Transactions on Industry Applications, vol. 55, no. 4, pp. 3411–3420, 2019.

[63] M. M. Esfahani, A. Hariri, and O. A. Mohammed, "A multiagent-based game-theoretic and optimization approach for market operation of multimicrogrid systems," IEEE Transactions on Industrial Informatics, vol. 15, no. 1, pp. 280–292, 2019.

[64] M. Starke, A. Herron, D. King, and Y. Xue, "Implementation of a publish-subscribe protocol in microgrid islanding and resynchronization with self-discovery," IEEE Transactions on Smart Grid, vol. 10, no. 1, pp. 361–370, Jan 2019.

[65] M. P. Singh and A. K. Chopra, "The internet of things and multiagent systems: Decentralized intelligence in distributed computing," in 2017 IEEE 37th International Conference on Distributed Computing Systems (ICDCS), 2017, pp. 1738–1747.

[66] S. D. J. McArthur, E. M. Davidson, V. M. Catterson, A. L. Dimeas, N. D. Hatziargyriou, F. Ponci, and T. Funabashi, "Multi-agent systems for power

engineering applications—part i: Concepts, approaches, and technical challenges," IEEE Transactions on Power Systems, vol. 22, no. 4, pp. 1743–1752, 2007.

[67] I. Gorton, Yan Liu, and J. Yin, "Gridoptics(tm): A design for plug-and-play smart grid software architecture," in 2012 First International Workshop on Software Engineering Challenges for the Smart Grid (SE-SmartGrids), 2012, pp. 38–41.

[68] C. Liu, K. K. Chai, X. Zhang, E. T. Lau, and Y. Chen, "Adaptive blockchain-based electric vehicle participation scheme in smart grid platform," IEEE Access, vol. 6, pp. 25 657–25 665, 2018.

[69] A. Al-Obaidi, H. Khani, H. E. Farag, and M. Mohamed, "Bidirectional smart charging of electric vehicles considering user preferences, peer to peer energy trade, and provision of grid ancillary services," International Journal of Electrical Power and Energy Systems, vol. 124, p. 106353, 2021. [Online]. Available: http://www.sciencedirect.com/science/article/pii/S0142061520307468

[70] Z. Su, Y. Wang, Q. Xu, M. Fei, Y. Tian, and N. Zhang, "A secure charging scheme for electric vehicles with smart communities in energy blockchain," IEEE Internet of Things Journal, vol. 6, no. 3, pp. 4601–4613, 2019.

[71] J. Kang, R. Yu, X. Huang, S. Maharjan, Y. Zhang, and E. Hossain, "Enabling localized peer-to-peer electricity trading among plug-in hybrid electric vehicles using consortium blockchains," IEEE Transactions on Industrial Informatics, vol. 13, no. 6, pp. 3154–3164, 2017.

[72] E. Münsing, J. Mather, and S. Moura, "Blockchains for decentralized optimization of energy resources in microgrid networks," in 2017 IEEE Conference on Control Technology and Applications (CCTA), 2017, pp. 2164–2171.

[73] Y. Amanbek, Y. Tabarak, H. S. V. S. K. Nunna, and S. Doolla, "Decentralized transactive energy management system for distribution systems with prosumer microgrids," in 2018 19th International Carpathian Control Conference (ICCC), 2018, pp. 553–558.

[74] Y.-C. Tsao, V.-V. Thanh, and Q. Wu, "Sustainable microgrid design considering blockchain technology for real-time price-based demand response programs," International Journal of Electrical Power & Energy Systems, vol. 125, p. 106418, 2021. [Online]. Available: http://www.sciencedirect.com/science/article/pii/S014206152030911X

[75] J. Guerrero, A. C. Chapman, and G. Verbič, "Decentralized P2P energy trading under network constraints in a low-voltage network," IEEE Transactions on Smart Grid, vol. 10, no. 5, pp. 5163–5173, Sep. 2019.

[76] F. Luo, Z. Y. Dong, G. Liang, J. Murata, and Z. Xu, "A distributed electricity trading system in active distribution networks based on multi-agent coalition and blockchain," IEEE Transactions on Power Systems, vol. 34, no. 5, pp. 4097–4108, Sep. 2019.

[77] M. Afzal, Q. Huang, W. Amin, K. Umer, A. Raza, and M. Naeem, "Blockchain enabled distributed demand side management in community energy system with smart homes," IEEE Access, vol. 8, pp. 37 428–37 439, Feb. 2020.

[78] W. Hou, L. Guo, and Z. Ning, "Local electricity storage for blockchain-based energy trading in industrial internet of things," IEEE Transactions on Industrial Informatics, vol. 15, no. 6, pp. 3610–3619, Feb. 2019.

[79] T. Morstyn and M. D. McCulloch, "Multiclass energy management for peer-to-peer energy trading driven by prosumer preferences," IEEE Transactions on Power Systems, vol. 34, no. 5, pp. 4005–4014, Sep. 2019.

[80] M. P. Singh and A. K. Chopra, "The internet of things and multiagent systems: Decentralized intelligence in distributed computing," in 2017 IEEE 37th International Conference on Distributed Computing Systems (ICDCS), June 2017, pp. 1738–1747.

[81] F. Perkonigg, D. Brujic, and M. Ristic, "Platform for multiagent application development incorporating accurate communications modeling," IEEE Transactions on Industrial Informatics, vol. 11, no. 3, pp. 728–736, June 2015.

[82] A. Elmitwally, M. Elsaid, M. Elgamal, and Z. Chen, "A fuzzy-multiagent self-healing scheme for a distribution system with distributed generations," IEEE Transactions on Power Systems, vol. 30, no. 5, pp. 2612–2622, Sep. 2015.

[83] W. Li, Y. Li, C. Chen, Y. Tan, Y. Cao, M. Zhang, Y. Peng, and S. Chen, "A full decentralized multi-agent service restoration for distribution network with DGs," IEEE Transactions on Smart Grid, vol. 11, no. 2, pp. 1100–1111, Jul. 2019.

[84] M. Yokoo, E. H. Durfee, T. Ishida, and K. Kuwabara, "The distributed constraint satisfaction problem: formalization and algorithms," IEEE

Transactions on Knowledge and Data Engineering, vol. 10, no. 5, pp. 673–685, Sep. 1998.

[85] N. A. El-Taweel and H. E. Z. Farag, "Voltage regulation in islanded microgrids using distributed constraint satisfaction," IEEE Transactions on Smart Grid, vol. 9, no. 3, pp. 1613–1625, May 2018.

[86] N. A. El-Taweel and H. E. Farag, "Multi-agent coordination of distributed energy storage systems for mitigating renewable energy resources high ramp-rate issues," in 2017 IEEE Electrical Power and Energy Conference (EPEC), Oct 2017, pp. 1–6.

[87] M. Rostami and S. Lotfifard, "Distributed dynamic state estimation of power systems," IEEE Transactions on Industrial Informatics, vol. 14, no. 8, pp. 3395–3404, Nov. 2018.

[88] N. A. El-Taweel and H. E. Z. Farag, "Operation challenges of feeder shunt capacitors in islanded microgrids," in 2015 IEEE EPEC, Oct. 2015, pp. 191–196.

[89] "Ni scan engine performance benchmarks," Feb 2018. [Online]. Available: http://www.ni.com/product-documentation/7792/en/

[90] M. M. A. Abdelaziz, H. E. Farag, E. F. El-Saadany, and Y. A. . I. Mohamed, "A globally convergent trust-region method for power flow studies in active distribution systems," in 2012 IEEE PES General Meeting, Jul. 2012, pp. 1–7.

[91] M. Faizullin, A. Kornilova, A. Akhmetyanov, and G. Ferrer, "Twist-n-sync: Software clock synchronization with microseconds accuracy using mems-gyroscopes," Sensors, vol. 21, no. 1, 2021. [Online]. Available: https://www.mdpi.com/1424-8220/21/1/68

[92] X. Zhu and B. Mather, "Data-driven distribution system load modeling for quasi-static time-series simulation," IEEE Transactions on Smart Grid, vol. 11, no. 2, pp. 1556–1565, 2020.

[93] R. Shigenobu, M. Kinjo, P. Mandal, A. M. Howlader, and T. Senjyu, "Optimal operation method for distribution systems considering distributed generators imparted with reactive power incentive," Applied Sciences, vol. 8, no. 8, 2018. [Online]. Available: https://www.mdpi.com/2076-3417/8/8/1411

[94] S. S. and, "Blockchain based transactive energy systems for voltage regulation in active distribution networks," IET Smart Grid, vol. 3, pp. 646–656, October 2020. [Online]. Available: https://digital-library.theiet.org/content/journals/10.1049/iet-stg.2019.0286

[95] S. Aknine, S. Pinson, and M. F. Shakun, "An extended multi-agent negotiation protocol," Autonomous Agents and Multi-Agent Systems, vol. 8, no. 1, pp. 5–45, Jan. 2004.

[96] C. Cai, H. Duan, and C. Wang, "Tutorial: Building secure and trustworthy blockchain applications," in 2018 IEEE Cybersecurity Development (SecDev), Sep. 2018, pp. 120–121.

[97] C. Li, B. Palanisamy, and R. Xu, "Scalable and privacy-preserving design of on/off-chain smart contracts," CoRR, vol. abs/1902.06359, 2019. [Online]. Available: http://arxiv.org/abs/1902.06359

[98] F. Rahimi and A. Ipakchi, "Using a transactive energy framework: Providing grid services from smart buildings," IEEE Electrification Magazine, vol. 4, no. 4, pp. 23–29, 2016.

[99] P. Yuan, X. Xiong, L. Lei, and K. Zheng, "Design and implementation on hyperledger-based emission trading system," IEEE Access, vol. 7, pp. 6109–6116, 2019.

[100] A. R. Rajput, Q. Li, M. Taleby Ahvanooey, and I. Masood, "Eacms: Emergency access control management system for personal health record based on blockchain," IEEE Access, vol. 7, pp. 84 304–84 317, 2019.

[101] W. H. Kersting, "The modeling and application of step voltage regulators," in 2009 IEEE/PES Conference Exposition, 2009, pp. 1–8.

[102] F. Bu, K. Dehghanpour, Y. Yuan, Z. Wang, and Y. Zhang, "A data-driven game-theoretic approach for behind-the-meter pv generation disaggregation," IEEE Transactions on Power Systems, vol. 35, no. 4, pp. 3133–3144, 2020.

[103] T. Fang, Q. Zhou, F. Ding, X. Wu, Z. Li, and H. Tang, "Response time of reactive power based on different definitions and algorithms," Journal of Modern Power Systems and Clean Energy, vol. 9, no. 2, pp. 440–449, 2021.

[104] M. V. Kirthiga, S. A. Daniel, and S. Gurunathan, "A methodology for transforming an existing distribution network into a sustainable autonomous micro-grid," IEEE Transactions on Sustainable Energy, vol. 4, no. 1, pp. 31–41, Jan. 2013.

[105] S. V. Akram, P. K. Malik, R. Singh, G. Anita, and S. Tanwar, "Adoption of blockchain technology in various realms: Opportunities and challenges," Security and Privacy, vol. 3, no. 5, pp. 109–125, Apr. 2020.

[106] J. Han, C. Choi, W. Park, I. Lee, and S. Kim, "Smart home energy management system including renewable energy based on ZigBee and PLC," IEEE Transactions on Consumer Electronics, vol. 60, no. 2, pp. 198–202, May 2014.

[107] U. Zafar, S. Bayhan, and A. Sanfilippo, "Home energy management system concepts, configurations, and technologies for the smart grid," IEEE Access, vol. 8, pp. 119 271–119 286, June 2020.

[108] S. Saxena, H. E. Z. Farag, A. Brookson, H. Turesson, and H. Kim, "A permissioned blockchain system to reduce peak demand in residential communities via energy trading: A real-world case study," IEEE Access, vol. 9, pp. 5517–5530, 2021.

[109] J. C. Fuller, K. P. Schneider, and D. Chassin, "Analysis of residential demand response and double-auction markets," in 2011 IEEE PES Meeting, Oct. 2011, pp. 1–7.

[110] P. H. Divshali, B. J. Choi, and H. Liang, "Multi-agent transactive energy management system considering high levels of renewable energy source and electric vehicles," IET Generation, Transmission Distribution, vol. 11, no. 15, pp. 3713–3721, 2017.

[111] C. Jiang, R. Torquato, D. Salles, and W. Xu, "Method to assess the power-quality impact of plug-in electric vehicles," IEEE Transactions on Power Delivery, vol. 29, no. 2, pp. 958–965, 2014.

[112] J. W. Smith, R. Dugan, and W. Sunderman, "Distribution modeling and analysis of high penetration pv," in 2011 IEEE Power and Energy Society General Meeting, July 2011, pp. 1–7.

[113] P. Hietaharju, M. Ruusunen, and K. Leiviskä, "A dynamic model for indoor temperature prediction in buildings," Energies, vol. 11, no. 6, pp. 1477–1497, Jun. 2018.

[114] Y. Li, Z. Yan, S. Chen, X. Xu, and C. Kang, "Operation strategy of smart thermostats that self-learn user preferences," IEEE Transactions on Smart Grid, vol. 10, no. 5, pp. 5770–5780, Jan. 2019.

[115] W. Tushar, T. K. Saha, C. Yuen, D. Smith, and H. V. Poor, "Peer-to-peer trading in electricity networks: An overview," IEEE Transactions on Smart Grid, vol. 11, no. 4, pp. 3185–3200, July 2020.

[116] J. Nicolaisen, V. Petrov, and L. Tesfatsion, "Market power and efficiency in a computational electricity market with discriminatory double-auction pricing," IEEE Transactions on Evolutionary Computation, vol. 5, no. 5, pp. 504–523, Oct. 2001.

[117] B. Sütterlina, T. A. Brunner, and M. Siegristc, "Who puts the most energy into energy conservation? A segmentation of energy consumers based on energy-related behavioral characteristics," Energy Policy, vol. 39, no. 12, pp. 8137 – 8152, Dec. 2011.

[118] M. N. Faqiry and S. Das, "Double-sided energy auction in microgrid: Equilibrium under price anticipation," IEEE Access, vol. 4, pp. 3794–3805, Jul. 2016.

[119] V. Venizelou, G. Makrides, V. Efthymiou, and G. E. Georghiou, "Residential consumption responsiveness under time-varying pricing," in 2018 IEEE International Energy Conference (ENERGYCON), Jun. 2018, pp. 1–6.

[120] C.-H. Yoo, I.-Y. Chung, H.-J. Lee, and S.-S. Hong, "Intelligent control of battery energy storage for multi-agent based microgrid energy management," Energies, vol. 6, no. 10, pp. 4956–4979, Sep. 2013.

[121] S. Saxena, H. Farag, A. Brookson, H. Turesson, and H. Kim, "Design and field implementation of blockchain based renewable energy trading in residential communities," in 2019 2nd International Conference on Smart Grid and Renewable Energy (SGRE), 2019, pp. 1–6.

[122] C. Ma, X. Kong, Q. Lan, and Z. Zhongding, "The privacy protection mechanism of hyperledger fabric and its application in supply chain finance," Cybersecurity, vol. 2, no. 5, pp. 1–9, Jan. 2019.

[123] T. T. A. Dinh, J. Wang, G. Chen, R. Liu, B. C. Ooi, and K.-L. Tan, "Blockbench: A framework for analyzing private blockchains," in 2017 ACM Conference on Data Management, Mar. 2017, pp. 1085–1100.

[124] L. Electronics, "Cost of transformers," Jan. 2020. [Online]. Available: https://www.larsonelectronics.com/category/719/100-112-5-kva-industrial-transformers[AccessedJan.2020]

[125] R. Nawzad, "Short-time overloading of power transformers," 2011.

[126] J. Johnson, R. Ablinger, R. Bründlinger, B. Fox, and J. Flicker, "Design and evaluation of sunspec-compliant smart grid controller with an automated hardware-in-the-loop testbed," Technology and Economics of Smart Grids and Sustainable Energy, vol. 2, 09 2017.

[127] R. Fu, X. Huang, Y. Xue, Y. Wu, Y. Tang, and D. Yue, "Security assessment for cyber physical distribution power system under intrusion attacks," IEEE Access, vol. 7, pp. 75 615–75 628, 2019.

[128] F. Rahman, M. Farmani, M. Tehranipoor, and Y. Jin, "Hardware-assisted cybersecurity for iot devices," in 2017 18th International Workshop on Microprocessor and SOC Test and Verification (MTV), 2017, pp. 51–56.

[129] M. Conti, N. Dragoni, and V. Lesyk, "A survey of man in the middle attacks," IEEE Communications Surveys Tutorials, vol. 18, no. 3, pp. 2027–2051, 2016.

[130] U. Meyer and S. Wetzel, "On the impact of gsm encryption and man-in-the-middle attacks on the security of interoperating gsm/umts networks," in 2004 IEEE 15th International Symposium on Personal, Indoor and Mobile Radio Communications (IEEE Cat. No.04TH8754), vol. 4, 2004, pp. 2876–2883 Vol.4.

[131] M. Zholbaryssov, C. N. Hadjicostis, and A. D. Dominguez-Garcia, "Privacy-preserving distributed coordination of distributed energy resources," in 2020 59th IEEE Conference on Decision and Control (CDC), 2020, pp. 4689–4696.

[132] S. M. Blair, M. H. Syed, A. J. Roscoe, G. M. Burt, and J. Braun, "Measurement and analysis of pmu reporting latency for smart grid protection and control applications," IEEE Access, vol. 7, pp. 48 689–48 698, 2019.

Appendices

A.1 List of Thesis Publications

[1] **S. Saxena** and H.E. Farag, "Distributed Voltage Regulation Using Permissioned Blockchains and Extended Contract Net Protocol", *accepted in International Journal of Electrical Power and Energy Systems*, Mar. 2021.

[2] **S. Saxena**, H.E. Farag and N.A. El-Taweel, "A Distributed Communication Framework for Multi-Agent Smart Grids Based on Data Distribution Service", *submitted in Electric Power Systems Research (Major Revision)*, May. 2021.

[3] **S. Saxena**, H.E. Farag, A. Brookson, H. Turesson, and H. Kim, "A Permissioned Blockchain System to Reduce Peak Demand in Residential Communities via Energy Trading: A Real-World Case Study", *IEEE Access*, vol. 9, pp. 5517-5530, 2021.
doi:10.1109/ACCESS.2020.3047885.

[4] **S. Saxena**, H.E. Farag, H. Turesson, and H. Kim, "Blockchain Based Transactive Energy Systems for Voltage Regulation in Active Distribution Networks", *IET Smart Grid*, vol. 3, no. 5, pp. 646-656, Oct. 2020. doi:10.1049/iet-stg.2019.0286.

[5] **S. Saxena**, H.E. Farag, A. Brookson, and L. St-Hilaire, "Utility Operated Transactional Energy Frameworks", Technical Report submitted to LDC Tomorrow Fund, Mar. 2020. [Available Online]: https://bit.ly/3vds5YF

[6] **S. Saxena**, H.E. Farag, A. Brookson, H. Turesson, and H. Kim, "Design and Field Implementation of Blockchain Based Renewable Energy Trading in Residential Communities," *2019 2nd International Conference on Smart Grid and Renewable Energy (SGRE)*, Doha, Qatar, Nov. 2019, pp. 1-6.
doi:10.1109/SGRE46976.2019.9020672.

[7] **S. Saxena**, N. A. El-Taweel, H. E. Farag and L. S. Hilaire, "Design and Field Im-

plementation of a Multi-Agent System for Voltage Regulation Using Smart Inverters and Data Distribution Service," *2018 IEEE Electrical Power and Energy Conference (EPEC)*, Toronto, ON, Oct. 2018, pp. 1-6. doi:10.1109/EPEC.2018.8598367.

[8] **S. Saxena**, H.E. Farag, N.A. El-Taweel, and L. St-Hilaire, "Managing Volt/VAR in Active Distribution Networks Using Distributed Generation Units and Peer to Peer Communication", Technical Report submitted to LDC Tomorrow Fund, Apr. 2018. [Available Online]: shorturl.at/agD17

A.2 Thesis Multimedia

The work in this thesis has generated several demonstration and informational videos that describe how the proposed communication and control frameworks have been deployed to the Kortright Centre Microgrid (KCM), located in Vaughan, Ontario. A description and link to each video is given in the list below.

- **Voltage Regulation Using Smart Inverters and Data Distribution Service (DDS):** Primer video to introduce the problem of voltage regulation, and how it can be solved by utilizing the proposed distributed communifcation framework that is built upon DDS. https://youtu.be/RnXo0Lt7vUI
- **Voltage Regulation DERMS Software Demo:** Demonstration video that shows how Distributed Energy Resources (DERs) can regulate voltage at the KCM by modulating real and reactive power. https://youtu.be/iVUiqXaG9mE
- **Real World P2P Energy Trading on Blockchains EXPLAINED:** Primer video that describes the infeasible rise in peak demand caused by the electrification of residential communities, and how the proposed blockchain-based, transactive energy system can reduce this demand by over 50% while enabling further trust between prosumers and distribution system operators (DSOs). https://youtu.be/_woIfSYOey4
- **Blockchain Transactive Energy Dashboard DEMO:** Demonstration video that shows the proposed blockchain-based, transactive energy system facilitating a residential energy trading system at the KCM to reduce energy imports from the DSO. https://youtu.be/XHQd-nqL8HM